UNIVERSITÀ DEGLI STUDI DI PALERMO
Dipartimento di Energia, ingegneria dell'Informazione modelli Matematici (DEIM)
Corso di Dottorato di Ricerca in Ingegneria Elettrica – XXXI CICLO
ING-IND/33 - Sistemi elettrici per l'energia

REGULATION DROOP COEFFICIENTS IN ISLANDED MICROGRIDS

IL DOTTORE
TRAN THI TU QUYNH

IL TUTOR
PROF. ELEONORA RIVA SANSEVERINO

IL COORDINATORE
PROF. MAURIZIO CELLURA

IL COTUTOR
PROF. MARIA LUISA DI SILVESTRE

CICLO XXXI
NOVEMBRE 2018

ACKNOWLEDGMENTS

First and foremost, I would like to express my sincere gratitude to my supervisor, Prof. Eleonora Riva Sanseverino, whose expertise, understanding, and patience, added considerably to my graduate experience. She gave me the academic freedom to explore my fields of interests while her deep knowledge and continual involvement prevented me from being distracted. I appreciate her vast knowledge and skill in many areas, and her assistance in writing reports as well as publications.

Besides my advisor, I would like to thank Prof. Maria Luisa Silvestre and Prof. Gaetano Zizzo for the time and effort they invested in reviewing this dissertation. I would like to extend special thanks to Prof. Tuan, Mr. Tung Lam Nguyen and colleagues, whose support to help me validating the simulation model at National Institute of Solar Energy, France. Many thanks to Dr. Richard Rocheleau, Dr. Cung Vu, Dr. Leon Roose and other colleagues for your support to exchange and further improve my skills and experiences in 6-months at Hawaii Natural Energy Institute.

A very special thanks goes out to Prof. Maurizio Cellura who has helped me alot, given the best condition to me to complete this PhD course in University of Palermo. I must also acknowledge Dr. Binh Doan Van and Dr. Ninh Nguyen Quang, Mr. Hoai Nam Nguyen for their suggestions for my scholarship applications and other supports. Without their supports, I would not have been in Palermo for this PhD course. I would also like to thank my family for the support they provided me through my entire life and in particular, without whose encouragement and editing assistance, I would not have finished this thesis.

I wish to thank the Italian Ministry of Foreign affairs and International Cooperation (MAECI), The Directorate General for the Promotion of the Italian Economic System (DGSP) for their support to the research activity within the frame of the Scientific cooperation Italy-Vietnam 2017-2019 (Project ‘Greening the power systems with solar power for Greenhouse gas emission reduction in Vietnam’).

In conclusion, I recognize that this research would not have been possible without the financial assistance of the University of Palermo, the Department of Electrical, Electronic and Telecommunication at the University of Palermo and the support of Institute of Energy System to me to have time to take this PhD course and express my gratitude to those agencies.

TABLE OF CONTENTS

LIST OF FIGURES

LIST OF TABLES

LIST OF SYMBOLS AND ABBREVIATIONS

DG	Distributed generator
OPF	Optimal Power Flow
GSO	Glow-worm Swarm Optimization
OF	Objective Function
ICT	Information and Communications Technology
PWM	Pulse Width Modulator
ACO	Ant Colony Optimization
PSO	Particle Swarm Optimization
P_{Gi}	Real power generated of the i-th generator
Q_{Gi}	Reactive power generated of the i-th generator
K_{Gi}	Frequency droop coefficient of the i-th generator
K_{di}	Voltage droop coefficient of the i-th generator
$f_{x,i}$	Frequency at the i-th generator
V_i	Output voltage at the i-th generator
f_{0i}	Frequency of the i-th generator at no load
V_{0i}	Voltage of the i-th generator at no load
K_{Gmaxi}	Maximum value of frequency droop coefficient of the i-th generator
P_{Gmaxi}	Rated power of i-th generator
n_G	Number of generators in microgrid
n_d	Number of load buses
P_{Li}	Real power demand of the i-th load
$I_{branchi}$	Current flowing in the i-th branch of the microgrid
$I_{maxbranchi}$	Ampacity of the i-th branch of the microgrid
n_{branch}	Number of transmission branches in the microgrid

f_{max}	Frequency upper limit
f_{min}	Frequency lower limit
P_i	Injected power at bus *i*
P_{loss}	Power losses of the microgrid
n_{bus}	Number of buses of the microgrid
V_i	Voltages at buses *i*
δ_i	Phase angles of the voltages at bus *i*
Y_{ij}	Admittance of the *ij* branch
θ_{ij}	Phase angle of Y_{ij};
n_{br}	Number of branches connected to bus *i*.
Δf	Frequency deviation
P_{0i}	Real power of the load in the operating point
Q_{0i}	Reactive power of the load in the operating point
α	Real power exponents
β	Reactive power exponents
K_{pf}	Coefficient, ranging from 0 to 3.0
K_{qf}	Coefficient ranging from -2.0 to 0
ΔP	Real power deviation
x(t)	Location of glow-worms in the search space at iteration t
l(t)	Value of luciferin at iteration t
ρ	Luciferin decay constant
γ	Enhancement constant
$N_i(t)$	Set of neighborhood of glow-worm *i* at the *t*-th iteration
s	Step-size
r_d^i	Local decision range
K_P	Proportional gain constant

f_{sw}	The switching frequency of the PWM
T_i	Integral time constant
σ	Symmetrical distance
f_c	Crossover frequency
$L_v(s)$	LC filter transfer function
$P_v(s)$	PI controller transfer function
$G_{C,CL}(s)$	Inner current control transfer function
C_f	Filter parameters
L_f, R_f	Filter parameters
T_f	System time constant
$G_v(s)_{OL}$	Open loop transfer function
$G_v(s)_{CL}$	Close loop transfer function

CHAPTER I

INTRODUCTION

1.1. Preface

Although in the first half of the 21st century fossil sources still play a key role in supplying the energy needs of humanity, they are on the road to be exhausted and are the main causes of environmental pollution. Therefore, research has concentrated on technology for efficient exploitation of alternative and renewable energy sources. According to forecasted data since after 2050, renewable energy will hold a key role in energy supply for human consumption, holding a unique position and providing three quarters of global energy demand by 2100 [1]. In this scenario, microgrids technology is emerging as an efficient solution to supply clean electrical power at local level from renewable energy sources. Such microgrids may either be operated as grid connected or islanded from the utility power grid and are utilized in a variety of settings including commercial applications, community/utility deployment, institutional power systems, military installations, and off-grid microgrids that provide electricity to remote villages and other sites.

According to the Navigant research report of January 2018, 1869 microgrid projects, that represent nearly 21 gigawatts of capacity, are proposed, planned, under construction or operating worldwide. Asia Pacific and North America are leading contributors for almost three-quarters of all microgrid capacity. The Middle East & Africa gets the third place among all regions with more than 3 GW of total capacity while Europe only accounts for just 9% with 1,8 GW of the global microgrid capacity. With a growing energy demand and environmental issues, many countries have set targets to increase the penetration of renewable energies into their electricity generation systems. The integration of DERs into microgrids thus plays a major role in achieving these targets and balancing power in the electricity grid [2].

Many control strategies, such as droop control, master-slave control, and average current-sharing control, have been extensively implemented worldwide to operate parallel-connected inverters for load sharing in MG network. Among these methods, droop control is one of the most popular methodology for power sharing and stability support in microgrids and the frequency and voltage control in the power system are the key features to support the optimal power sharing between the generators [3-5]. In this thesis, a novel non-linear droop control is proposed. The droop curve is generated as a piecewise linear curve from the optimized operating points of the system under consideration for different values of the supplied load. For each Optimal Power Flow (OPF) [6], the droop coefficients are generated and these create small piecewise linear parts of the final droop curve. The operation is constrained by frequency and voltage limits.

It is well known that the load flow problem solution can provide infinite operating points if the generators set point is not fixed. For each loading condition, the solution to the OPF problem outputs a single solution. Such solution, in case of microgrids with inverter-interfaced units, is an expanded state of the system comprising the operating frequency and voltage. In this case, all microgrids' components are modeled as frequency and voltage dependent elements. The OPF is solved off-line for various loading conditions so as to construct the new droop as a piecewise linear curve.

The novelty of this approach is that the droop coefficients in the f-P plane and V-Q plane are set to provide, together with frequency and voltage regulation during transients, also the lowest value of the energy losses in the microgrid, both during a load variation and in steady-state, without any other adjustment in the set-points of the generators.

In Vietnam, the potential to develop new energy from renewable sources is very high, the power which is generated from renewable energy sources is considered to be an ideal complement to the power shortage. This will not only help to diversify sources of energy but also contribute to diversify risks, strengthening and ensuring

national energy security. Therefore, the research methods to develop and optimize operation for microgrids play an important role to help expand microgrid networks in Vietnam as well as to reduce costs and losses operation for Vietnam's power systems.

1.2. Research motivation

The interest in the micorgrid structures have increased due to their capability of enhancing the observability and controllability of the power flow in the systems, contributing for reducing system losses, improving the power quality and providing at the same time the necessary conditions for increasing the connection capacities for different distributed generation technologies.

The literature survey that will be detailed in the following sections shows the need to change power system operation modes since the increasing amount of renewable distributed generation (DG) units is strongly impacting existing power systems. This is more relevant when small systems like microgrids are considered. In these systems, most renewable DG units are indeed interfaced to the alternative current (AC) network via inverters whose physical characteristics largely differ from features of rotating units.

Therefore, it is necessary to considerate the overall microgrid's efficiency in the literature when dealing with primary regulation, analyze in detail the impact of different droop control methodologies on the system frequency stability and voltage dynamics in microgrid. In these situations, an improved primary droop regulation can keep frequency and voltage within desired limits and can relieve also volumes that secondary and tertiary regulation have to take over from primary control if limited load-generators variations occur in microgrids. The droop regulation in the f-P and V-Q planes can output the lowest value of the energy losses in the microgrid, both during a load variation and in steady-state.

1.3. Research objectives

To address the aforementioned difficulties, the following objectives are identified for this research work:

1) Improvement of overall efficiency in the microgrid by adopting a driven primary regulation procedure that keeps frequency and voltage within desired limits and can relieve also volumes that secondary and tertiary regulation have to take over from primary control, if limited load-generators variations occur in the microgrid.;

2) Modeling and analysis of the impact of droop control on the overall system stability in islanded microgrids under dynamic conditions in simulation environment;

3) Comparative analysis and sensitivity studies for assessing the impact of the proposed methods on the transient and steady-state behaviors of the power sharing, power losses, frequency stability and voltage dynamics.

1.4. Thesis outline

The thesis includes 7 chapters, as described below.

Chapter 2 presents basic concept and hierarchical control of microgrid networks. This chapter also presents the state-of-the-art and a critical literature survey on energy management, solutions for OPF and droop control methodologies in microgrids. This chapter also presents the potential of renewable energy resources and opportunities as well as barriers for developing microgrid technology in Vietnam.

Chapter 3 presents the proposed driven P-f primary regulation technique with frequency constraint for minimum power losses operation and the advantages of this new method compared to conventional droop control. It contains the description of the GSO algorithm that is used to solve the OPF problem. Moreover, the section describes the 4-bus test implementation in Matlab/Simulink environment; such implementation is useful to check the effectiveness of the proposed method as well as its improved reliability.

Chapter 4 presents the proposed primary regulation technique both in with voltage and frequency constraints for minimum power losses operation and the advantages of the new method compared to the conventional droop control. A 9-bus

test system simulation is employed to assess which regulation method is more effective for improving the power losses.

Chapter 5 presents the application of the proposed primary regulation technique for minimum power costs operation while meeting technical constraints. A test has been carried out for PV-Storage-Microturbine islanded microgrid to show the efficiency and the advantages of the proposed technique by comparing to a two levels architecture.

Chapter 6 presents a development of the regulation method proposed in Chapter 3. Instead of using droop curves to regulate the power sharing between generators, the value of the optimized control parameter are calculated in the optimization controller and transferred online to the inverter of generator at every time step for minimizing microgrid's power losses. The test system is modeled in real time. At first, a model of system is implemented in the RT-lab simulator to check operating parameters, then it is tested in hardware-in-the-loop simulation with participation of real PV systems to check stability of the system.

Finally, Chapter 7 presents the dissertation summary, contributions, and directions for future work.

The details of optimal results and load flow calculation results are shown in the appendix.

CHAPTER II

LITERATURE SURVEY

2.1. Basic concepts about microgrids and hierarchical control

Microgrids are small or medium scale electric distribution networks that include multiple loads, distributed energy resources and storage systems. These energy resources can either be generation units such as fuel cells, PV systems, wind energy sources, as well as storage or controllable loads, as shown in Figure 2.1. In a microgrid network, it is important to have at least one controllable distributed generator to enhance the flexibility of power. The loads in microgrids are the electrical components that consume electricity power. Loads can be lights, bulbs, heaters, air conditioners, electronic components, electrical machines, etc; they require electricity at different demand levels and with different quality depending on their use. The distributed energy resources and loads are connected by a physical network and operated by an advanced control technology to distribute the power flow in the system and provide energy usage information [7].

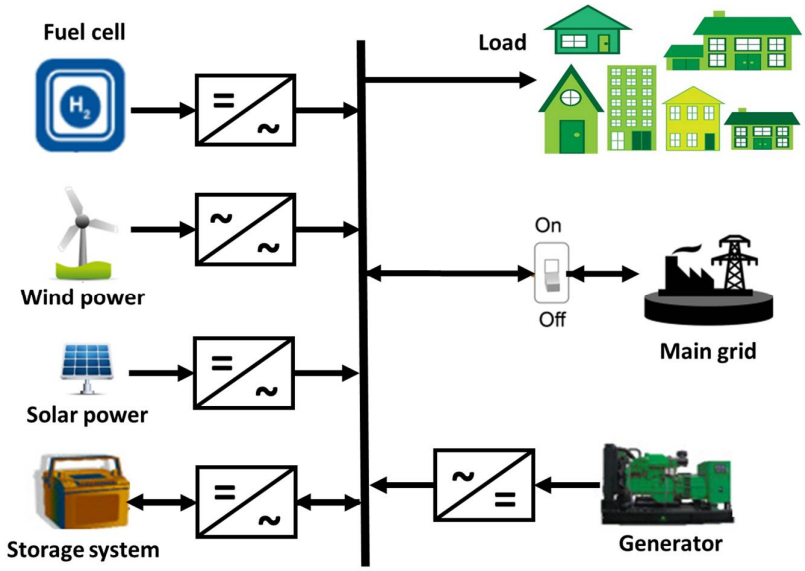

Figure 2.1. Microgrid system

Following the report of The United States Northeast Blackout of August 2003 impacted 50 million people and 61,800 MW of load [8], when electrical grids are run near critical capacity, a seemingly innocuous problem in a small part of the system can lead to a domino effect that takes down an entire electrical grid. However, in MGs, this risk can be alleviated by segmenting the grid into smaller functional units that can be isolated and operated autonomously if needed [9]. The energy efficiency and reliability of supply are improved by reducing the transmission length and integrating distributed generations. Through their decentralized architecture, MGs are also less vulnerable to attacks on individual pieces of key generation or transmission infrastructure compare to the centralized grid that contains large, complex components that are expensive and slow to replace if damaged. Moreover, the clean energy sources like solar PV and wind are used to address climate change, MGs can provide power to important facilities and communities using their distributed generation assets when the main grid goes down, therefore the environmental impact is decreased as well.

Microgrids can be operated either in grid-connected or islanded modes [10]. When operated in grid-connected mode, microgrids purchase electricity from the main grid to control voltage and power balance [11] or sell unused electricity to the main grid for maximizing the operational benefits [12]. Islanded microgrids, as small systems, suffer from a number of problems deriving from unpredictability of renewable-based Distributed Generators (DGs). In these systems, the frequency and voltage are the main features to be controlled so as to support the optimal power sharing between the generators [3, 4, 13]. Such power sharing is carried out at different regulation levels, ranging from the tertiary regulation level, acting on the scale of tens of minutes or hours, to the secondary and primary regulation (also called droop regulation) acting at the scale of seconds and milliseconds respectively.

In MGs, a three levels control hierarchical architecture [10] allows to provide good power quality. The meaning of three levels could be explained as below (see Figure 2.2):

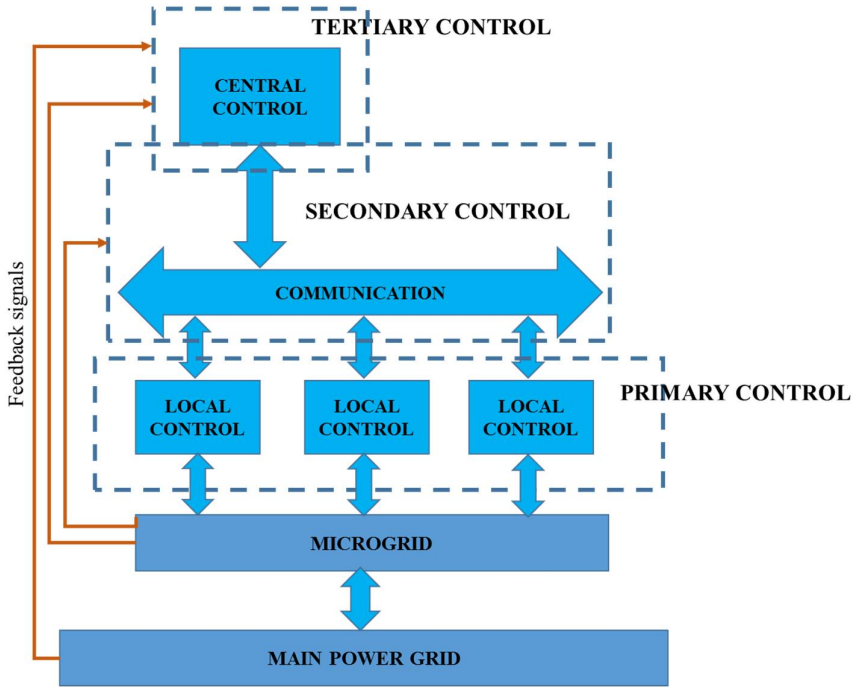

Figure 2.2. The hierarchical control structure of microgrid

- The primary control is usually designed to use droop-control method to stabilize the voltage and frequency for microgrids and regulate the power sharing between distributed generators. This control level is also used to mitigate the circulating currents between paralleled three-phase generators' converters that cause over-current phenomenon in the power electric devices and damage the capacitors.

- The secondary control is designed to compensate the voltage and frequency deviation caused by primary control. This control level has slower dynamics than the primary control level. By this way, the secondary control level can also be implemented to satisfy the power quality requirements.

- The tertiary control is the last control level that controls the power flow in the MG and between the MG and the grid. The tertiary control level also provides an economically optimal operation by solving optimization problems for minimizing power operating cost.

Beside the benefits, the rapidly increasing trend of microgrid integration into electricity grid presents technical, regulatory and economic barriers and problems,

where MG's grid interconnection, voltage stability, distribution system operation, control and protection are the key technical issues discussed [14-16], the barriers to microgrid promotion and deployment are:

- Matching solutions to the local needs: to access the benefits of flexibility and scalability solutions need to be designed which match the individual needs of a community. Whereas a centralized grid provides energy for whatever need, decentralized energy systems must be designed to match the local needs. This design process requires detailed understanding of load use, load specification, ability to pay and other site specific factors, adding complexity to design.

- Efficient loads for productive use: to access the benefits of flexibility, particularly the ability to power livelihoods, more efficient loads are required to ensure that powering these loads from renewable energy is affordable. However for non-domestic loads these efficiency improvements are yet to be easily available for end-users.

- In addition, there are a lot of barriers that relate to bad policy design, or discontinuity and/or insufficient transparency of policies and legislation, the institutional and administrative barriers, market barriers, such as inconsistent pricing structures that disadvantage are renewables, asymmetrical information, market power, subsidies for fossil fuels, and the failure of costing methods to include social and environmental costs.

2.2. Energy management system in MGs

In the future, MGs will be developed to take strong advantage of using clean and renewable energy sources. One of the main problems in MGs is to match production and consumption at the different time scales. For this reason, the highest control level implements OPF and Energy Management at minimum cost and minimum losses. The microgrid Energy management system (EMS) is expected to monitor the operational conditions and optimally dispatch power from distributed generators (DGs) and distributed energy storage nodes to supply the controllable and

critical loads. The microgrid EMS receives the load and energy resource forecasting data, customer information/preference, policy, and electricity market information to determine the best available controls on power flow, utility power purchases, load dispatch, and DG or distributed energy storage scheduling [17].

The latest research carried out optimal energy management in microgrids is based on different methods to find out the minimum cost operation while analyzing the technical and economic time dependent constraints. In most papers, the economic issue is considered in great details [18-22].

In [23-28], power management algorithms are applied. The optimization of a hybrid micro-grid system is investigated and the Particle Swarm Optimization (PSO) method is used to find a least-cost configuration of the system and to design its components. In other papers, mixed-integer nonlinear programming (MINLP) and mixed integer linear programming (MILP) [29-31] are proposed to manage energy production and demand. In [32], the operation problem of micro-grids is modeled considering the economical, technical and environmental issues, as well as uncertainties related to loads, wind speed and solar radiation and was solved by MINLP. In [33], a discrete-time MILP mathematical formulation is demonstrated to cope with the underlying uncertainty through a rolling horizon approach to optimize the management a micro-grid. In [34], a MILP model is presented to identify optimal design for the integration of distributed generation units and micro-grids in the power grid, a case study is applied for an area in South Australia. A robust optimization algorithm for scheduling the dispatchable units is presented in [35] and formulated in the MILP frame. From these studies, the optimization has just satisfied constraints about energy balance and capacity limitation both of generators and storage system, the technical issues like power loss minimization, frequency variation, currents below lines ampacity have been mentioned but not yet implemented in details. Also some works focus on energy storage systems management [16,17] which are critical for energy and power balance.

2.3. Solutions for optimal power flow in MGs

The OPF problem is usually dealt with in the Distribution Management System (DMS) to find the optimal operating points in the electric power system in order to achieve the minimum operating costs as well as minimum power losses. The time scale for deploying such function range from minutes to tens of minutes. In this way, electricity demands are also met while ensuring security conditions. Therefore, the OPF solution in power systems as well as in microgrids is necessary.

Recently, many studies have been done to calculate the OPF in microgrid systems. These studies generally consider the participation of inverter-based devices, which are designed, by means of lower control levels deployed between milliseconds and seconds, to compensate the voltage and frequency deviations.

Some recent research works concern the optimal power flow problem in islanded microgrids. In most cases, approaches rely on numeric solution approaches. In [36, 37], the authors use Newton-Raphson method to solve a set of nonlinear algebraic equation for power network. In [38], the Newton trust-region method is implemented to consider some case studies for both balanced and unbalanced microgrid test systems. Matlab's *fsolve* function has been used in [39] to calculate the power flow in three-phase balanced and unbalanced microgrids and supports the OPF solution based on an iterative strategy for non-linear optimization. Based on a quasi-Newton method, [40] also describes a methodology for unbalanced three-phase OPF for smart grid. But these solution approaches do not efficiently account for constraints.

Meanwhile, the heuristic solution approaches can overcome the weaknesses of the numeric solutions. In [41], a novel load flow analysis (LFA) and Particle Swarm Optimization are used to optimize the power sharing among sources in a microgrid. In another research [42], a fuzzy based Modified Artificial Bee Colony (MABC) algorithm is presented for solving the OPF problem. Recently, an Adaptive Multi Objective Harmony Search Algorithm is used in [43] to decrease power losses and improve load ability in islanded microgrids. In [44, 45], the Glow-worm Swarm

Optimization method is implemented to solve the OPF problem accounting for frequency [15] and line impedance constraints of the system [14,15].

2.4. Droop control methodologies

Recently, studies about droop control for microgrid systems have been used widely and focused on finding solutions for improving system stability. As an example, in [46], a new scheme for the control of parallel-connected inverters in an islanded microgrids is presented. The study uses the feedback from those variables that can be measured locally at the inverter. In this way, it is not necessary to establish a communication flow of control signals between the devices, with high advantages for large microgrids, where distances between inverters make communication impractical. In [47] the authors propose a new methodology for quickly and accurately calculating the average power for single-phase paralleled inverters intended to be applied in a droop-control microgrid system. In [48], the authors face the issue of frequency stabilization of islanded microgrids through Demand Response and generation-side management, using droop control and allowing them to share imbalances. Finally, in [49] the authors propose a direct current vector control mechanism integrated in the droop control method for improving microgrid's stability, reliability and power quality. There are three most famous droop control methodologies in the literature: linear, nonlinear and dynamic droop control.

Linear droop control (also known as conventional droop control) is carried out at the grid forming DG units[1] for primary regulation of frequency and voltage in microgrids and to rate power sharing between DG generators in the system [50-54] as an example, the system in Figure 2.3, including *i* distributed generators (DG_1, DG_2,…, DG_i) connected to a load bus.

[1] Grid forming inverters are tied to microgrids where they are required to assist in the regulation of both voltage and frequency

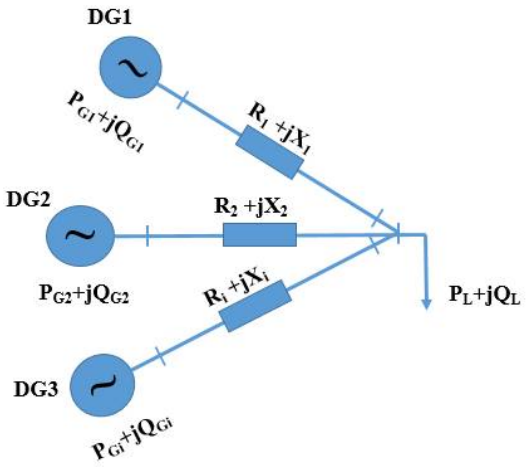

Figure 2.3. Distributed generators connected to a load through three cable lines.

The frequency and voltage adjustment of generators, which are integrated into the microgrid, can be implemented by linear droop control technique as follows:

$$P_{Gi} = - K_{Gi} (f - f_{0i}) \quad (2.1)$$

$$Q_{Gi} = - K_{di} (|V_i| - V_{0i}) \quad (2.2)$$

The values f_{0i} and V_{0i} are rated frequency and rated voltage, respectively. K_{Gi} and K_{di} parameters are frequency and voltage droop coefficients and are chosen based on the active rating of DGs and are typically kept constant in the computational process. The K_{Gi} value of each generator i-th, is defined as K_{Gmaxi}, is the ratio between maximum output power P_{Gmaxi} and maximum frequency deviation (f_{0i} - f_{min})

$$K_{G\max i} = \frac{P_{G\max i}}{f_{0i} - f_{\min}} = \frac{\Delta P_{\max i}}{\Delta f_{\max i}} \quad (2.3)$$

Δf_{max} is maximum acceptable frequency deviation and must be taken into consideration to limit the frequency deviation at P_{Gmaxi} [55]. Because the frequency of the microgrid is an universal signal, the sharing of real power demand between generators can be based on the droop coefficients K_{Gi}. Moreover, as a first application, this study only considers the frequency droop control. From (2.1), the microgrid operating frequency (f_x) for the i^{th} generator can be adjusted based on the droop relation as follows:

$$f_x = f_{0i} - \frac{1}{K_{Gi}} . P_{Gi} \quad (2.4)$$

When the load rises, the microgrid operating frequency is adjusted from f_x to f'_x and f_x must not be higher than the maximum acceptable frequency f_{max} and not lower than the minimum acceptable frequency f_{min} [55].

Figure.2.4 illustrates the variation of microgrid operating frequency f_x as a function of the active power provided from DG_1, DG_2,…,DG_i when the load changes, the active power of DG_1 changes from P_1 to P'_1, the active power of DG_2 changes from P_2 to P'_2. It can be seen that the active power variation of generators always stays proportional to its rated power in standard linear droop control method.

As shown by the curves, the variation of load leads to a slight change of the microgrid operating frequency f_x and the system after a few oscillations is again stable at a new microgrid operating frequency, f'_x.

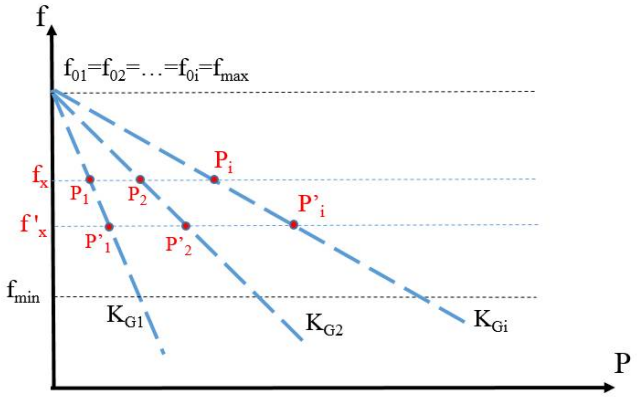

Figure.2.4. Linear power sharing with conventional droop control method.

In this case, these DG units are called grid forming units. The work [46] presents a scheme for parallel connected inverters control based on linear droop in a stand-alone AC system. The features can be measured at local level at the inverter premises, so that the system does not need control signals exchange between inverters. In [56], a compensating method is added to the conventional droop so as to add a power offset to the active power. In this way, the output power supplied by the inverters stays balanced as the output power of renewable sources varies. A detailed study shows

that this method has a more efficient performance as compared to existing methods also in terms of voltage harmonics mitigation, short-circuit behavior, as it takes the R to X line impedance ratio into account. The approach shows the power sharing under various operating conditions without any communication among units. In [57], the research is also based on the traditional droop control method and using the parallel voltage and current controller to maintain the power sharing in microgrids for both islanded and connected grid modes. In [58], a new control method for the parallel inverters operating in an island grid or connected to an infinite bus is described. Based on the linear droop regulation, frequency and voltage control are achieved without any communication between inverters.

A detailed analysis shows that this approach has a superior behavior compared to existing methods, regarding the mitigation of voltage harmonics, short-circuit behavior and the effectiveness of the frequency and voltage control, as it takes the R to X line impedance ratio into account. The conventional linear droop control is very simple and reliable, but power sharing based on rated power cannot provide an optimized operating point, for example, to minimize power losses in the system.

Differently from linear droop control in which constant droop coefficients are considered, nonlinear droop control is implemented with frequency and voltage droop relations whose parameters change as a function of the optimized output power for power sharing among the different sources. This method is described in details in the study presented in [59]. This research implements an optimized power sharing among different DGs, finding a solution that minimizes the operating cost. An experimental study was also carried out to prove the effectiveness of nonlinear droop control. The nonlinear droop control also is mentioned in the reference materials as [60-63].

Dynamic droop control method is considered as an expansion of the linear droop control. In this method, the no load voltage and no load frequency are utilized as dynamic signals to regulate the output power of each DG. In [64], an improved droop control method with automatic master to correct the voltage regulation is shown. A robust control scheme is provided in this case to keep a good stability and dynamic response. A robust control scheme is also provided to maintain a good stability and

dynamic response as the design of the normal condition. It also was described in [65]. Another research used the same way to regulate active power following the values of frequency at no load to reduce the fuel cost of DGs [66]. The work in [55] mentions a cost optimization based on a dynamic power sharing method. In this case, a linear unit commitment, based on a frequency droop scheme, is resolved to find out the amount of power that each generator should inject into the bus. To prove the results, some experimental tests are carried out. However, results are just concentrated on the power sharing issue, without considering frequency conditions. A cost optimization based on a dynamic power sharing method is mentioned in [67], where a linear unit commitment strategy based on a frequency droop scheme is solved to determine the amount of power that each generator should put into the power bus. Then, to prove results, some experimental tests are carried out in., however, the results are just concentrated to power sharing without considering frequency conditions. Table 2.1 summarizes the above analysis highlighting the advantages and disadvantages of the various approaches presented in the literature.

Table 2.1. The advantages and disadvantages of droop control methods.

	Conventional Droop Control	**Non-linear Droop Control**	**Dynamic Droop Control**	**Proposed Droop Control**
Simple	✓	-	-	✓
Easy to implement	✓	-	-	✓
Quick response	✓	-	-	✓
No communication signals between the inverters	✓	✓	✓	✓
Improved power sharing	-	✓	✓	✓
Improved stability	-	✓	✓	✓

2.5. Opportunities for developing microgrids in Vietnam

At present, Vietnam is focusing on exploration and development of renewable energy sources to supply electricity for local consumer demand, where the national grid is not available, such as remote islands and high mountains, be called communes. The Master Power Plan (MOIT, 2011) indicates the following: by September 2009 the national power grid was covering all 63 provinces and its cities and 536/547 districts (98%). Of these, 11 rural districts were not connected to power grid yet but electricity was distributed via local diesel power and local small hydro power plants.

On a community level 8,931/9,120 communes municipalities had access to electricity (97.93%) - in which 8,890 communes municipalities (97.5%) connected to power grid, 41 communes municipalities (0.5%) accessed electricity by local power production. The Mapping of the Off-grid Communities is shown in the Figure 2.5 [68]. By the end of 2020, the target of Vietnam is that 100% of the country's households should be electrified [69].

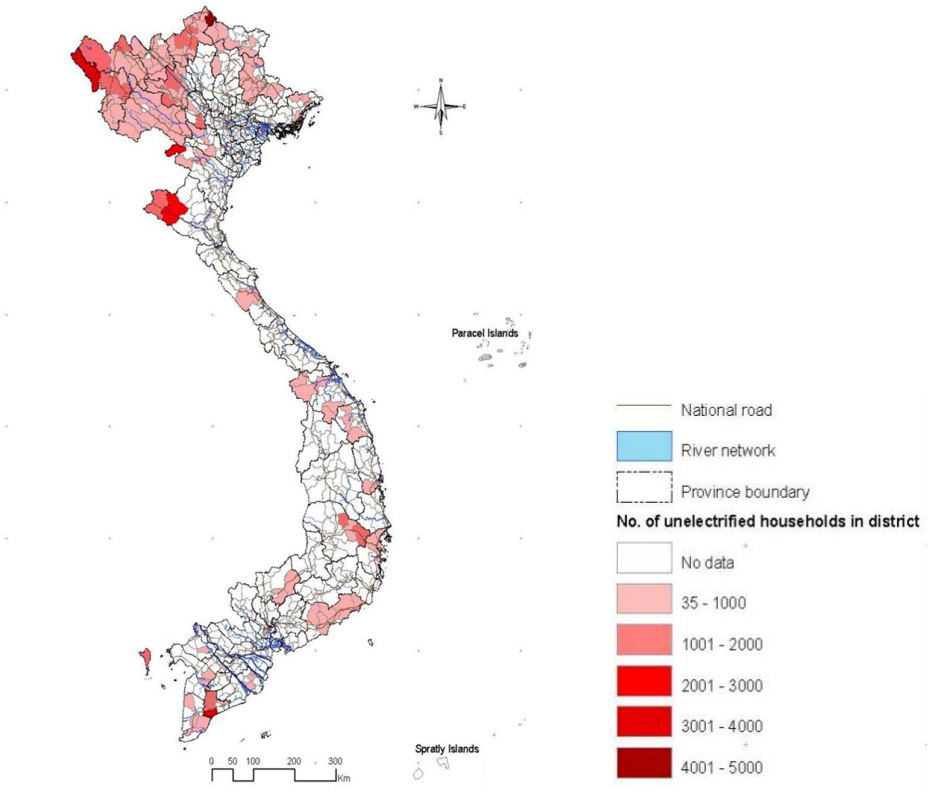

Figure 2.5. GIS Map of the number of households that don't have access to the National Grid

According to the report of United Nations Environment Programme (UNEP) and Global Environment Facility (GEF) in 2014, the number of people that do not have access to grid electricity in Southeast Asian countries [70] are shown in the Table 2.2 below .

Table 2.2. Off-grid lighting status for Southeast Asian countries

Parameters	Cambodia	Indonesia	Lao	Philippines	Thailand	Vietnam
Total population (million)	14,10	239,9	6,2	93,3	66,8	86,9
Off-grid population (million)	10,7	85,2	2,8	9,6	1,00	2,1
Percent population off-grid	75,8	35,5	45,16	10,28	1,5	2,41

From the data in table 2.2 compared to other countries in the region, it can be seen that the population that has not access to the national power grid in Vietnam is low, only 2.1%. Most of the households in these areas depend on conventional fuel burning that is polluting and damaging, both to the environment and their health. Generation of electricity through renewable means such as wind, solar, hydro and even geothermal energy could emerge as a great alternative in providing clean energy. With high potential for renewable energy sources, this figure can be reduced quickly in the future if the development policy renewable energy power is implemented appropriately. Therefore, the research methods to develop and optimize operation for microgrids play more important role to help expand microgrid networks in Vietnam as well as reduce costs and losses operation for Vietnam's power systems.

The potential of Renewable energy in Vietnam

Vietnam is one of the countries having renewable energy source in high potential distributing throughout the country. According to the estimation, biomass in potential from waste products or agricultural waste is about 10 million tons per year; biogas from garbage, animal manure and agricultural waste is approximately 10 billion m3 per year; small hydro power (<30 MW) is 4000 MW, and solar power radiation with average sunny radiation is 5 kWh/m^2 per day. Besides, with more than

3,400 km of coast, Vietnam has plentifully wind power source of about 500- 1000 kWh/m^2 / year in estimation. These renewable energy sources when being used will meet the rapidly growing demands [71].

Solar energy

Vietnam has one of the highest number of hours of sunshine annually in the world with approximately 2,000 to 2,500 on average and the solar map in Figure 2.6(a) shows that the southern regions in particular are suitable, reaching average solar intensity levels of 5 kWh per square meter per day. Vietnam has high potential for solar energy production. By 2030, Vietnamese generation system should produce 12 GW of solar energy annually, coming from insignificant levels today [72].

Currently, Vietnam has more than 30 projects at some stage of development ranging from 20-300 MW, and plans to invest a total of USD 3.3 billion into solar energy development. The country is preparing for large investments in the solar energy sector, and through the revised Vietnam's Power Development Plan 2011 [73] aims to increase solar power installed capacity from virtually nothing now to 0.8 GW in 2020 and 12 GW in 2030, the latter accounting for 3.3% of the total energy production that year [72].

Wind energy

Vietnam is considered to have the best wind resources in Southeast Asia. Located in the monsoon climate zone, and shaped by its over 3,000 km long coastline, Vietnam´s potential to develop and generate wind power is large. The World Bank recently identified great potential for harnessing wind energy in Vietnam´s south central regions and the Mekong Delta. Estimations from an existing 2011 wind atlas cite around 24 GW of potential.

According to the Renewable Energy Development Strategy 2016-2030, Vietnam will promote on-shore wind power until 2030 and assess the potential for off-shore wind resources as an electricity solution for after 2030.

The map of Vietnam's Solar energy and Wind energy is shown in the Figure 2.6.

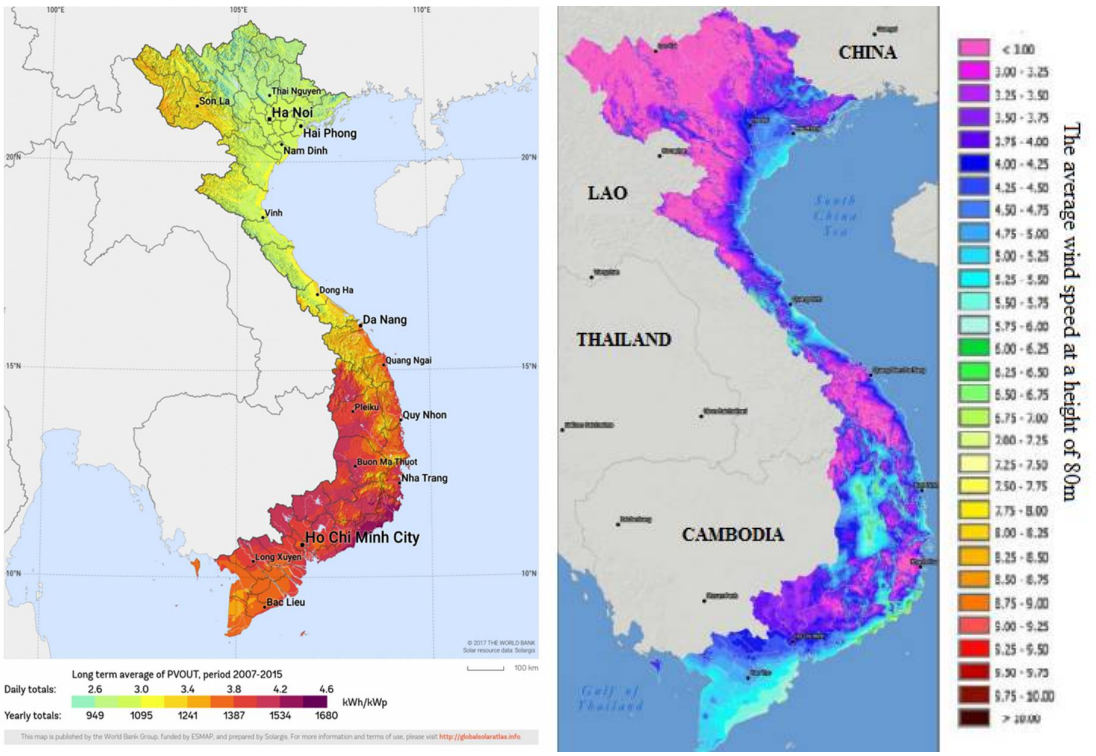

(a) (b)

Figure 2.6. The map of Vietnam's renewable energy resources (a) Solar energy (b) Wind energy[2]

Hydroelectric

The river system of Vietnam is dense, distributed in many different territories. Vietnam has 2,360 rivers over 10 km long. Of these, 90% are small rivers and streams, which are favorable for the development of the community. At present, hydropower in Vietnam is "divided" into four major categories: micro hydroelectric systems, owned by households in mountainous rural areas, have capacities in the range of 200 - <1000W, which are sufficient for lighting in the case of water sources.

- Grid-connected hydroelectric systems provide power only to independent mini grid systems with a typical power output of 1kW to 1MW.

[2] Source: Renewable Energy in Vietnam report, Hanoi, Vietnam, August 2017

- Grid-connected hydro systems have power ranges from 1MW to 30MW.

- Large hydropower with a capacity is over 30MW.

Biomass energy

Biomass is an important source of energy in Vietnam, and being an agricultural country, Vietnam has a high level of biomass energy potential. Agricultural waste is most abundant in the Mekong Delta region, responsible for approximately 50% of the waste of the whole country, and in the Red River Delta, producing 15% of the country's waste. It is estimated that approximately 90% of domestic energy consumption in rural areas is derived from biomass such as fuel wood, agricultural residues and charcoal. Moreover, biomass fuel is also an important source of energy for small industries located mainly in rural areas. According to a report of the Vietnam Energy Association, in total biomass could amount to up to 9 billion kWh in 2020 and 80 billion kWh in 2050. There are still many obstacles, such as high investment and low returns. The government is working on more supporting policies and land and tax incentives to reduce the costs of importing spare parts and equipment.

Currently, there are 5 types of renewable energy that have been exploited to produce electricity in Vietnam with a total installed capacity of about 1215 MW, these including: small hydropower (1000 MW), biomass (152 MW), domestic waste (8 MW), solar (3 MW) and wind (52 MW). The current status of renewable energy just obtained about 3,4% [71] of the overall energy in potential.

Barriers on microgrid project development in Vietnam

• High investment costs of renewable energy technology solutions

• Difficult access to financial resources at different stages of project/enterprise development

• Limited access to tailor-made financing for end-users

• Legal and institutional framework and uniform legal framework

• Lack of adequate incentive mechanism

• Lack of national/province RE development master plan.

National Policy Framework

Policy frameworks have great influence on the development and implementation of microgrid networks in Vietnam. Vietnamese Government has built a clear policy framework with a set of principles, long-term goals, and national commitments to the program as below.

In the Master Power Plan, the strategy to develop and create rural power supply is indicated. Government will stimulate EVN to develop the national power grid to supply power to 100% households by 2020. The aims are (MOIT, 2011):

- To further develop the national power system to supply efficiently and with highly quality sufficient electricity to meet the power demand for production and residential purposes in rural areas. In case areas cannot meet conditions to access to national power grid, the Government provides investment and support policies for development of local power resource to ensure that by 2020 the ratio of electricity available households is 100%.

- To provide support policies to help developing socio-economic situations, including developing power supply system for provinces and poor households in remote areas, especially if it concerns ethnic minorities, in order to strengthen ethnic's solidarity, maintain defense security, ensure the living and production of people, and improve physical and mental living.

- To have a Governmental program to development investment and power supply to every hamlets and minority ethnics of Tay Nguyen.

- To upgrade rural power grid to increase supply capability and electricity quality; reduce power loss in power lines.

The rural electrification (REII) project is expected to fund such developments. The objective of the REII, which became effective in 2005, is to improve access to good, affordable electricity services to rural communities in an efficient and

sustainable manner. Financed with a US$200 million IDA credit and US$5.25 million GEF grant, would be achieved through:

- A major upgrading and expansion of rural power networks in about 1,200 communes.

- Conversion of the existing ad-hoc local electricity management systems to local distribution utilities (LDUs) as legal entities recognized under Vietnamese law, to improve management of power distribution in rural areas, ensure financial sustainability, and enable future mobilization of private funds.

- Capacity building assistance for the LDUs, provincial authorities, participating regional PCs, and national authorities involved in the planning and regulation of rural electrification.

The main contents related to rural electrification are the following:

- Law on Electricity dated 14 December 2004 - Decision No. 1208/QD-TTg

- The National Power Development Plan 2011-2020 with a vision to 2030 (Master Plan VII), dated 21 July 2011;

- Decision 1855/QD-TTg Development Strategy of Energy's National Renewable Vietnam 2020 vision in 2050 dated 27 December 2007;

- Decision 177/2007/QD-TTg approved "Development scheme development of biofuels by 2015, with a vision to 2025" dated 20 November 2007;

- Circular No. 97/2008/TT-BTC, by Ministry of Finance about "Circular on implementing state support policies for investment, development of electricity in rural, mountainous and island areas" dated on 28 October 2008;

- Decision No. 8217/QD-BCT Approval of Renewable Energy Development Plan for Delta, midland area up to 2020 and 2030 vision dated 28 December 2012;

It can be seen that the opportunities for biomass, wind, solar, hydro and geothermal have a high potential in Vietnam. Hydro energy is already extensively implemented in Vietnam, solar and wind project for off-grid communities are also

developed but on a less commercial basis. The policy framework is elaborated upon and it can be concluded that there is a strong need for an improved enabling environment, consisting of - but not limited to - a further developed policy framework that supports the (commercial) development of access to renewable energy. The optimization research for microgrid networks needs to be carried out in parallel to promote the effectiveness of existing projects as well as being applied for future projects.

CHAPTER III

DRIVEN P-F PRIMARY REGULATION FOR MINIMUM POWER LOSSES OPERATION IN ISLANDED MICROGRIDS

3.1. Introduction

The droop control is widely used to regulate frequency and voltage and to adjust the power sharing between the generators in a microgrid. In the following, a comparison between the linear droop control method and a primary regulation method designed to reduce power losses is presented.

In Chapter II, the linear droop control technique is introduced and presented in details. It is observed that, in standard linear droop control, the change of the real power demand of generators always stays proportional to its rated power. The strength of conventional droop control is in its simplicity and reliability, but power sharing based on rated power cannot provide a good solution for optimized operation.

In this Chapter, a driven primary regulation method, based on simple and easy to implement algorithms, is proposed with the aim of minimizing the power losses in an islanded microgrid. Based on the OPF solution, the droop coefficients in the droop control function are adjusted following the variation of the loading conditions, and a unique piecewise droop curve for the controlled generator is built from a set of optimized operating points. In this way, the distributed generator's power output can be adjusted more flexibly, the operational efficiency of the microgrid is increased, and the power losses are reduced. The novelty of the approach, with respect to the state of the art, is, therefore, the use of non-costant droop coefficients in order to enhance the overall efficiency of the microgrid while preserving its stability. This issue is of particular interest for diesel-based islanded microgrids that face, constantly, the issue of reducing their dependency from fossil fuels and of enhancing the quality of the supply, also reducing voltage drops and power losses.

From a technical point of view, the contributions of the approach are listed below:

1) The proposed primary droop regulation improves the overall efficiency of the microgrid by adopting a Glow-worm Swarm Optimization (GSO) procedure.

2) The proposed primary droop regulation keeps frequency within desired limits and can relieve also volumes that secondary and tertiary regulation have to take over from primary control, if limited load-generators variations occur in the microgrid.

3) Building a test model and scenarios for implementing the proposed droop control in Matlab/Simulink environment under dynamic conditions to check operating parameters.

3.2. Problem formulation

In literature, some examples can be found showing that, in practical applications, K_G can be adjusted [26]. For example, in [27], it is proved that the coefficient K_G of wind turbine is not constant. When wind direction and speed fluctuate, the output power changes and this means that the real power of the wind generator transferred to the primary frequency control changes. As a consequence, the value of K_G should be picked out under various wind speeds. It is worth to highlight that, also in [19][66], different droop relations are required to resynchronize the system in different operating conditions.

The proposed driven primary regulation method for inverter-interfaced units in isolated microgrids presented in the following is an expansion of the conventional droop control method described in section 2.4. The new droop curves are built by changing the load in the microgrid and assessing through the OPF the relevant value of K_{Gi}, which is considered as the only adjustable parameter producing a new real power sharing among the two generators. The droop coefficients K_{Gi} of all the generators are selected optimally in a given range [K_{Gmini}; K_{Gmaxi}], according to the limitations of output power and frequency. For every load condition, an OPF problem

is solved for finding a minimum-losses operating state, assuming that every generator is able to regulate its frequency droop coefficient.

The OPF underlying the construction of the piecewise linear droop control law is formulated as indicated in [28]. The objective of the OPF problem is the minimization of the power losses of the microgrid and can be written as it follows:

$$\text{Min} \quad OF_{(K_G)} = P_{\text{Loss}} = \sum_{i=1}^{n_{\text{bus}}} P_{i(K_G)} \tag{3.1}$$

where n_{bus} is the total number of buses of the microgrid and $P_{i(KG)}$ is the injected power at bus *i* given by:

$$P_{i(K_G)} = \sum_{j=1}^{n_{br}} |V_i||V_j||Y_{ij}|\cos(\theta_{ij} - \delta_i + \delta_j) \tag{3.2}$$

where :

V_i and V_j are the voltages at buses *i* and *j*, respectively;

δ_i and δ_j are the phase angles of the voltages at bus *i*, *j*;

Y_{ij} is the admittance of the *ij* branch;

θ_{ij} is the phase angle of Y_{ij};

n_{br} is the number of branches connected to bus *i*.

The OPF is solved considering the following constraints:

$$\begin{cases} \sum_{i=1}^{n_G} P_{Gi} = \sum_{i=1}^{n_d} P_{Li} + P_{loss} \\ K_{Gimin} \le K_{Gi} \le K_{Gimax} \\ P_{Gimin} \le P_{Gi} \le P_{Gimax} \\ i = 2 \div n_G \\ f_{min} \le f \le f_{max} \\ I_{branchj} \le I_{\max branchj} \\ j = 2 \div n_{branch} \\ V_{min} \le V_i \le V_{max} \end{cases} \quad (3.3)$$

where:

n_G is the number of generators in microgrid;

n_d is the number of load buses;

P_{Gi} is the real power generated by DGi;

P_{Li} is the real power demand of the i-th load;

P_{loss} indicates the total real power losses of migrogrid;

$I_{branchj}$ is the current flowing in the j-th branch of microgrid;

$I_{maxbranchj}$ is the ampacity of the j-th branch of microgrid.

n_{branch} is the number of transmission branch in microgrid;

In the problem formulation, loads are modeled as frequency and voltage dependent terms, as expressed below [29]:

$$P_{Li} = P_{0i} |V_i|^{\alpha} (1 + K_{pf} . \Delta f) \quad (3.4)$$

$$Q_{Li} = Q_{0i} |V_i|^{\beta} (1 + K_{qf} . \Delta f) \quad (3.5)$$

where:

Δf is the frequency deviation;

P_{0i} and Q_{0i} are the real and reactive power of the load in the operating point;

α, β are the real and reactive power exponents [30][74];

K_{pf} is a coefficient ranging from 0 to 3.0;

K_{qf} is a coefficient ranging from -2.0 to 0 [29].

The coefficients K_{Gi} are the decision variables of the optimization problem, although they are not explicitly appearing in the objective function (3.1), they are contained in the expression (2.1) of generated powers in inverter interfaced units. The solution found for each load condition is an optimal operating point characterized the following state variables:

- The amplitude and displacement of the voltage phasors at the P-Q buses.

- The amplitude and displacement of the voltage phasors at all the P-V buses except the reference bus (Q_i depends on V_i by (2.2));

- The voltage amplitude at the reference bus;

- The frequency of the system in the range [f_{min}, f_{max}].

The power flow solution has thus $2*n_{bus}$ nodes and $2*n_{bus}$ variables.

Consider the power sharing between two generators DG_1 and DG_2, as shown in Figure 3.1, where the frequencies f_{0i} are considered equal to f_{max}. The droop coefficients of DG_2 is kept constant (continuous brown line) while K_{G1} of DG_1 is varied (from the blue to the red dashed line) allowing to modify the real power contribution of each generator to the overall load demand.

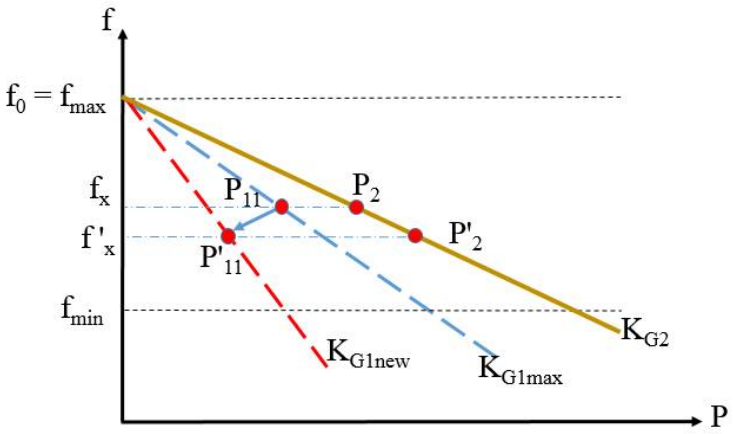

Figure 3.1. Power sharing with new droop control method among two generating units.

Finally, to ensure the stability of the system while adopting the new droop law, the frequency of the microgrid should be a monotonic function satisfying the following property [49]:

$$f(P_i) > f(P_i + \Delta P_i) \quad \text{for } P_i * \Delta P_i > 0 \tag{3.6}$$

This requirement is to get a single droop value for every changing load condition and to provide a negative feedback in the droop relations.

Regarding the power loss minimization issue, it is worth to underline that in a system with parallel inverters, the losses can be separated into two terms. The first is generated by the currents flowing from the generators to the loads, and is the power losses component considered in this thesis. The second term is generated by the circulation currents between paralleled three-phase generators' converters. The method to calculate this second power loss component is presented in [75]. At present, there are many research studies on methods to eliminate this loss component [10, 76-78], but this issue is beyond the scope of this thesis.

3.3. Glow-worm Swarm Optimization Algorithm

The optimization problem here considered (5)-(9) is highly non-linear and multimodal. For this reason, to solve this problem, a swarm intelligence algorithm is a good choice. There are three most popular swarm techniques: Ant Colony

Optimization (ACO), Particle Swarm Optimization (PSO) and Glow-worm Swarm Optimization (GSO). In [79], the various papers are reviewed and gave evidences that the glow-worm swarm has high ability of looking for global optimization and has a fast convergence rate, achieving more stable and accurate results compared to other methods. For these reasons, GSO is selected as a key tool to solve the optimization problem in this chapter.

GSO is a relatively recent heuristic method proposed by K.N. Krishnanad and D. Ghose [80]. The optimization algorithm starts from a random distribution of solutions in the search space of the objective function. The objective function values are then encoded into a function that is called 'luciferin' and is calculated for each solution (firefly), in this way, the better objective function, the greater the firefly's brightness. Fireflies will move towards solutions that have a higher luciferin value within a dynamic range. In the last iteration, the solution with the highest luciferin value will be the solution of problem. The steps of the GSO algorithm are reported below:

- Step 1: Start.

- Step 2: Collect input data regarding the microgrid (including real power and reactive power of generators, bus voltages, features of the lines, droop parameters, etc.).

- Step 3: Initialize a population of glow-worms randomly. Every glow-worm is a potential solution of optimization problem.

- Step 4: Generate luciferin l_o, local decision range r_o at time t=0.

- Step 5: The objective function is calculated by running the OPF for each solution and is stored in vector J(x).

- Step 6: Update the value of luciferin $l_i(t+1)$ using (3.7):

$$l_i(t+1) = (1-\rho)l_i(t) + \gamma J(x_i(t+1)) \tag{3.7}$$

where ρ is the luciferin decay constant ($0 < \rho < 1$) and γ is the enhancement constant ($0 < \gamma < 1$). These paramters have been determined based on extensive numerical experiments and kept fix in this thesis, ρ=0.4, γ=0.6 [80].

- Step 7: Find the neighborhood agents having stronger luciferin in the local decision range.

- Step 8: Update the probability of glow-worm *i* moving to neighbor *j* in the *t* iteration denoted by $p_{ij}(t)$:

$$p_{ij}(t) = \frac{l_j(t) - l_i(t)}{\sum_{k \in N_i(t)} l_k(t) - l_i(t)} \tag{3.8}$$

where $N_i(t)$ is the set of neighborhood of glow-worm *i* at the *t*-th iteration.

- Step 9: Update the location of glow-worms as following:

$$x_i(t+1) = x_i(t) + s\left(\frac{x_j(t) - x_i(t)}{\| x_j(t) - x_i(t) \|}\right) \tag{3.9}$$

where s is the step-size.

- Step 10: Update the local decision range $r_d^i(t+1)$:

$$r_d^i(t+1) = \min[r_s, \max[0, r_d^i(t) + \beta(n_t - | N_i(t) |)]] \tag{3.10}$$

- Step 11: Iterate the step from 5 to 10 until reach the maximum iterations number.

- Step 12: Show the results.

The main stages of the GSO algorithm are shown in the flow chart and is given in Figure 3.2.

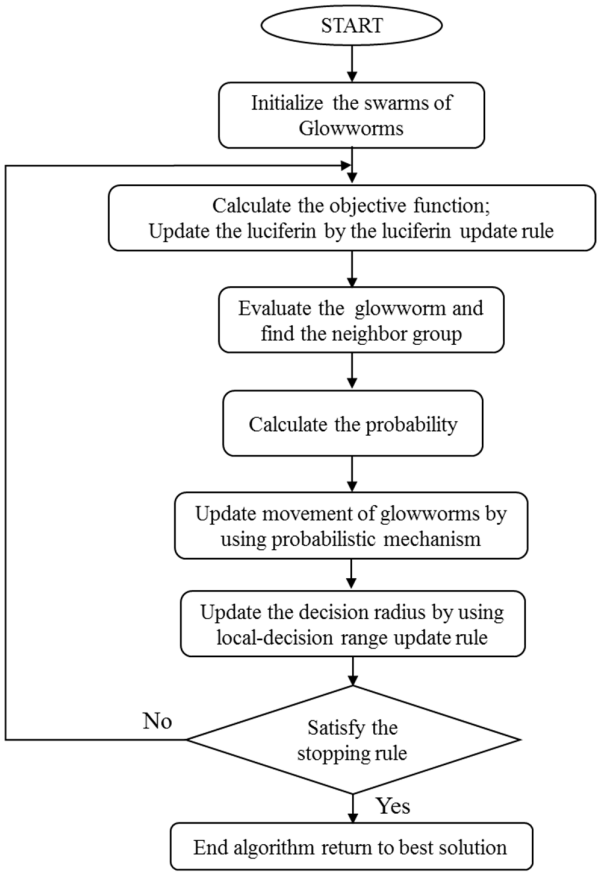

Figure. 3.2. Flowchart of GSO algorithm

The whole system has been implemented in Matlab\Simulink environment, as described in the following section. Figure 3.3 describes the pseudocode of GSO algorithm.

Initialize a population Archive A randomly, population has m glow-worms, m is archive size
Repeat Until ***Termination Condition***
Do m times
    Step 1: Deterministic ***choice (selection)*** *of the base vector*
    Step 2: Probabilistic ***choice (selection)*** *of the target vector (Roulette Wheel technique based on l(t)). find the best point with the best resource,* ***considering frequency, line ampacity and energy storage system constraints***
    Step 3: ***Recombination***
END m
Step 4: create ***new population (replace A)***
END.

Figure. 3.3. Pseudocode of GSO algorithm

3.4. Simulation of the Droop Control Loop

The droop control loop, implementing the proposed regulation method and containing the constraints of the optimization problem, is shown in Figure 3.4.a. A Phase-Locked Loop (PLL) is used to remove disturbance signals and keep the system frequency stable at its reference values [5,36]. The structure of phase-locked loop is illustrated in the Figure 3.4.b.

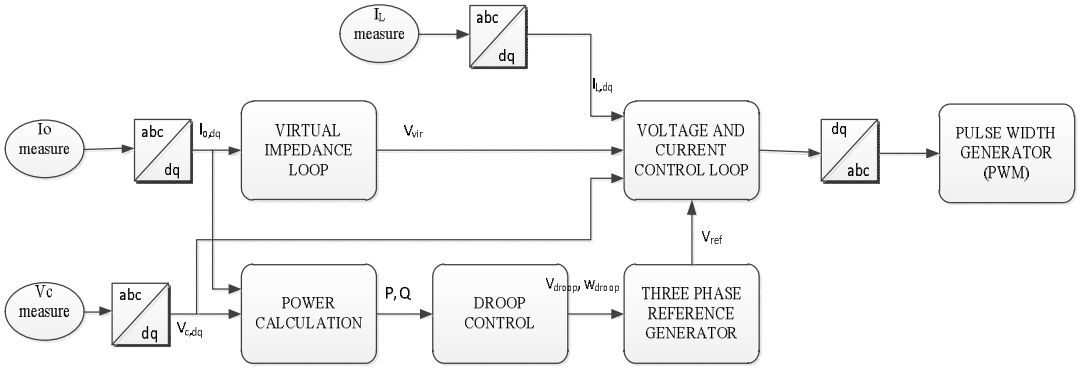

(a)

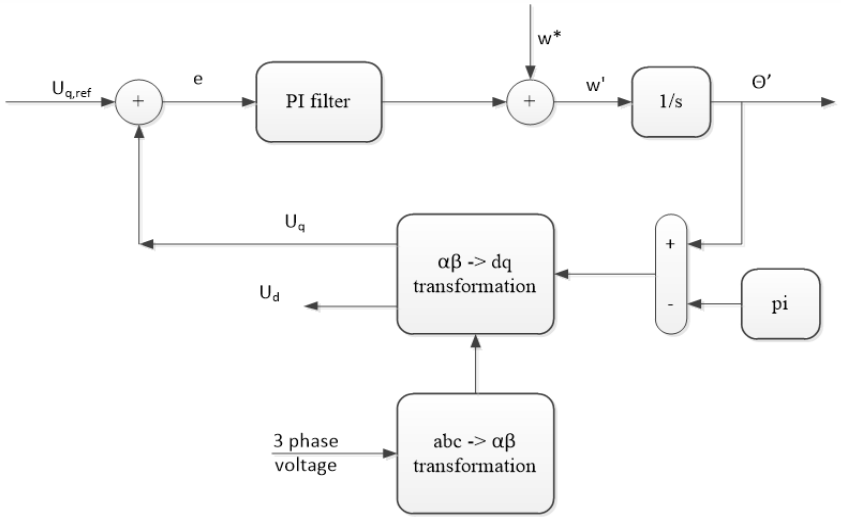

(b)

Figure 3.4. Simulation block diagram: (a) Block diagram of the control system of one inverter; (**b**) Structure of phase-locked loop.

As shown in Figure 3.3.a, the control signals are transferred to the control loops (PI controllers) to generate the reference signals for the pulse width modulator (PMW). The symmetrical optimum method is used to adjust the PI controller [37].

The process model transfer function is expressed as follows:

$$G(s) = \frac{K_P}{(1+T_\alpha.s)(1+T_e.s)} \tag{3.11}$$

$$T_\alpha = \frac{1}{2 f_{sw}} \tag{3.12}$$

$$T_e = \frac{\sigma^2}{T_i} \tag{3.13}$$

where K_P is the proportional gain constant; f_{sw} is the switching frequency of the PWM; T_i is the integral time constant and σ is defined as the symmetrical distance between $1/T_i$ and $1/T_e$ to crossover frequency f_c. The recommended value for σ is between 2 and 4. By increasing σ, the system will have a better damping and higher phase margin, but its response will become slower [38]. The block diagram of the outer voltage PI controller is presented in Figure 3.5.

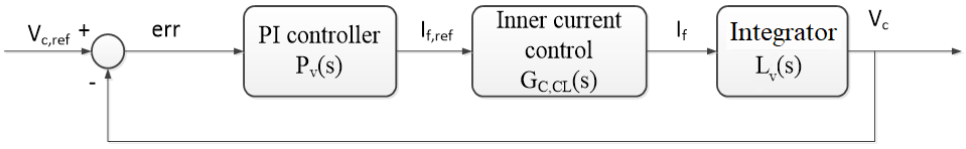

Figure 3.5. Block of the outer voltage PI controller.

Figure 3.5 shows a PI controller $P_v(s)$, an inner current control block $G_{C,CL}(s)$ and the integrator block $L_v(s)$, whose transfer functions are:

$$P_v(s) = K_P \frac{1+T_i.s}{T_i.s} \tag{3.14}$$

$$L_v(s) = \frac{V_c(s)}{I_L(s)} = \frac{1}{C_f s} \tag{3.15}$$

$$G_{C,CL}(s) = \frac{1}{2T_\alpha .s + 1} \tag{3.16}$$

where C_f is filter parameters.

The open loop $G_v(s)_{OL}$ and close loop $G_v(s)_{CL}$ transfer functions of the current controller are defined as it follows:

$$G_v(s)_{OL} = P_v(s).G_{C,CL}(s).L_V(s) = K_p.\left(\frac{1+T_i.s}{T_i.s}\right).\frac{1}{1+2T_\alpha .s}.\frac{1}{C_f.s} \tag{3.17}$$

$$G_v(s)_{CL} = \frac{K_P.(1+T_i.s)}{K_P.(1+T_i.s)+T_i.s.(1+T_\alpha .s).C_f} \tag{3.18}$$

The block of the outer current PI controller is presented in Figure 3.6.

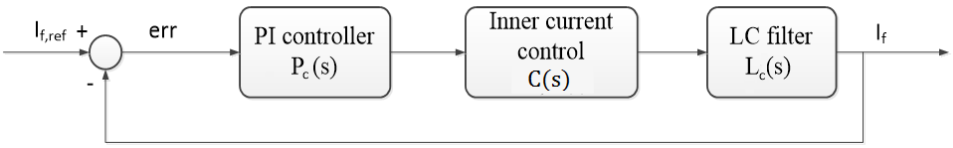

Figure 3.6. Block of the outer current PI controller.

The transfer function of the current loop can be expressed as:

$$P_C(s) = K_P \frac{1+T_i.s}{T_i.s} \tag{3.19}$$

$$L_c(s) = \frac{I_L(s)}{U_L(s)} = \frac{1}{L_f s + R_f} = \frac{1}{R_f(1+T_f s)} \quad \text{with} \quad T_f = \frac{L_f}{R_f} \tag{3.210}$$

where L_f and R_f are the filter parameters and T_f is the system time constant.

$$C(s) = \frac{1}{1 + T_{\alpha}.s} \tag{11}$$

The open $G_c(s)_{OL}$ and close loop $G_c(s)_{CL}$ transfer functions of the current controller are defined as it follows:

$$G_c(s)_{OL} = P_c(s).C(s).L_c(s) = K_p.\left(\frac{1 + T_i.s}{T_i.s}\right).\frac{1}{1 + T_{\alpha}.s}.\frac{1}{R_f(1 + T_f.s)} \tag{3.22}$$

$$G_c(s)_{CL} = \frac{K_P.(1 + T_i.s).\dfrac{1}{R_f}}{K_P.(1 + T_i.s).\dfrac{1}{R_f} + T_i.s + T_i.s.(1 + T_{\alpha}.s).(1 + T_f.s)} \tag{12}$$

3.5. Application to 4-bus system

The effects of the proposed regulation method on the real power sharing between *DG*s are analyzed in a simple case study. The test microgrid in Figure 3.7 is based on the 4-bus test system issued by IEEE [81]. However, the parameters are modified to be more appropriate for the proposed problem. A system with two generators indicated as DG_1 and DG_2 and two loads, is considered.

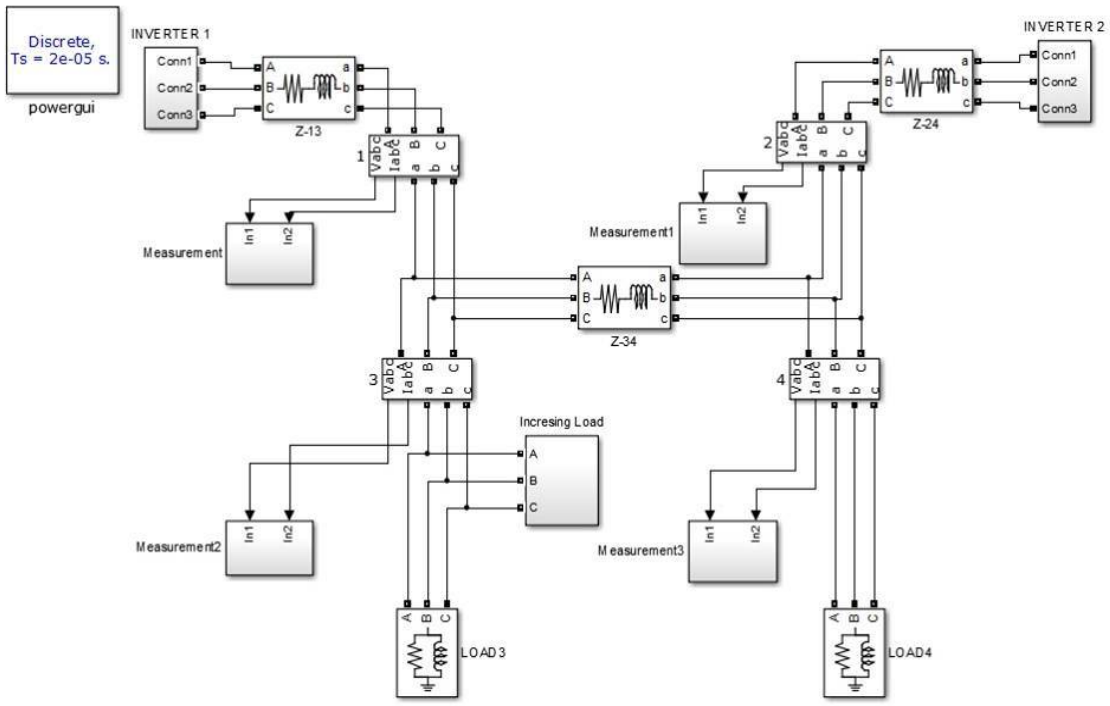

Figure 3.7. Test microgrid.

The electrical parameters of the microgrid are reported in Table 3.1.

Table 3.1. Electric parameters of the microgrid branches.

Branch	**R (pu)**	**X (pu)**	**R/X**	$I_{maxbranch}$ **(pu)**
1–3	0.22229917	0.02873961	7.7	0.5396
2–4	0.22229917	0.02873961	7.7	0.5396
3–4	0.22229917	0.02873961	7.7	0.5396

The generator DG_1 can provide real power in the range 0–0.3 pu, while DG_2 can operate in the range 0–0.2 pu. The no load-frequency f_0 is assumed the same for DG_1 and DG_2 and equal to 1.02 pu. The system frequency limits are set to f_{min}=0.98 pu and f_{max}=1.02 pu, meaning that the frequency must be within +/-1Hz of 50Hz.

In the considered case study, the droop coefficient K_{G1} of DG_1 is varied for adjusting the output power of the generators. K_{G1max} is assumed equal to 7.5, while the coefficient K_{G2} of DG_2 is assumed invariable and equal to 5 in all the examined

cases. The load at bus 4 is assumed equal to 0.1 pu while the load at bus 3 varies in the range from 0.1 pu to 0.37 pu with a step equal to +0.02 pu.

If the droop coefficients are too high, it can lead system to instability. If the droop coefficients are too low, it result in low responding of inverters [63]. Therefore, For testing the proposed method in different conditions, the maximum of droop coefficient $KG1$ in this work will be fix at 7.5 and the minimum value will be evaluated in two cases that are 6 (20% less than the maximum value) and 5 (40% less than the maximum value), respectively. Three scenarios where the adjusting of droop coefficients can improve the effectiveness of system as well as ensure the system stability are considered:

- Scenario 1, implementing the conventional droop control method
- Scenario 2, implementing the proposed optimized control method with $KG1$ selected optimally in the range [5–7.5]
- Scenario 3, implementing the proposed optimized control method with $KG1$ selected optimally in the range [6–7.5]

As shown in Section 3.2, the new droop curves of the generators are built by solving the OPF problem. Therefore, for the proposed example, there are two droop curves of DG_1 constructed to reduce the power losses for the considered test microgrid. The first curve is built with K_{G1} selected optimally in the range [5–7.5] (Scenario 2) and is illustrated in Figure 3.8.a. The second is built with K_{G1} in the range [6–7.5] (Scenario 3) and is shown in the Figure 3.8.b. The conventional droop control curve (Scenario 1) is also represented in Figure 3.8 to show the improvements obtained with the proposed optimized control method.

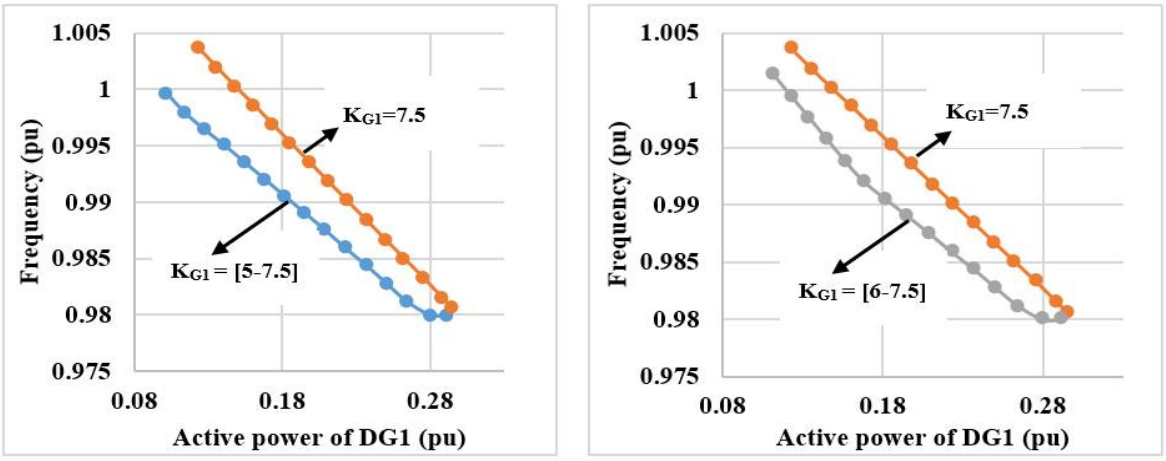

(a) (b)

Figure 3.8. P-f relation curves (**a**) P-f relation of DG_1 with K_{G1} selected optimally in the range [5–7.5]; (**b**) P-f relation of DG_1 with K_{G1} selected optimally in the range [6–7.5];

The active power P_{G1} of the generator DG_1, the power losses Ploss and the frequency f as function of K_{G1} are listed in Table 3.2. The detail of results are shown in Appendix I.

Table 3.2. New operating points of DG_1 droop curve in the three scenarios.

	Initial Load		**Scenario 1**				**Scenario 2**				**Scenario 3**			
	P_{L3}	P_{L4}	K_{G1}	P_{G1}	**Ploss**	f	K_{G1}	P_{G1}	**Ploss**	f	K_{G1}	P_{G1}	**Ploss**	f
1	0.1	0.1	7.5	0.1233	0.0049	1.0036	5.01	0.1022	0.0045	0.9996	6.01	0.1118	0.0046	1.0014
2	0.12	0.1	7.5	0.1357	0.0058	1.0019	5.18	0.1144	0.0055	0.9979	6.00	0.123	0.0056	0.9995
3	0.14	0.1	7.5	0.1482	0.0069	1.0002	5.42	0.1279	0.0066	0.9964	6.00	0.1343	0.0067	0.9976
4	0.16	0.1	7.5	0.1607	0.0082	0.9986	5.66	0.1414	0.0079	0.995	5.99	0.1456	0.0080	0.9957
5	0.18	0.1	7.5	0.1732	0.0096	0.9969	5.85	0.1550	0.0093	0.9935	5.99	0.1569	0.0094	0.9938
6	0.2	0.1	7.5	0.1858	0.0112	0.9952	6.02	0.1686	0.0110	0.992	6.02	0.1685	0.0110	0.992
7	0.22	0.1	7.5	0.1985	0.0129	0.9935	6.17	0.1821	0.0127	0.9905	6.17	0.1821	0.0127	0.9905
8	0.24	0.1	7.5	0.2112	0.0147	0.9918	6.32	0.1958	0.0146	0.989	6.32	0.1958	0.0146	0.989
9	0.26	0.1	7.5	0.2239	0.0168	0.9901	6.44	0.2094	0.0167	0.9875	6.44	0.2094	0.0167	0.9875
10	0.28	0.1	7.5	0.2368	0.019	0.9884	6.54	0.2231	0.0189	0.9859	6.55	0.2232	0.0189	0.9859
11	0.3	0.1	7.5	0.2496	0.0214	0.9867	6.65	0.2369	0.0213	0.9844	6.65	0.2369	0.0213	0.9844
12	0.32	0.1	7.5	0.2626	0.0239	0.985	6.74	0.2507	0.0238	0.9828	6.74	0.2506	0.0238	0.9828
13	0.34	0.1	7.5	0.2755	0.0266	0.9833	6.82	0.2645	0.0265	0.9812	6.82	0.2645	0.0265	0.9812
14	0.36	0.1	7.5	0.2886	0.0295	0.9815	7.01	0.2805	0.0295	0.98	7.01	0.2803	0.0295	0.98
15	0.37	0.1	7.5	0.2952	0.0311	0.9806	7.29	0.2918	0.0311	0.98	7.29	0.2918	0.0311	0.98

3.6. Discussion

In the previous Figure 3.7, the underlying droop curve is a piecewise line that is composed by a set of 15 optimal operating points at different load demand conditions. With a different adjustment range of frequency coefficient, a different shape of the P–f curve is constructed. In order to figure out this set of optimized operating point, the program has to collect the information of power grid topology, load demands and power capacity of distributed generators, so for every specific microgrid, an unique droop control relation will be considered. In Table 3.2, it can be noticed that the scenario 2 with K_{G1} in the range [5–7.5] gives the best results in terms of power losses reduction with respect to scenario 1. Indeed, power losses are reduced of about 8% as compared to the conventional droop control method ((0.0049-0.0045)*100/0.0049=8,16%). The improvement is illustrated clearly at low power demand where the power sharing is needed to be adjusted for optimizing the microgrid's operation.

The power losses in scenarios 2 and 3 are quite similar, but the variation of the adjustment range for the frequency coefficient leads to the variation of the power sharing between the generators and other parameters of islanded microgrid as shown in Figure 3.9.

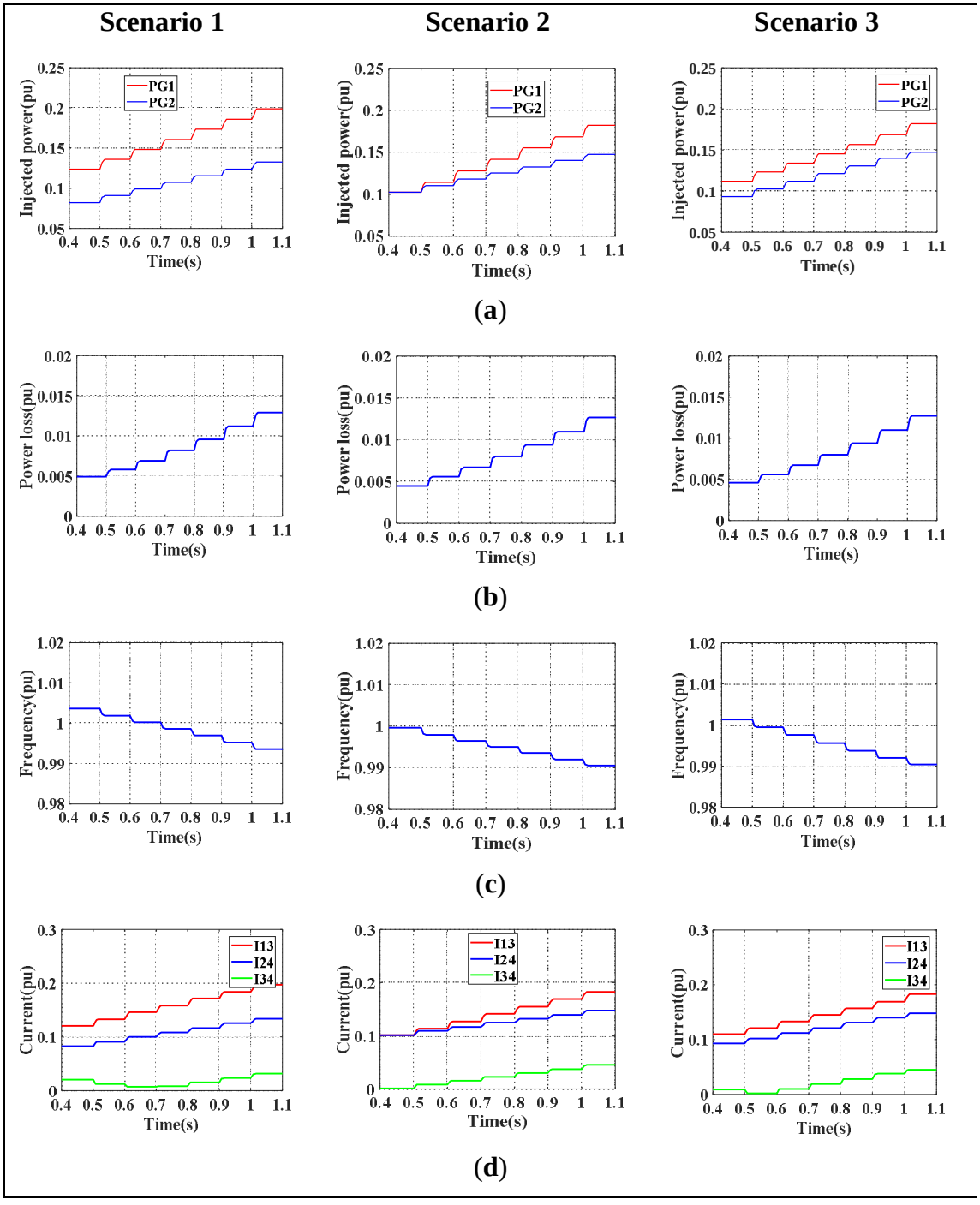

Figure 3.9. Simulation results: (a) Real power of the distributed generators in the three scenarios; (b) Power losses of the microgrid in the three scenarios; (c) System frequency in the three scenarios; (d) Current of branches in the three scenarios.

Figure 3.9.a shows the power sharing between the two DGs in the three scenarios. The wider range of droop coefficients, the greater adjustability of the

generators, this explains why the power output of the distributed generators in the three cases is different. As a consequence, the frequency of the islanded microgrid is improved in each of scenario. With K_{G1} constant at 7.5 (scenario 1), the frequency fluctuates from 0.9918 pu to 1.0036 pu, while with K_{G1} in the range from 6 to 7.5, the frequency changes from 0.989 to 1.0014 and with K_{G1} varying in the range from 5 to 7.5, the frequency only changes from 0.989 to 0.9996. In all cases, the frequency stay within the constrained operating limits from 0.98 pu to 1.02 pu. Figure 3.9.c shows that the frequency response is smooth: system frequency fluctuates within the imposed limits from 0.992 pu to 0.998 pu, without abnormal peaks or nadir. This trend demonstrates the stability of the proposed control method.

The values of the currents in the microgrid branches are shown in Figures 3.9.d. The change in power sharing leads to the current flowing in transmission lines also changes. It observed that all values are smaller than the related limit $I_{maxbranch}$.

From the results, it can be seen that the new proposed droop control method demonstrates its powerful efficiency compared to conventional droop method, the microgrid operates more effectively at every load variation. By this way, the frequency is kept within desired limits and the volumes are relieved for secondary and tertiary regulation which have to take over from primary control, if limited load-generators variations occur in the microgrid. Thus the optimized droop coefficients are calculated independently based on optimal power flow process, this approach can be applied efficiently and flexibly even when the P-f and Q-V are not directly coupled in distribution grid.

3.7. Conclusions

This chapter presented an improved droop regulation methodology for islanded microgrids. In the new methodology, solving an OPF problem, new feasible and optimized set points for distributed generators are found to minimize the microgrid operation losses and satisfy the grid and generators constraints. In this way, the frequency is kept within the desired limits and the energy volumes are relieved for secondary and tertiary regulation purposes. The GSO algorithm is selected to solve

the OPF problem, for its ability of looking for global optimization and its fast convergence rate.

A case study was implemented for demonstrating the effectiveness of the proposed method in different loading conditions and a Matlab/Simulink model was built for testing the operating characteristics of the system. The achieved results were compared to those obtained with the conventional droop regulation. It was shown that, when a load variation occurs, the proposed droop regulation adjusts the droop coefficients, minimizes the power losses, and maximizes the efficiency of power sharing between distributed generators.

The optimization procedure, that currently considers only the minimization of the microgrid's power losses, can be modified in order to generate new droop regulation curves for larger systems, and to minimize also the microgrid's operating cost. Moreover, the new regulation method can be applied to battery storage systems since they are currently showing their potential to enhance system stability in grid-connected and in islanded microgrids.

CHAPTER IV

DRIVEN P-f AND Q-V PRIMARY REGULATION FOR MINIMUM POWER LOSSES OPERATION IN ISLANDED MICROGRIDS

4.1. Introduction

In chapter III, an improved droop regulation methodology in P-f curve for islanded microgrids has been presented to enhance the overall efficiency of the microgrid while preserving its stability. In this chapter, an improved droop control with changing droop coefficients, both in P-f and in Q-V curves, is proposed as an improved primary regulation driven by minimum losses OPF.

Distributed generation inverters are generally operated in parallel with P-f/Q-V and P-V/Q-f droop control strategies. Due to mismatched resistive and inductive line impedance, power sharing and output voltage of the parallel DG inverters deviate from the reference value. This leads to instability in the microgrid system. Adding virtual resistors and virtual inductors in the control loop of droop controllers improve the power sharing and stability of operation. But, this leads to voltage drop. Therefore, an improved P-f/Q-V and P-V/Q-f droop control is proposed. Simulation results demonstrate that the proposed control and the selection of parameters enhance the output voltage of inverters. By this way, not only frequency but also voltage is regulated at primary level. With the networks considered to be lossy, its operation principle and control method are explained. Simulation results of a 9-node 3-inverter system that the proposed control and the selection of parameters enhance the output voltage of inverters are then presented to validate the effectiveness of the proposed control method.

4.2. The P-f and Q-V droop control for minimum power losses operation

Consider a microgrid system with i DG units connected to the loads through resistive-inductive lines. With conventional linear droop control, the frequency and

voltage primary adjustment of DGs can be implemented by linear droop control technique as already outlined in chapter 2 equations (4.1) and (4.2):

$$P_{Gi} = - K_{Gi} (f – f_{0i}) \quad (4.1)$$

Where K_{Gi} is the frequency droop coefficient chosen based on active rating of DGs; f_{0i} is rated frequency.

$$Q_{Gi} = - K_{di} (|V_i| – V_{0i}) \quad (4.2)$$

Where K_{di} is voltage droop coefficients, chosen based on the reactive rating of DGs; V_{0i} is rated voltage.

In linear droop control, the values of K_{Gi} and K_{di} are usually constant and equal to the maximum value. K_{Gmaxi} and K_{dmaxi} can be determined as shown in equations (4.3) and (4):

$$K_{G\max i} = \frac{P_{G\max i}}{f_{0i} - f_{\min}} \quad (4.3)$$

Where: P_{Gmaxi} is the maximum generated active power of generator i, f_{min} is minimum acceptable frequency,

$$K_{d\max i} = \frac{Q_{G\max i}}{V_{0i} - V_{\min}} \quad (4.4)$$

Where: Q_{Gmaxi} is maximum generated reactive power of generator i, V_{min} is minimum acceptable voltage.

In this research, the already described non-linear primary regulation method employs optimized droop coefficients both in P-f and in Q-V planes. In each run, the droop parameters K_{Gi} K_{di} of generators are chosen optimally in the range [K_{Gmini}; K_{Gmaxi}] and [K_{dmini}; K_{dmaxi}], respectively.

Such as already mentioned in Chapter 3, this droop control method could be implemented in a system which includes fast response generators like wind generators, PV systems which have fast response storage. The works in [82], [83]

prove that the droop parameters of generators can be adjusted. The different K_G and K_d values should be chosen under different generated output power. In this case, different droop relations are needed for the resynchronization with the grid in different operating conditions.

The OPF, for each loading condition, outputs a minimum loss operating state. The latter is an expanded state comprising system's frequency and the droop parameters. The OPF underlying the identification of the piecewise linear droop law is expressed as shown in [84].

The formulation of the problem here and in the preceding chapter must use same symbols and same equations and here you also need to recall it.

The active power and reactive power injected at bus i can be expressed as follows:

$$P_i = \sum_{i=1}^{n_{\text{bus}}} \sum_{j=1}^{n_{br}} |V_i||V_j||Y_{\text{ij}}| \cos(\theta_{\text{ij}} - \delta_i + \delta_j) \tag{4.5}$$

$$Q_i = -\sum_{i=1}^{n_{\text{bus}}} \sum_{j=1}^{n_{br}} |V_i||V_j||Y_{\text{ij}}| \sin(\theta_{\text{ij}} - \delta_i + \delta_j) \tag{4.6}$$

Where:

n_{br} is the number of branches which are connected to bus i

n_{bus} is the number of buses in microgrid.

V_i, δ_i are the voltages and phase angle of the voltage at bus i; V_j, δ_j are the voltage and phase angle of the voltage at bus *j*. These values depend on K_d and K_G at droop buses;

Y_{ij} is the admittance of branch ij; θ_{ij} is the phase angle of $Y_{ij;}$

The objective function of the OPF, which is the total real power losses, can be expressed as follows:

$$P_{\text{Loss}} = \sum_{i=1}^{n_{\text{bus}}} \sum_{j=1}^{n_{br}} |V_i||V_j||Y_{\text{ij}}| \cos(\theta_{\text{ij}} - \delta_i + \delta_j) \tag{4.7}$$

Assume that the generator G1 is available to regulate droop coefficients for the n_G generators in an islanded microgrid system and to drive the contribution of each source to the overall load demand, the other generators have the fixed droop coefficients K_{Gi} and K_{di}. The objective function (6) must be subjected to following constraints:

$$\begin{cases} \sum_{i=1}^{n_G} P_{Gi} = \sum_{i=1}^{n_d} P_{Li} + P_{loss} \\ \sum_{i=1}^{n_G} Q_{Gi} = \sum_{i=1}^{n_d} Q_{Li} + Q_{loss} \\ K_{G1min} \le K_{G1} \le K_{G1max} \\ K_{d1min} \le K_{d1} \le K_{d1max} \\ f_{min} \le f \le f_{max} \\ V_{min} \le V_i \le V_{max} \end{cases} \tag{4.8}$$

The solutions were found for each loading condition is one steady state operating point with a single frequency and voltage assuming as reference bus (with zero displacement) one of the grid forming units buses. The problem is solved by a Glow-worm Swarm Optimization (GSO) method, a heuristic method [80] which has been implemented within Matlab environment and that was already described on chapter 3 section 3.3.

For example, an islanded microgrid system including 2 generators is considered. DG1 has ability to adjust droop coefficients, DG2 has fixed droop coefficients. The model of droop coefficients regulation method can be shown in the Figure 4.1.

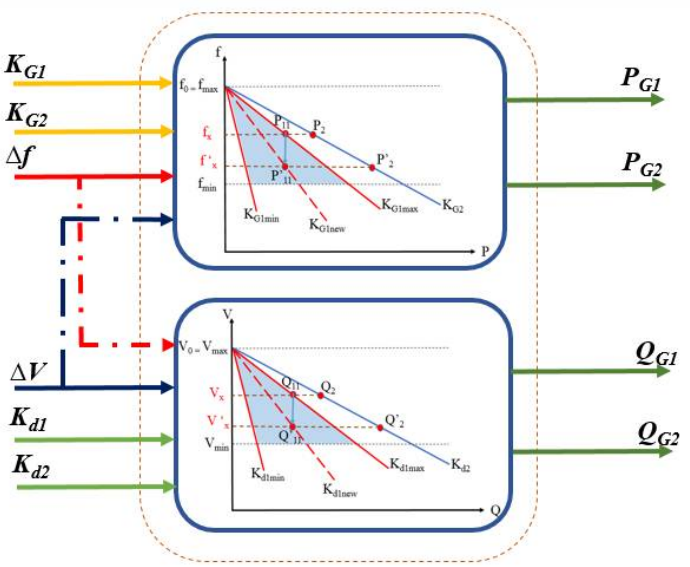

Figure. 4.1. The model of droop coefficients regulation method

The expression of droop coefficients regulation methodology for power sharing between generators can be depicted as in Figure 4.2. As depicted in the figure, each optimized operating point corresponds to a single value of V and a single value of f, thus a 3-d surface can be considered instead than a line in the planes P-f and Q-V planes.

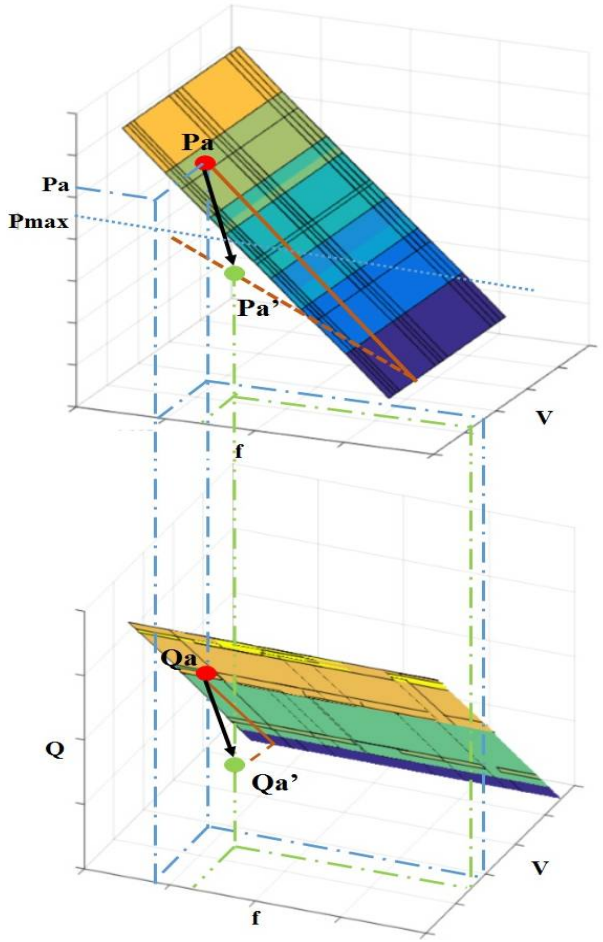

Figure.4.2. Expression of droop coefficients regulation methodology

The function of the droop control law should be monotonic to get a negative feedback in the control relations and to get the single droop value for every variation of load [85].

4.3. Application to a 9-bus system

A test system which includes 9 nodes is considered first to illustrate the effectiveness of the improved regulation methodology, see Figure. 4.3.

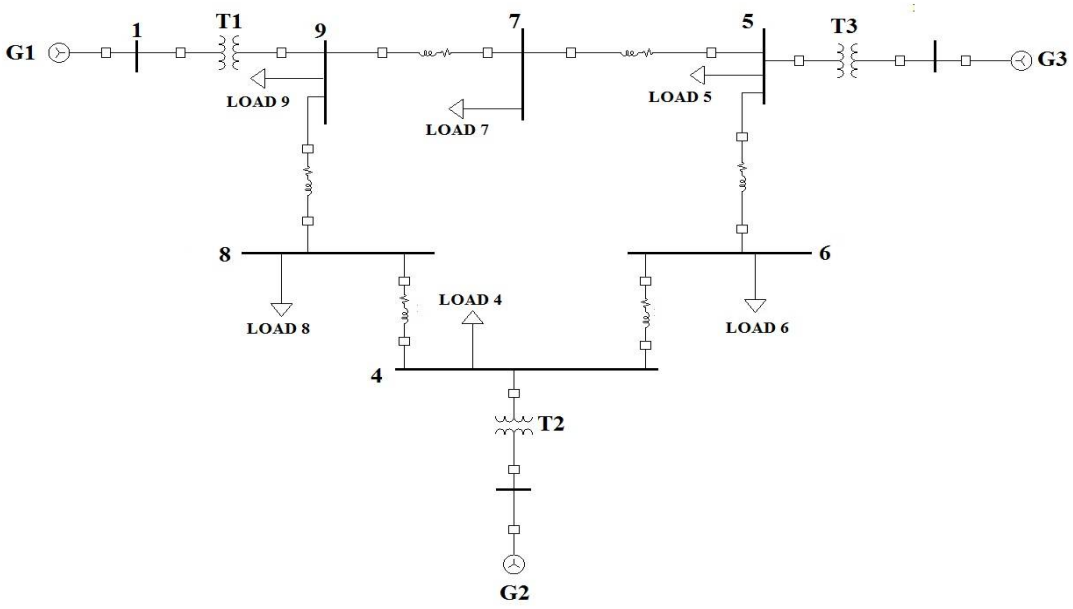

Figure. 4.3. 9-bus system.

In this network, generator DG1 has active power supply capacity that ranges between 0 and 1,2 pu, reactive power supply capacity that ranges between 0 and 0,72 pu; DG2 has active power supply capacity that ranges between 0 and 0,8 pu, reactive power supply capacity that ranges between 0 and 0,48 pu; DG3 has fixed generated power at 0,1 pu active power and 0,05 pu reactive power. The slope $K_{G2,}$ K_{d2} of DG2 is is changed to adjust the output power, K_{G2max} equals 20 and K_{d2max} equals 6; The slope $K_{G1,}$ K_{d1} of DG1 are fixed to 30 and 9, respectively.

The frequency ranges between f_{min} =0,98 pu and f_{max}=1,02 pu, namely within +/-1Hz of 50Hz; f_0 of DG1 and DG2 is set to 1,02 pu. The voltage ranges between V_{min} =0,96 pu and f_{max}=1,04 pu; V_0 of DG1 and DG2 is set to 1,04 pu.

The electric features of transmission line in the 9-bus system is shown in the following Table 4.1.

Table 4.1. The electric feature of transmission line in 9-bus system in pu

From	To	R(pu)	X(pu)	Transformer tap
1	9	0,000	0,089	1
2	4	0,000	0,089	1
9	8	0,032	0,161	1
9	7	0,059	0,170	1
5	7	0,032	0,161	1
5	3	0,000	0,089	1
6	4	0,039	0,170	1
8	4	0,032	0,161	1
5	6	0,032	0,161	1

To emphasize the effectiveness of the regulation method for power sharing between the two generators DG1 and DG2, assume that the largest load in the network varies, this is located at bus 9, and assume that the loads at the other buses does not change. All considered loading conditions are shown in Table 4.2.

Table 4.2. Load changing in the system in pu

Load	All case	
	PL(pu)	QL(pu)
Load 4	0,1	0,014
Load 5	0,12	0,02
Load 6	0,12	0,02
Load 7	0.24	0,04
Load 8	0,12	0,02

Case	Load 9	
	PL(pu)	QL(pu)
1	0,640	0,174
2	0,690	0,177
3	0,740	0,180
4	0,840	0,186
5	0,94	0,188
6	1,040	0,191
7	1,190	0,200
8	1,340	0,174

At first, the conventional droop control is applied for both generators DG1 (K_{G1} = 30, K_{d1} = 9; and DG2 (K_{G2} = 20, K_{d1} = 6). Then, the proposed non-linear droop

regulation is implemented only for DG_2; K_{G2} is regulated with OPF (ranging between 12 and 20), K_{d2} is regulated with OPF (ranging between 4 and 6).

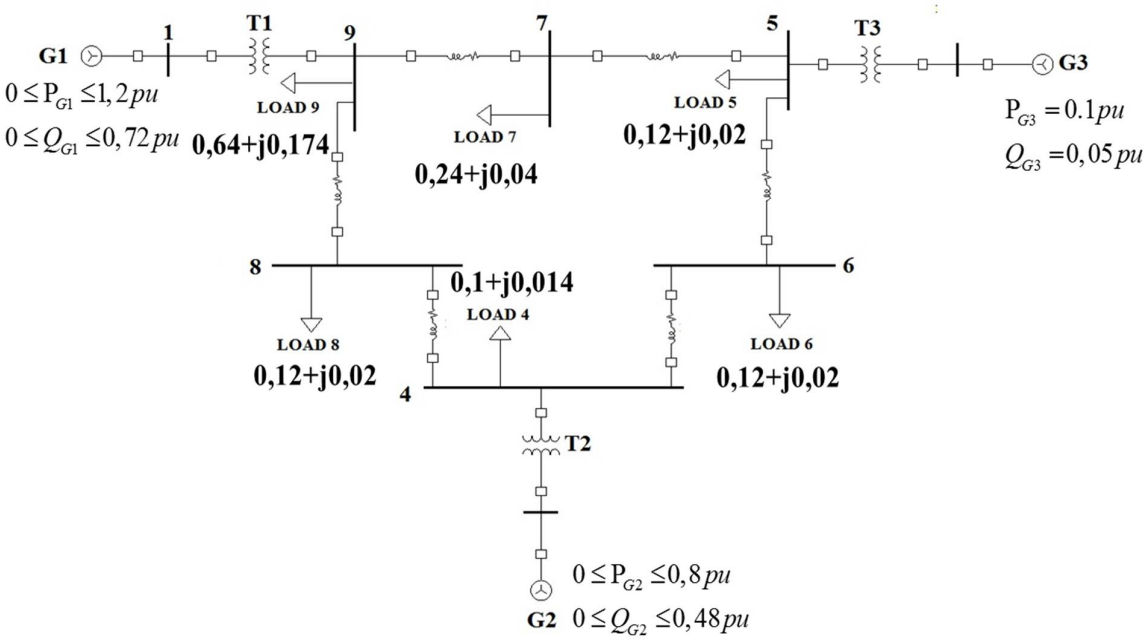

Figure. 4.4. 9-bus system

The comparison of results after calculations are in pu and are reported in Table 4.3.

Table 4.3. The results of K_G and power generated of generators in pu with linear droop regulation

Case	KG2	Kd2	PG1	PG2	QG1	QG2
1	20,0	6,0	0.7432	0.4955	0.2248	0.1111
2	20,0	6,0	0.7724	0.515	0.233	0.1138
3	20,0	6,0	0.8016	0.5344	0.2414	0.1167
4	20,0	6,0	0.8599	0.5732	0.259	0.1229
5	20,0	6,0	0.9179	0.612	0.2747	0.1286
6	20,0	6,0	0.9759	0.6506	0.2922	0.1353
7	20,0	6,0	1.0626	0.7084	0.3239	0.1483
8	20,0	6,0	1.149	0.766	0.3631	0.165

Table 4.4. The results of K_G, active power of generators, power losses and frequency in pu with new droop coefficients method

Case	KG2	Kd2	PG1	PG2	QG1	QG2
1	12.3	4.1	0.8741	0.3580	0.2377	0.1025
2	12.1	4.2	0.9108	0.3690	0.2447	0.1060
3	12.0	4.9	0.9480	0.3796	0.2483	0.1131
4	12.0	4.4	1.0162	0.4068	0.2698	0.1143
5	12.1	4.1	1.0827	0.4355	0.2881	0.1156
6	12.0	4.5	1.1507	0.4622	0.3021	0.1237
7	14.0	5.0	1.1991	0.5595	0.3278	0.1371
8	17.8	5.5	1.1995	0.7101	0.3641	0.1579

To express clearly the improvement of real power losses by using the droop coefficients regulation, the value of power losses in pu is multiplied by 100. In table 4.4, the droop coefficient KG2 is regulated in the range from 12 to 17,8 and Kd2 is in the range from 4,1 to 5,5. Therefore, the power sharing between DG1 and DG2 is regulated to increase the generated power from DG1 and decrease the generated power from DG2, the power changing of DG1 and DG2 are described in the Figure 4.5 – Figure 4.8.

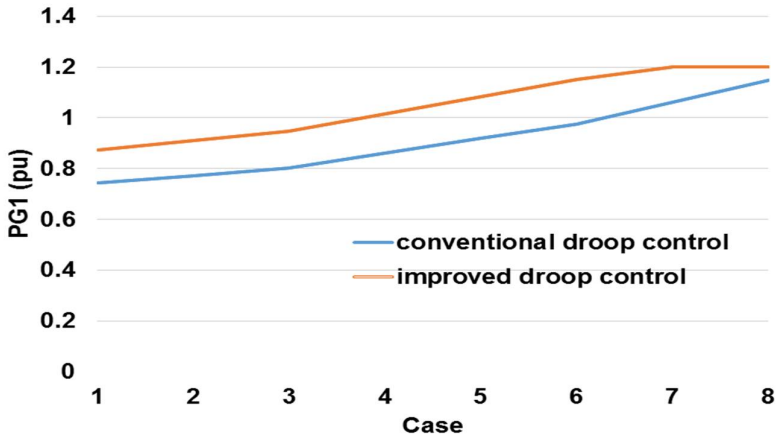

Figure. 4.5. The active power generated from DG1 with two regulation methods

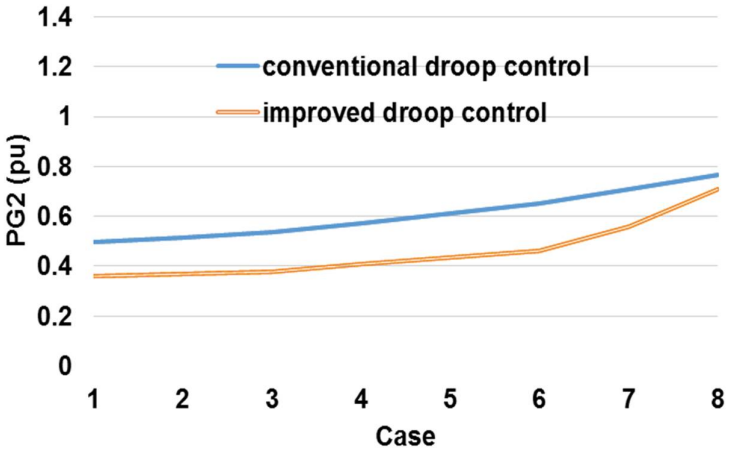

Figure. 4.6. The active power generated from DG2 with two regulation methods

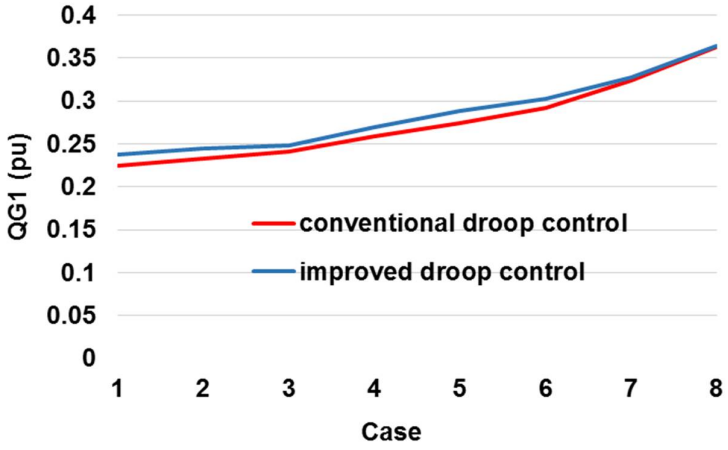

Figure. 4.7. The reactive power generated from DG1 with two regulation methods

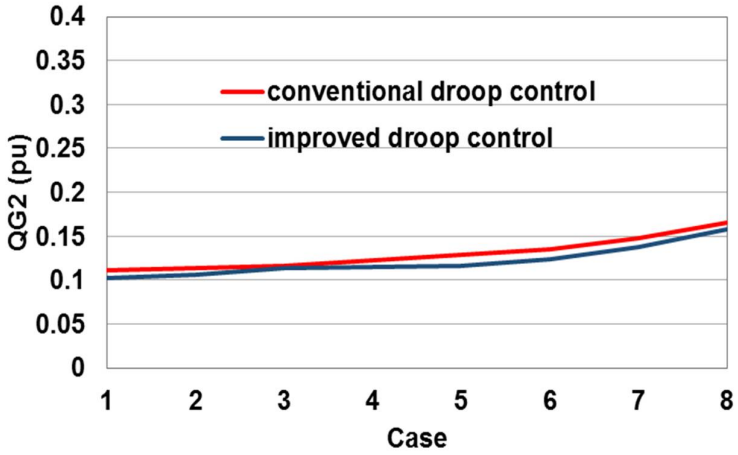

Figure. 4.8. The reactive power generated from DG2 with two regulation methods

Because the main node that needs provided energy is bus 9 which is located near the DG1 and gets the heaviest load demand,-by this power sharing regulation, the losses from DG2 to bus 9 will drop. The improvement of power losses is illustrated in Table 4.7.

Table 4.5. The improvement of Power losses

Case	Conventional droop control			Improved droop control		
	KG2	**Kd2**	**Ploss*100**	**KG2**	**Kd2**	**Ploss*100**
1	20.0	6.0	0.5125	12.3	4.1	0.4248
2	20.0	6.0	0.5396	12.1	4.2	0.4262
3	20.0	6.0	0.5704	12.0	4.9	0.4295
4	20.0	6.0	0.643	12.0	4.4	0.4399
5	20.0	6.0	0.7296	12.1	4.1	0.4582
6	20.0	6.0	0.8313	12.0	4.5	0.4842
7	20.0	6.0	1.0136	14.0	5.0	0.6313
8	20.0	6.0	1.2334	17.8	5.5	1.0348

It can be observed that the power losses were reduced a lot as compared to the conventional droop control method, of about 18%. For optimizing the regulation, it can be seen that the value of frequency and voltage is regulated to their limit at every loading condition. The most clear is case 8, where frequency changes from 0,9909 pu to 0,9800 pu, the voltage at all buses reduces slightly also and, of course, all values are in their limitation.

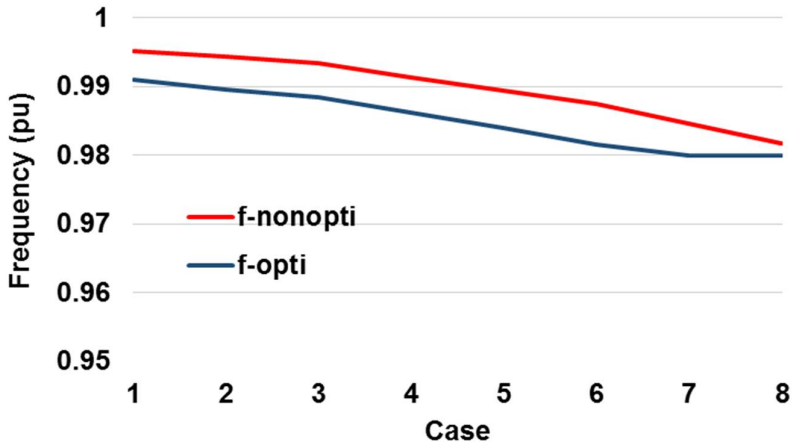

Figure. 4.9. Frequency of system with two regulation methods

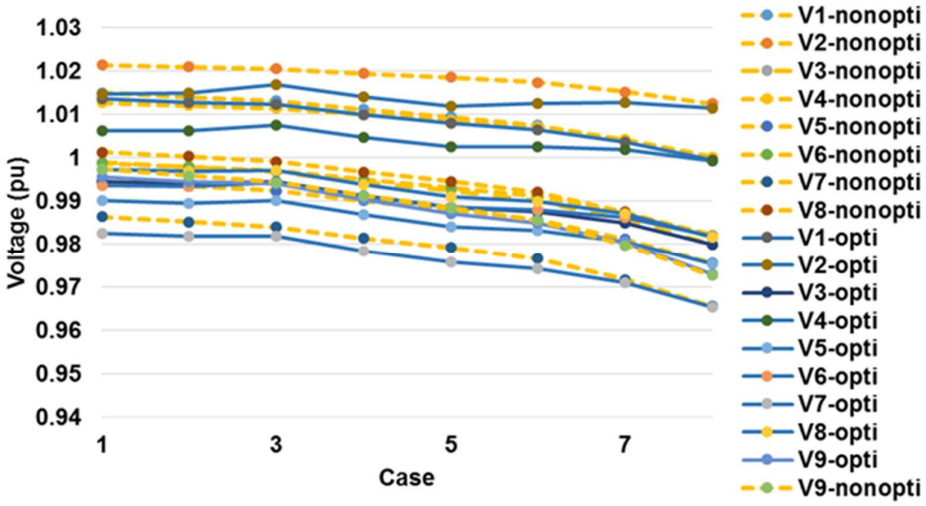

Figure. 4.10. The voltage of buses with two regulation methods

Figures 4.9 and 4.10 show that voltage is improved at all buses, while frequency stays within the limitation. The detail of results are shown in Appendix I.

4.4. Conclusion

In this chapter, an improved droop regulation method has been proposed for inverter interfaced units in islanded microgrids with ability to satisfy the voltage and frequency constraints. The results have been compared with conventional droop control to prove the effectiveness.

CHAPTER V

DRIVEN PRIMARY REGULATION FOR MINIMUM POWER COSTS IN ISLANDED MICROGRIDS

5.1. Introduction

In this chapter, differently from the preceding chapters, the issue of cost minimization is considered. The problem formulation considers operational costs of generation units to manage and control islanded micro-grids. In order to achieve the desired results, two approaches are compared. On one hand a 2 levels approach is considered for technically feasible cost optimization OPF, on the other a one level approach optimizing at the same time costs and technical feasibility is considered. These two approaches have different calculation methodologies but have the same objective function namely minimizing the operation cost while ensuring technical requirements for islanded microgrid. A test for a PV-Storage-Microturbine islanded micro-grid has been considered to compare results of the two approaches.

5.2. The two levels approach

The detail of two levels architecture has been shown in [86]. The architecture includes two different sub-levels: the energy management (EM) and optimal power flow (OPF). The organization of the new layer is shown in Figure. 5.1 below [5]:

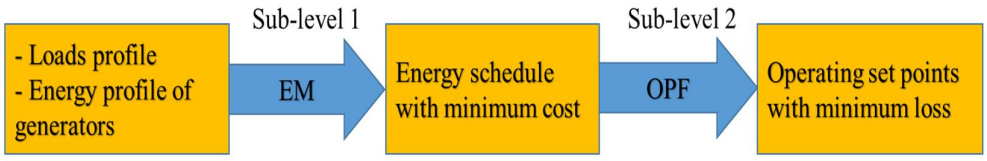

Figure. 5.1. Control levels for microgrids.

The first sub-level provides a feasible and minimum cost operating point which are subjected to constraints about energy balance between loads and generation and the constraints on the power supplied by different kinds of generators. To solve

problem in this sub-level, the Mixed Integer Linear Programming is used, the model is implemented in The General Algebraic Modeling System (GAMS). The results of problem are the range of variation of the generation units in 24 hours.

- The second sub-level solves the optimal power flow, devising the set points of inverter-interfaced generation units and rotating machines with a minimum power loss in a point which is nearby the minimum cost optimum. The objective function must satisfy the equality constraints about the balance between generated power and total demands plus losses in the system and inequalty constraints about admissible ranges of K_G, admissible range of variation of the frequency Δf, and current in every branch below I_{branch_i}. The problem in this sub-level will be solved by using GSO method that was described in Chaper III.

5.3. Problem formulation

For this problem, the solution will provide a feasible and minimum cost operating point while satisfying the technical constraints. The objective function of the first sub-level is the cost of energy supplied by the n_G units expressed by the following equation:

$$\text{Cost} = \sum_{i=1}^{n_G} \sum_{h=1}^{n_{time}} C_i . E_{Gi}(h) \tag{5.1}$$

where

C_i is the energy cost which is supplied at each time slot h by the i-th generator units.

$E_{Gi}(h)$ is the energy which is generated by generator i at each time slot h. Numerically, this term also corresponds to the average power injected by the i-th generator into the grid at hour h.

n_G is the number of generators

n_{time} is the number of time slot.

The posed problem is subjected to hard technical constraints about power balance between loads and generators and the constraints on the power supplied by each generator at every hour h that can range between a minimum and a maximum.

$$\sum_{j=1}^{n_G} P_{Gj}(h) + P_{bat}(h) = \sum_{j=1}^{n_L} P_{Lj}(h) + P_{Loss}(h) \quad (5.2)$$

where:

n_L is the number of loads in the system

$P_{bat}(h)$ is the power injected/released by storage system at hour h

$P_L(h)$ is the power supplied to the load at hour h

$P_{Loss}(h)$ is the estimated power losses of the system at hour h.

A. Energy sources

In the considered modeling of the system, in order to provide a reliable solution to the problem, the droop inverter interfaced generation units will provide for frequency regulation in primary regulation. It was already observed that optimizing the droop coefficients, namely varying their value, allows to better meet technical constraints [21] by adding some degree of freedom, while not affecting stability.

The power generated with droop regulation of DG units can be illustrated in equations (3) and (4):

$$P_{Gi}(h) = - K_{Gi\_h}(f(h) - f_{0i}) \quad (5.3)$$

$$Q_{Gi}(h) = - K_{di\_h}(|V_i(h)| - V_{0i}) \quad (5.4).$$

The energy provided by the i-th generator at hour h can be defined in terms of its power as:

$$E_{Gi}(h) = P_{Gi}(h)*\Delta t \quad (5.5)$$

where

K_{Gi_h}, K_{di_h} are the droop constants at hour h

f_{0i}, V_{0i} are rated values of frequency and voltage, respectively

f(h), V_i(h) are variables of frequency and voltage at bus i, at time slot h, respectively.

As a result, keeping fixed for simplicity reasons, the K_{di_h} terms (they do not affect much the operation of the system which is mostly active), the only optimization variables of the problem are the K_{Gi_h} terms.

For the generators which include storage system or battery, the power will be expressed as:

$$P_{G+bat}(h) = P_G(h) + P_{bat}(h) \quad (5.6)$$

$$P_{G+bat}(h) = -K_{G\_h}(f(h) - f_{0i}) \quad (5.7)$$

In this way, the power of storage systems also participates in the droop-control process to keep the system stability.

a. Storage system

The emergency mode of operation requires adequate control and management systems to provide a stable islanded operation or to locally exploit a service restoration procedure in the advent of a general blackout. In these situations, the additional storage capacity provide by the EV can help in the regulation of frequency and voltage and possibly supporting the service restoration procedures. The energy of storage systems and can be described in terms of their power as:

$$E_{bat}(h) = P_{bat}(h).\Delta t \quad (5.8)$$

Where P_{bat}(h) is the power of storage system at time slot h. P_{bat} will depend on the operation mode of the battery which is defined based on the difference between the generation capacity of the PV system and the demand of loads. P_{bat}(h) is positive when the storage system is discharging and negative when it is charging. The State of Charge, SoC, is a positive variable whereas the power can get negative and positive values both within defined ranges. The SoC value at time h-1 and the battery output power during the period as describe as below

$$SoC_{bat}(h) = SoC_{bat}(h-1) - P_{bat}(h) \quad (5.9)$$

Moreover, the state of charge at hour 0 and at hour 24 are imposed to be the same.

B. Power losses

At the second sub-level, the power losses of the microgrid will be minimized. The power losses of the micro-grid at time slot *h* will be calculated based on the power injected into the power grid at bus i and can be expressed as follows:

$$P_{loss}(h) = \sum_{i=1}^{n_{bus}} \sum_{j}^{n_{br}} |V_i(h)||V_j(h)||Y_{ij}|\cos(\theta_{ij} - \delta_i(h) + \delta_j(h)) \quad (5.10)$$

Where:

Y_{ij} is the admittance of branch ij

θ_{ij} is the phase angle of Y_{ij}

n_{br} is the number of branches

$V_i(h)$, $V_j(h)$, $\delta_i(h)$, $\delta_j(h)$ are the voltage and phase angles at buses i, j respectively at time slot h.

C. Variables boundaries

The above functions must satisfy inequalty constraints about admissible ranges of K_{Gi_h}, admissible range of variation of the frequency Δf, and maximum current flowing in the i-th branch at hour h, $I_{branch\_i}(h)$, as shown below:

$$K_{Gmini} \leq K_{Gi} \leq K_{Gmaxi}, \text{ i=1 to } n_{Gd} \quad (5.11)$$

$$\Delta f = f_0 - f \leq 0.02 \quad (5.12)$$

$$I_{branch\_i}(h) \leq I_{maxbranch\_i}, \text{ i=1 to } n_{br} \quad (5.13)$$

where:

K_{Gmini}, K_{Gmaxi} are the boundary values of the droop parameters, that are the only problem's variables

Δf is the operating frequency deviation

I_{branch_i} is the current of branch i-th

$I_{maxbranch\_i}$ is the maximum curent of branch i-th

n_{Gd} is the number of droop interfaced generators

n_{bus} is the number of buses in the system.

Regarding the storage system, these boundaries can be written as:

$$SoC_{\min} \le SoC_{bat}(t) \le SoC_{bat\min} \tag{5.14}$$

$$P_{bat\min} \le P_{bat}(h) \le P_{bat\max} \tag{5.15}$$

where SoC_{min} , SoC_{max}, P_{min} and P_{max} are the maximum and minimum values that the energy and power of the battery can acquire. To solve this problem, the GSO is used and the model is implemented on a Matlab platform. The elementary time interval can be 15 minutes or one hour for scheduling. In this chapter, a time slot (h) of one hour in 24 hours will be chosen to demonstrate the results of the problem.

5.4. The one level approach

The aim of problem is still to minimize Cost function (5.1) in 24 hours, under the constraints (5.2),(5.7),(5.8),(5.10),(5.11),(5.12-5.14) recalled above. In this case, the system is not optimized with reference to power losses. Load flow calculations for verifying constraints and computing the objective function are carried out as described in [21],[23]. If the system hosts only more droop inverter interfaced units, the independent variable of this problem $\mathbf{K_G}$ is a matrix as described below.

$$K_G = \begin{bmatrix} K_{G1-1}, K_{G2-1} \ldots K_{Gn_{Gd}-1} \\ K_{G1-2}, K_{G2-2} \ldots K_{Gn_{Gd}-2} \\ \ldots. \\ K_{G1-h}, K_{G2-h} \ldots K_{Gn_{Gd}-h} \end{bmatrix} \tag{5.15}$$

Although $\mathbf{K_G}$ doesn't appear in power balance equations and objective function, it influences the value of real power injections that in turn are related to the status of

the system. Such status is composed by the matrix of voltages, the matrix of displacements and the vector of frequencies.

$$V = \begin{bmatrix} V_{1-1}, V_{2-1} \ldots V_{n_{\text{bus}}-1} \\ V_{1-2}, V_{2-2} \ldots V_{n_{\text{bus}}-2} \\ \ldots. \\ V_{1-h}, V_{2-h} \ldots V_{n_{\text{bus}}-h} \end{bmatrix}; \quad (5.16)$$

$$\delta = \begin{bmatrix} \delta_{1-1}, \delta_{2-1} \ldots \delta_{n_{\text{bus}}-1} \\ \delta_{1-2}, \delta_{2-2} \ldots \delta_{n_{\text{bus}}-2} \\ \ldots. \\ \delta_{1-h}, \delta_{2-h} \ldots \delta_{n_{\text{bus}}-h} \end{bmatrix} \quad (5.17) \qquad ; \qquad f = \begin{bmatrix} f_1 \\ f_2 \\ \ldots. \\ f_h \end{bmatrix} \quad (5.18)$$

The parameters of this problem are thus C_i, K_{di_h}, f_{0i}, V_{0i} and the impedances of distribution lines Y_{bus} as well as the boundary values of the inequality constraints. The conventional methods such as Lagrange or Linear programing can't be used for the highly non-linear above problem. In this case, GSO has proved to be a good tool to solve problem, even when the load in the problem is unbalanced.

5.5. Application for 6-bus system

A test was implemented for a sample islanded micro-grid, demonstrated in Figure 5.2. System includes two microturbines (DG1 and DG3), the power supply capacities range from 10kW to 30kW. Operation cost of DG1 and DG3 is C1, 0,01€/kWh and C2, 0,013€/kWh, respectively. A solar photovoltaic generator integrated with a storage system are located at DG2, the photovoltaic plant (PV plant) has maximum power 40kWp. The charge E_0 is 20kWh, the energy capacity of battery ranges from 4kWh to 40kWh. the power capacity of battery ranges from -4kW to 8kW. The comparison results will be implemented to show the effectiveness of method.

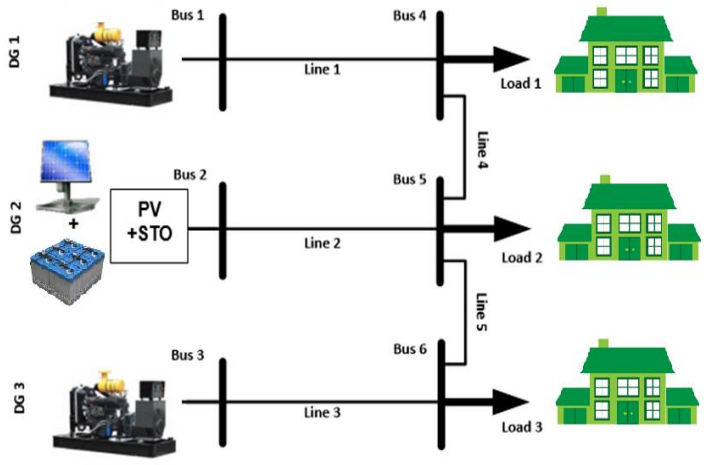

Figure.5.2. Sample micorgrid system

Table 5.1 presents rhe parameters of transmission lines

Table 5.1. The transmission line parameters of system

	Branch	**R (pu)**	**X (pu)**	**Imax (pu)**
1	4-5	0,081285	0,022662	0,4
2	4-1	0,056711	0,024943	0,5
3	5-2	0,056711	0,024943	0,5
4	5-6	0,081285	0,022662	0,4
5	6-3	0,056711	0,024943	0,5

The energy profile of PV system at DG2 is shown in the following Figure 5.3.

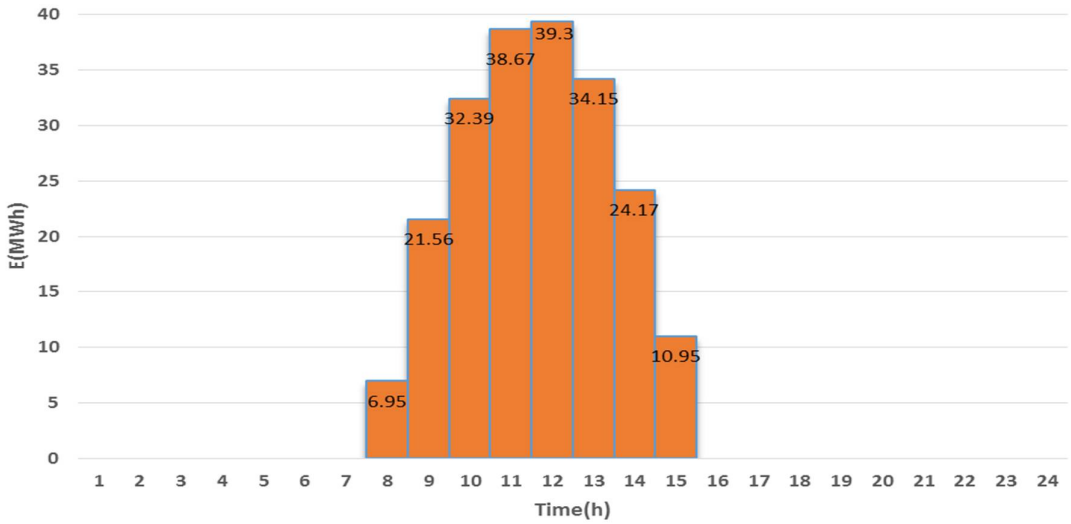

Figure. 5.3. Energy profile of PV generator

The energy profiles of load 1, load 2 and load 3 are shown in Figure 5.4.

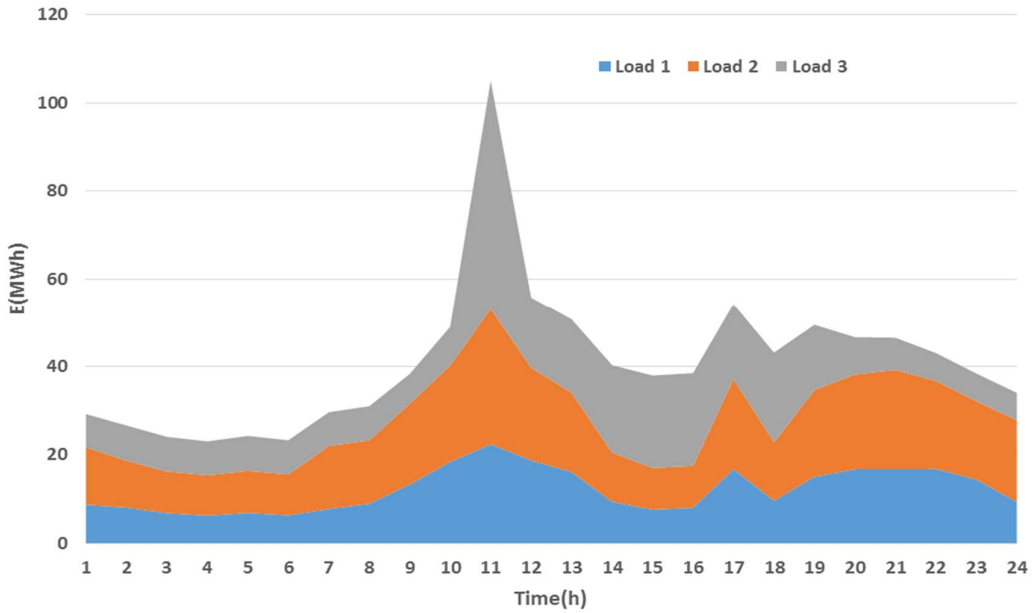

Figure. 5.4. Energy profile of loads

5.6. Results and discussion

After optimizing the production cost of the system, the scheduling of energy generated from PV system and microturbines are shown in Figure 5.5 and Figure 5.6.

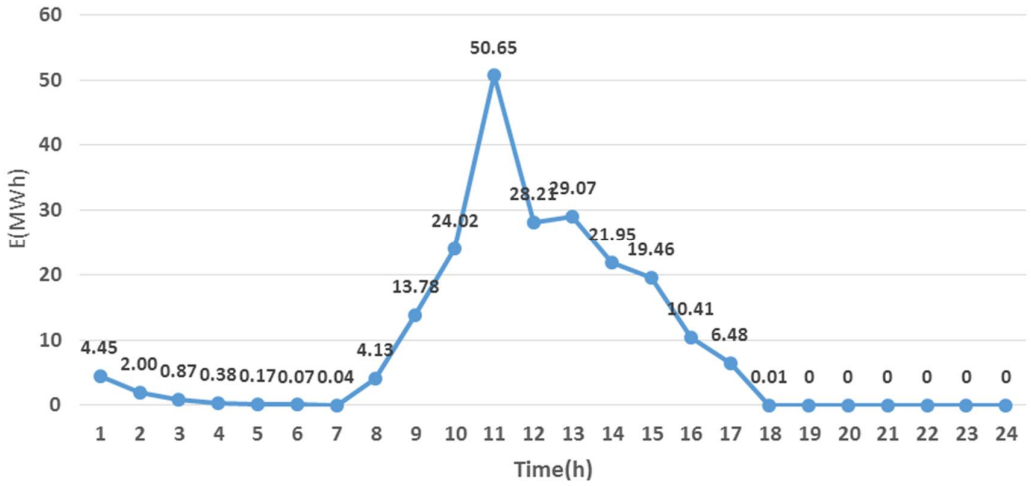

Figure. 5.5. Energy generated by PV and storage system in 24 hours

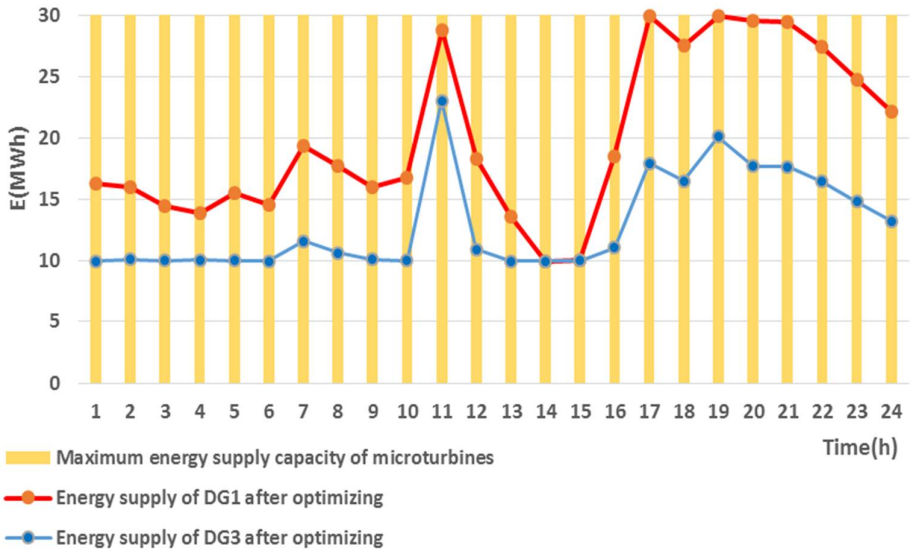

Figure. 5.6. Energy generated by microturbines in 24 hours

It appears, as expected that, the power generated by PV+storage system has been adjusted to provide energy support for microturbines. The charged or dischagred energy of storage system in every hour is maximized to reduce energy cost as well as support for system to adapt to technical restrictions. In Figure 5.6, the amount of energy generated from DG3 is less than the energy generated by DG1 because its cost is slightly higher. In the calculation process, all constraints are tested to ensure that

all conditions are within their limitation. The results are illustrated in Figure 5.7 and Figure 5.8.

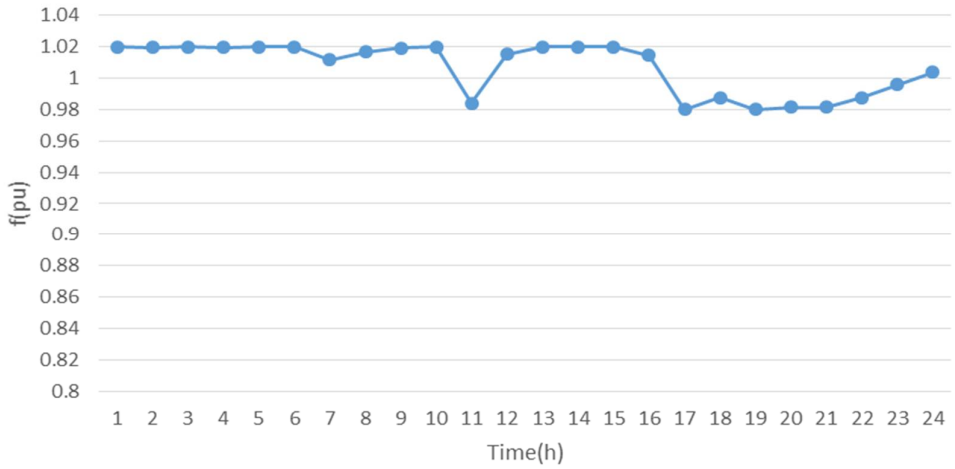

Figure. 5.7. Frequency of system

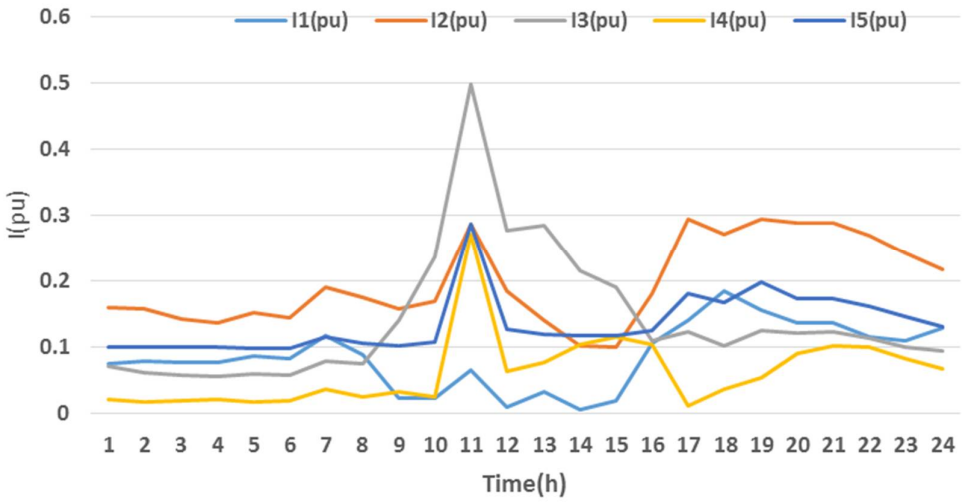

Figure. 5.8. Current of transmission lines

It can be seen that the technical constraints are satisfied. In Figure 5.7, the frequency has just changed in the limitation from 0,98 pu to 1,02 pu. At the peak load points, for instance, 11:00, 17:00, 18:00-21:00, frequency is fall down to 0,98 pu. At the low load points as 1:00-6:00, the frequency is the highest at 1,02 pu. The values of the transmission line currents are alos below the limits I_{max} and the normal

limitation for voltage stays between 0,95pu and 1,05pu. At peak point, 11:00, the maximum current is on branch 5-2 at 0,5pu.

To illustrate the feasibility of the method, the achieved operating cost is compared to the operating cost of tested system in paper [86] which was caculated using a two levels architecture.

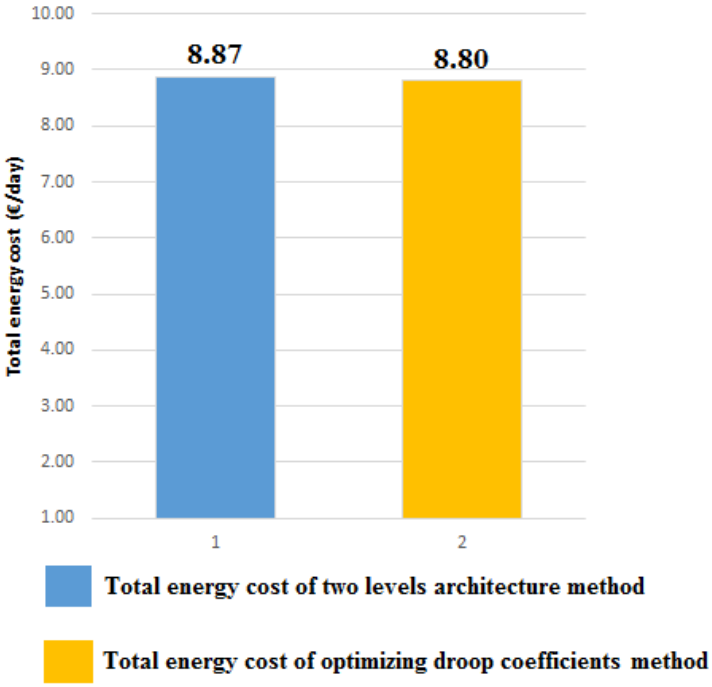

Figure. 5.9. The comparison between operating energy costs of the method proposed here and the one in [17]

The comparison of the 2 methods is shown in Figure 5.9. According to the chart, the difference of values is very small, about 0,1%. It means that the proposed method can acquire a minimum operating cost as well, thus the method is reliable and effective. The detail of results are shown in Appendix I.

5.7. Conclusion

In this approach, the GSO method was applied to keep the energy operation cost for the system to a minimum by regulating droop coefficients in a 24 hours time frame. A test was implemented on a sample 6-bus system to verify the results. The

achieved results demonstrated that this method is effective, feasible and can adapt to all technical constraints, whereas it can get a minimum operating cost.

Further studies will investigate the possibility to have different generators with different speed of response. In this case, some generators will be considered with constant output power others will be variable and will take part to the OPF because speed of response is higher and can follow loads change or sudden power generation variations. Also, a rolling horizon approach for the whole architecture needs to be considered in order to compensate possible weather changes or loads requests. Finally, the price of electricity from the PV and storage system have not been considered, although for the battery a cost can be considered due to the Dept of discharge issue and the number of operations producing a reduction of their lifetime. The demand side management programs is also considered. A rolling horizon approach can be deployed to cope with possible sudden weather variations.

CHAPTER VI

HARDWARE-IN-THE-LOOP SIMULATION DRIVEN PRIMARY REGULATION IN ISLANDED MICROGRIDS

6.1. Introduction

The basic idea in hardware-in-the-loop simulation is that of including a part of the real hardware in the simulation loop during system development. Rather than testing the control algorithm on a purely mathematical model of the system, one can use real hardware (if available) in the simulation loop. For instance, actuators are notoriously difficult to model and, if available, can be included in the simulation loop to improve the validity of the simulation. Furthermore, the testing and the evaluation of the system are carried out in real-time. This ensures that the embedded control system can deliver the control input within the desired sampled period. This is important as the lack of control signal at the end of the sample period can affect stability [87].

In this chapter, an experimental study is carried out to test operating characteristics of the system when the P-f droop coefficients change to adapt with load changing conditions in 24 hours. So the theoretical background and related simulations are reported in chapter III.

The system is modeled in real time but the time of scheduling is scaled down from hour to minutes. At first, a model of system is implemented in the RT-lab simulator to check operating parameters, then it is tested in hardware-in-the-loop simulation with participation of real PV systems to check stability of the system.

6.2. Optimization program

The optimization program is the core of test system which sets decision variables based on optimizing the objective fuction. As already widely explained in Chapter III of this thesis, an Optimal Power Flow for islanded microgrids finds at

each operating condition, namely for a new load value and/or renewable generation injection, a minimum loss operating state. The latter is an *expanded state* which includes the system's frequency and the droop parameters [84]. From the expression of the generic power injection at bus i:

$$P_{i(K_G)} = \sum_{j=1}^{n_{br}} |V_i||V_j||Y_{ij}|\cos(\theta_{ij} - \delta_i + \delta_j) \qquad (6.1)$$

In (6.1), as expressed in Chapter III, V_i and V_j are the i and j bus voltages, depending on K_d and K_G at droop buses; δ_i and δ_j are the phase angles of the i and j bus voltages, depending on K_d and K_G at droop buses; Y_{ij} is the admittance of branch ij; θ_{ij} is the phase angle of $Y_{ij;}$ n_{br} is the number of branches connected to bus i; n_{br} is the number of branches connected to bus i.

One of the main objectives of OPF is the minimization of real power loss of the system although its formulation may also consider minimum cost. Considering losses, it can be expressed as follows.

$$OF_{(K_G)} = P_{\text{Loss}} = \sum_{i=1}^{n_{\text{bus}}} P_{i(K_G)} \qquad (6.2)$$

Where n_{bus} is the number of buses in the system.

For example, considering a simple system includes 4-bus with 2 generators as expressed in the Figure 6.1.

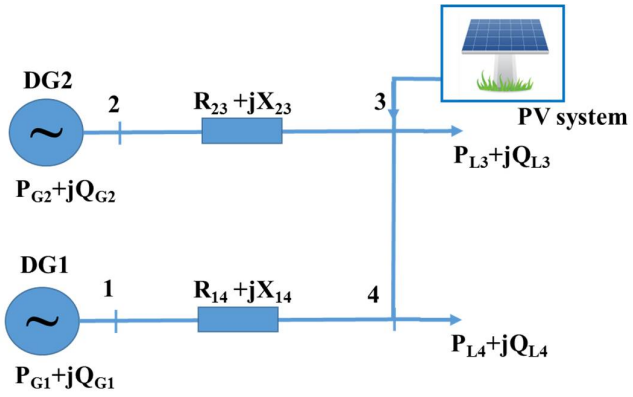

Figure. 6.1. Test system

Assume that DG2 is a generator that is able to adjust its frequency droop coefficient. The following constraints must thus hold:

$$\begin{cases} \sum_{i=1}^{n_G} P_{Gi} = \sum_{i=1}^{n_d} P_{Li} + P_{loss} \\ K_{G2min} \le K_{G2} \le K_{G2max} \\ P_{Gimin} \le P_{Gi} \le P_{Gimax}, \\ i = 2 \div n_G \\ f_{min} \le f \le f_{max} \\ V_{min} \le V \le V_{max} \end{cases} \tag{6.3}$$

Where the n_G is the number of generators in the microgrid, n_d is the number of load buses. For further details about the problem formulation, please refer to Chapter III of this work.

6.3. Communication structure

In the experiments, the approach is slightly different from the one described in chapters III, IV and V. Here the droop curve was changed on-line as the OPF was running in times that were compatible with the operation.

In this way, at every time step, the optimization controller was producing a new operating point described by the droop constant K_{G1} thus improving the power losses in the system. The only adjustable parameter producing a new power sharing among generators is here taken as K_{G2}.

At first, the linear droop control is applied to both generators. Then, with the new regulation method, some experiments are implemented with different values of K_{G2} obtained from the resolution of the OPF. The communication network is shown in the Figure 6.2. The program to find K_{G2} for minimizing power losses of the system is run in the Optimization controller block and then the value of the optimized control parameter is transferred back to the power network model. In these experiments, K_{G1} is kept fixed at 8.75. The range of variation of K_{G2} was taken as large as possible in its range.

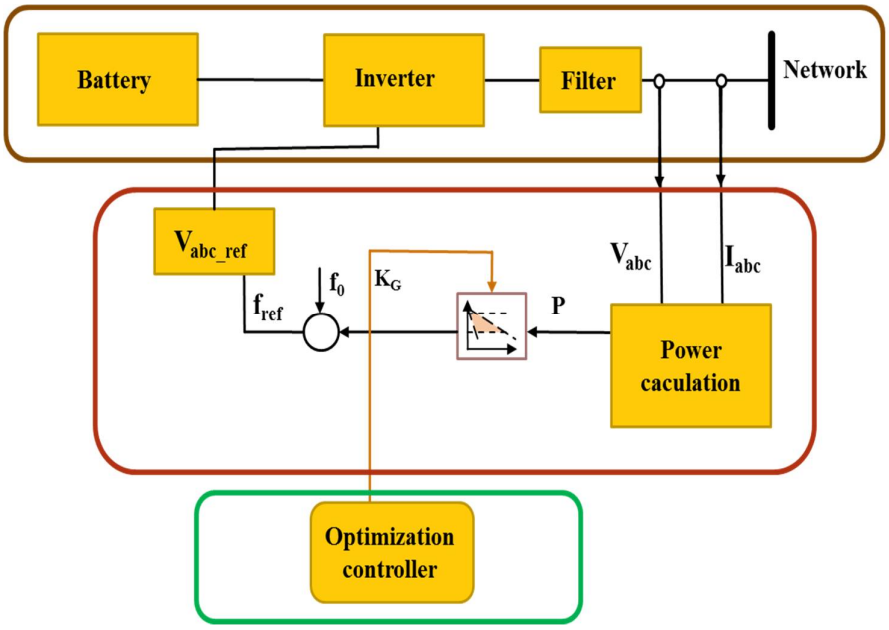

Figure. 6.2. Communication Network

The computer information using for simulation is shown as below:

Window edition: Windows 7 Professional. Copyright 2009 Microsoft Corporation. All rights reserved

System Processor: Inter® core ™ 2 Quad CPU Q9650 @ 3.00GHz (4CPUs)

Installed memory (RAM) 4.00 GB

System type 32 bits operating system

System manufacture Dell Inc

System model OptiPlex 960

BIOS Phoenix ROM BIOS PLUS version 1.10 A08

DirectX version DirectX11

The system is modelled in real time but the time of scheduling is scaled down from hour to minutes.

6.4. Case study simulation in RT lab

To analyze the effects of the controller parameters on the power sharing of generators, a simple test system is considered. At bus 1 and bus 2 two generators are connected to two set of loads at bus 3 and bus 4 and a set of PV system at bus 3, as

shown in Figure. 6.1, is considered. Before the HIL experimental test, some simulations have been carried out. These, differently from those presented in Chapter III of this work have been carried out in RT-LAB simulation environment which is immediately applicable for HIL implementation. The experiments described in this section have been implemented in a laboratory scale at the National Institute of Solar Energy (INES) in France.

The model of test system is shown in the Figure 6.3:

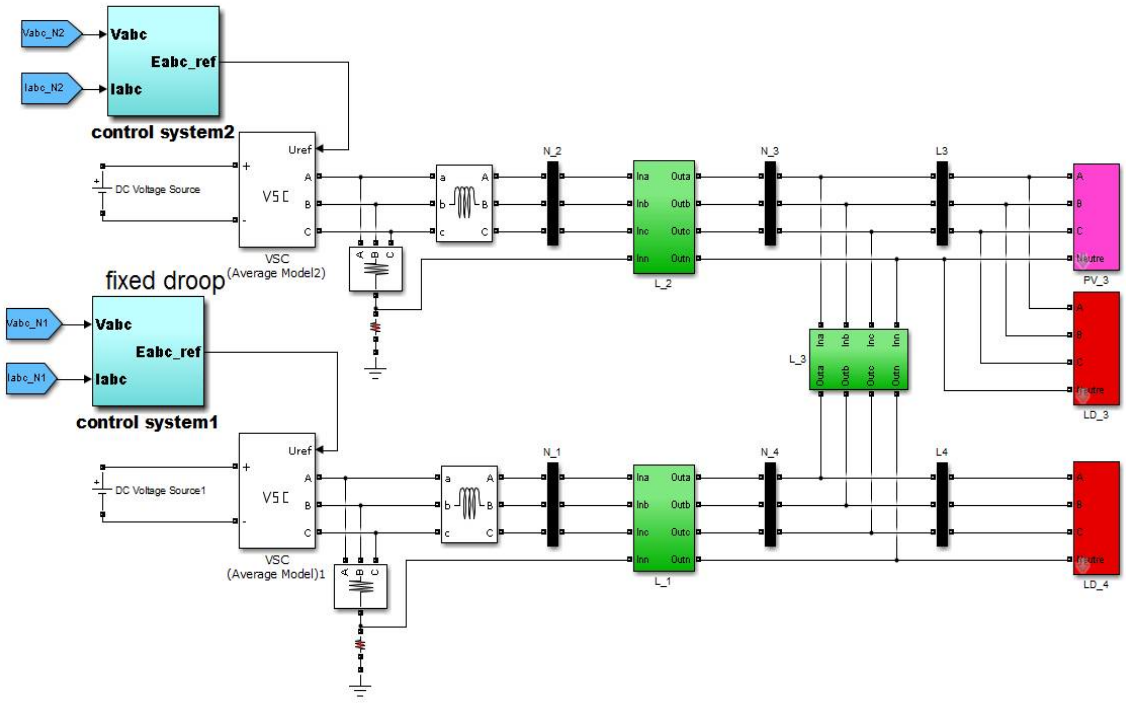

Figure. 6.3. The model of 4-bus test system in RT-lab simulator.

The generator DG1 has a power supply capacity ranging from 0 to 0,35 pu, DG2 has power supply capacity ranging from 0 to 0,45 pu. In this case, the slope KG2 of DG2 will be changed in the range to adjust the output power. The constraint for frequency in the system is set to fmin = 0,98 pu and fmax= 1,02 pu, meaning that the frequency must be within +/-1Hz of 50Hz. The frequency f0 of DG1 and DG2 is set the same and equal to 1,02 pu. The electric features of transmission lines in the 4-bus system are shown in the following Table 6.1:

Table 6.1. Electric features of 4-bus system

From	To	R (Ohm/km)	X(Ohm/km)	L(km)
1	4	0.43	0.14444	0.5
2	3	0.43	0.14444	2.5
3	4	0.43	0.14444	0.5

As it appears from Figure 6.2, bus 3 is also connected to a PV generation system, whose measured production curve in a generic day is reported in Figure 6.4.

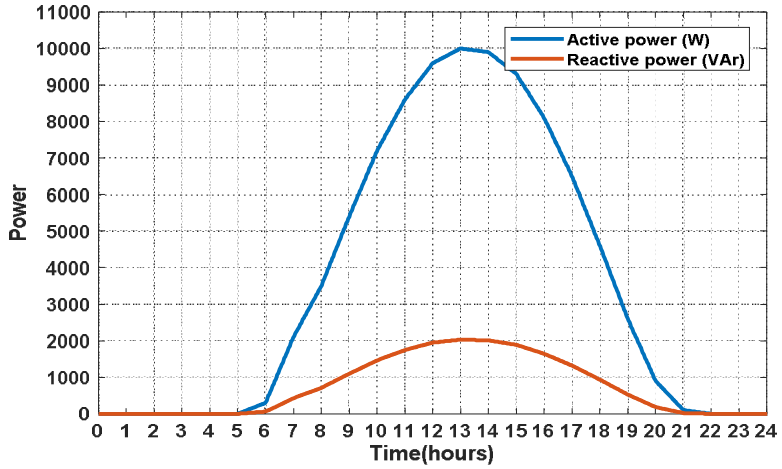

Figure. 6.4. Power profile of PV system

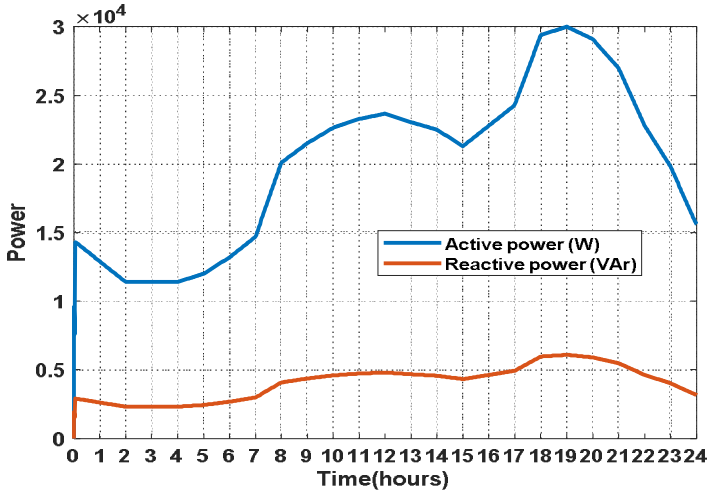

Figure. 6.5. Energy demand at load 3 in 24 hours

Figure 6.5 instead shows the assumptions made for the load consumption at bus 3. While Figure 6.6 shows real and reactive power consumptions at bus 4, which is a purely consuming node.

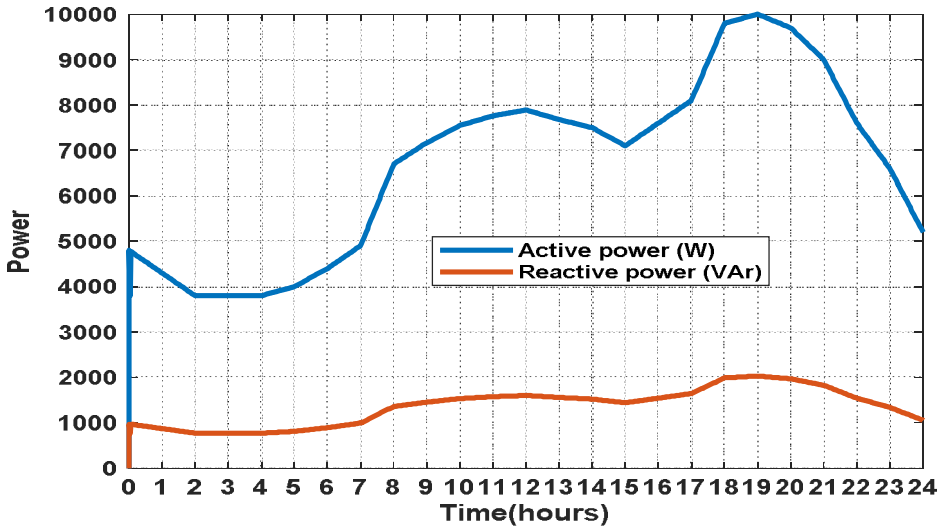

Figure 6.6. Energy demand at load 4 in 24 hours

Going to a comparison between linear droop and the new minimum losses droop, the following experiments show the effectiveness of the approach. In these experiments, in the non optimized operation, K_{G2} is set to 11.25, and K_{G1} is kept fixed to 8.75

Figure 6.7 shows a comparison in the 24 hours of the generated power at the inverted interfaced unit where the optimized droop curve is set.

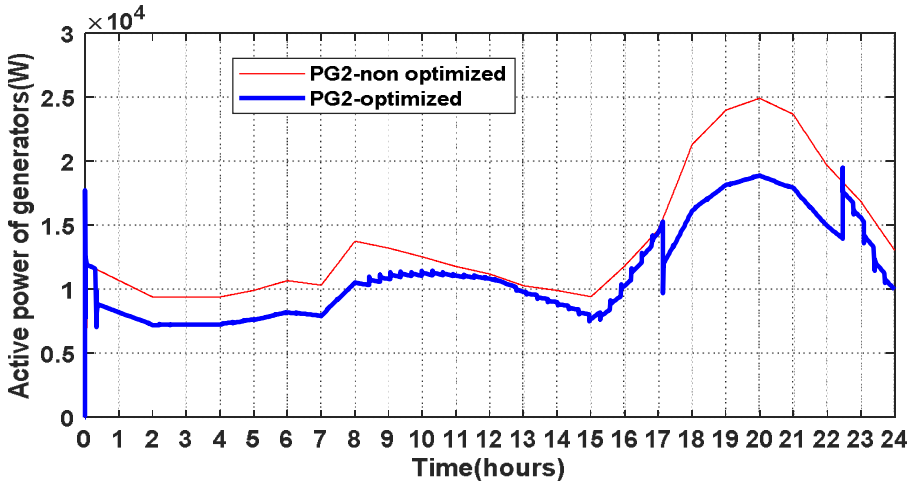

Figure 6.7. Active power of generator DG2 with and without optimized droop regulation

Figure 6.8 shows a comparison along the 24 hours of the power losses in the system considering the new droop technique and the standard droop.

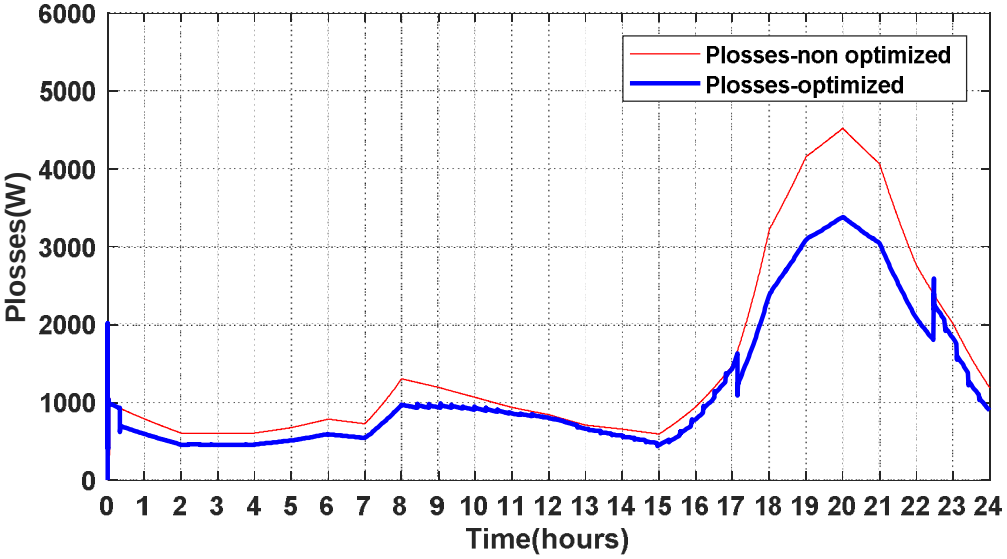

Figure 6.8. Power losses of system with and without optimized droop regulation

Figure 6.9 shows a comparison along the 24 hours of the frequency in the system considering the optimized droop technique and the standard droop.

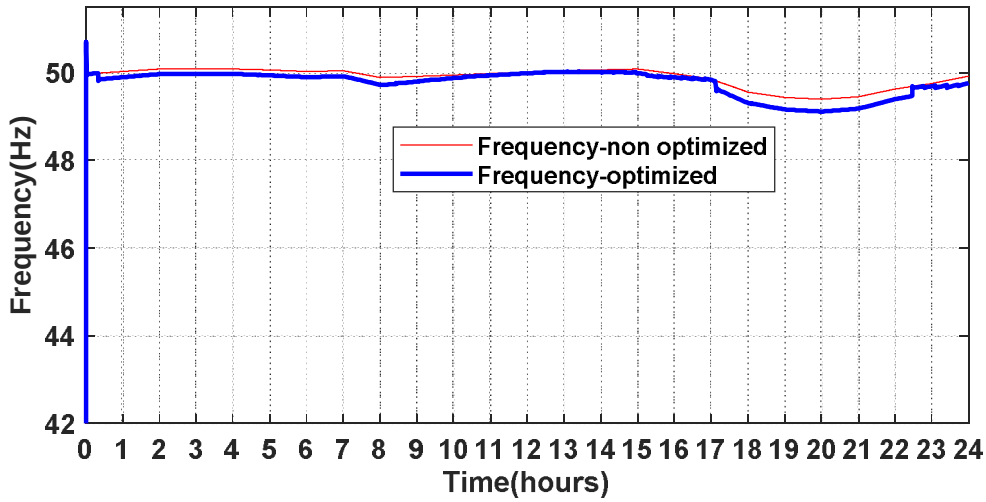

Figure 6.9. Frequency of system with and without optimized droop regulation

Finally Figure 6.10 shows the bus voltages along the 24 hours operation considering the new droop technique.

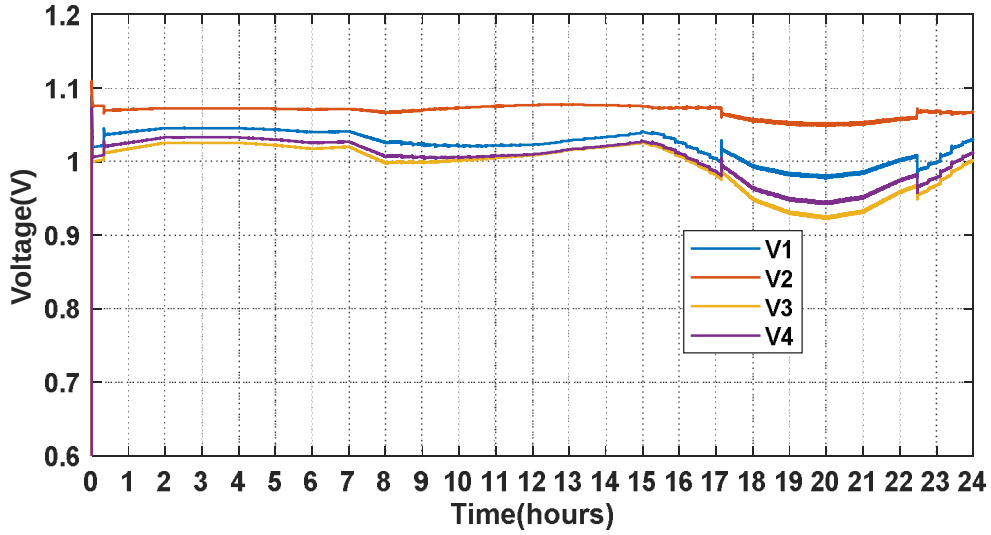

Figure 6.10. Voltage at 4 buses with optimized droop regulation

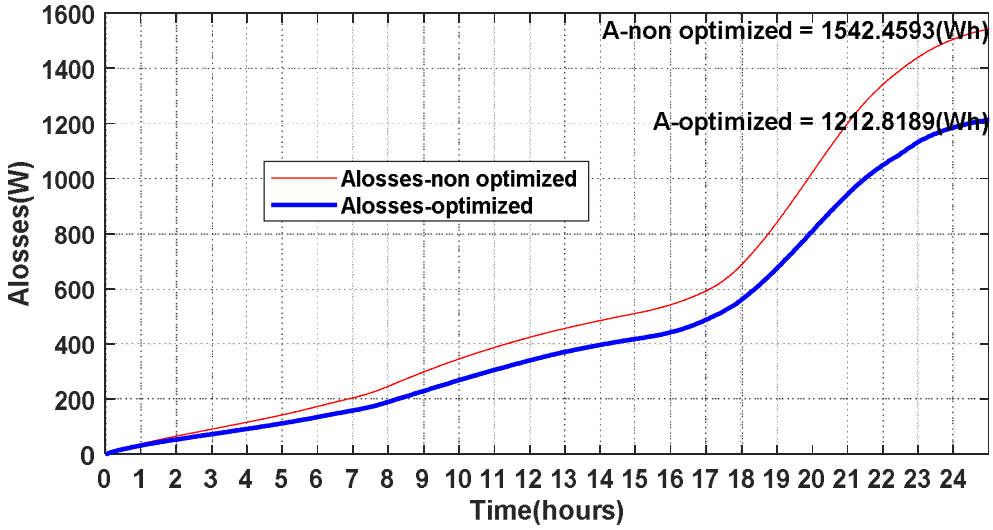

Figure 6.11. Improvement of energy losses with and without optimized droop regulation

System frequency fluctuates within the limitation, as shown in Figure 6.9, from 49.5 Hz to 50.6 Hz. The frequency response in Figure. 6.9 shows that the response of frequency is smooth. The DG2 is adjusted to inject enough power in the system in a way that minimizes power losses for the system. The energy losses illustrated in Figure. 6.11 shows that the new regulation method gives smaller losses operation as compared to conventional regulation method of about 21%.

6.5. Hardware in the loop simulation

To prove the effectiveness of the system under the optimized droop law, this study presents a laboratory hardware in the loop implementation of the test system described in Figure 8 to validate important features, such as stability. In this case, for practical reasons, a smaller system of 3 buses is simulated in RT-lab simulator to express the advantage of this new method as well as to verify the operating properties of system. The model of the 3-bus test system is expressed as in Figure 6.12.

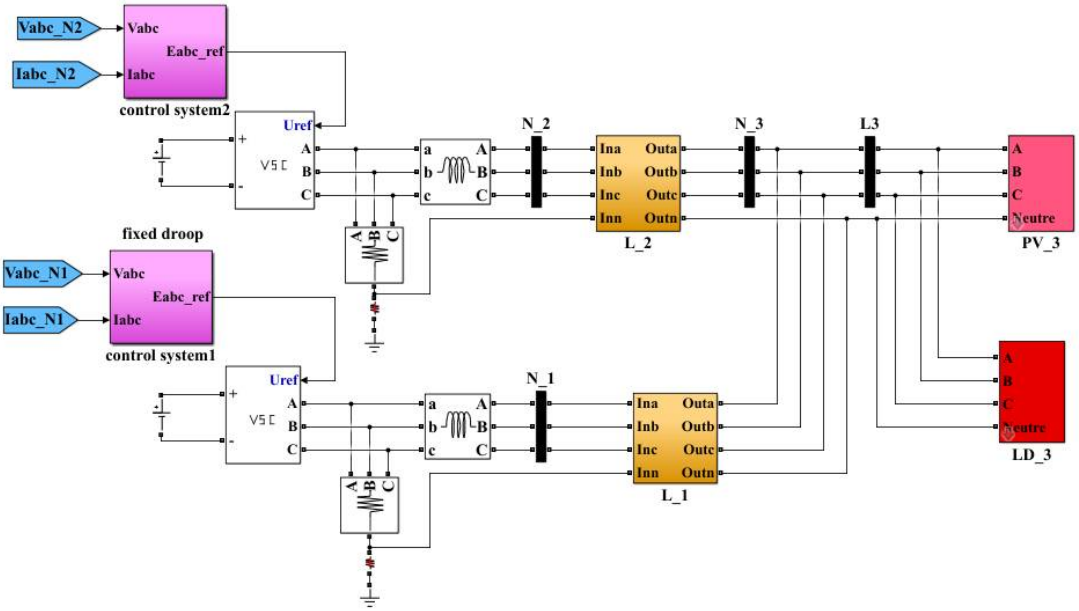

Figure 6.12. The model of 3-bus test system in RT-lab simulator

The maximum power capacity of DG1 is 35kW and maximum power capacity of DG2 is 45kW. The energy demand data set at node 3 will be simulated as a set of peak loads for hours 1 to 24 in a day. The energy profiles of these set of loads are demonstrated in the Figure 6.13. The peak hour load demand at load 3 is 30kW.

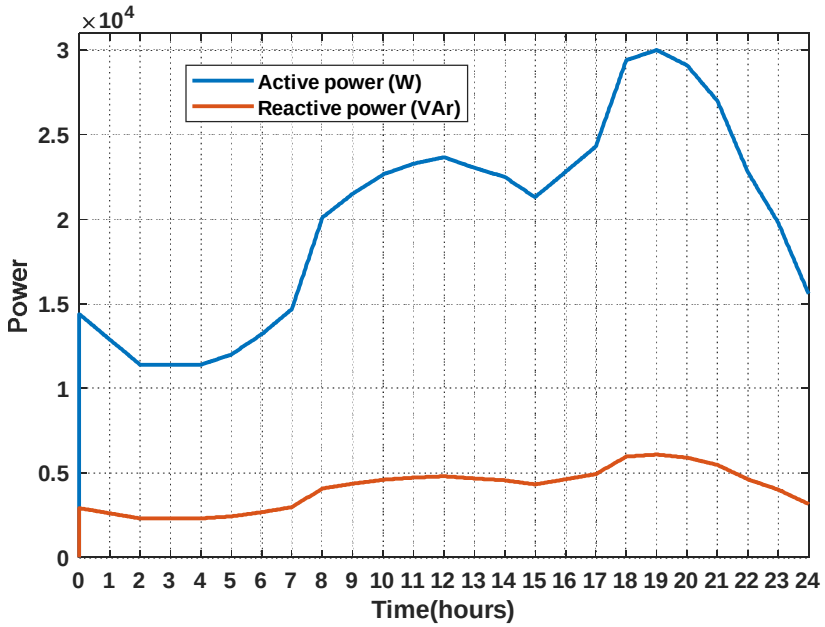

Figure 6.13. The load profile at node 3 in 24h hours

The energy profile of PV system is shown in the Figure 6.14

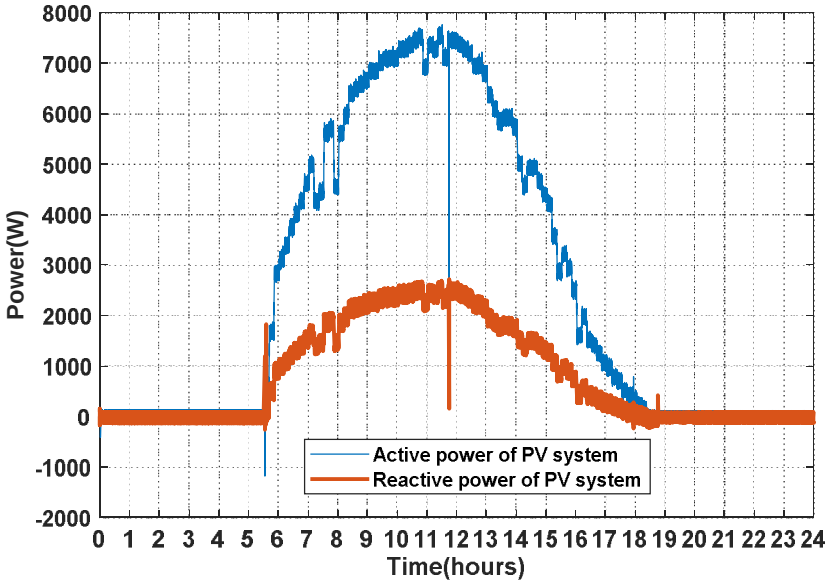

Figure 6.14. The energy profile of PV system in 24 hours

The electric features of transmission lines in the 4-bus system are shown in the following Table 6.2:

Table 6.2. Electric features of 4-bus system

From	To	R (Ohm/km)	X(Ohm/km)	L(km)
1	3	0.43	0.14444	1
2	3	0.43	0.14444	2.5

At the software level, the online driven droop regulation has been implemented in OPAL-RT simulator. In this work, OPAL-RT 5142 simulator is used. There is one host computer with a RT software installation connected with RT simulator via a Transmission Control Protocol/Internet Protocol (TCP/IP). The Optimization Program (OP) will be developed in Matlab (R2010a) environment with GSO algorithm to solve problem at another computer. This program is called by RT-lab through a tool of Matlab Script. The OP and real-time platform communicate to each others by the User Datagram Protocol (UDP) over Ethernet.The configuration of Hardware in the loop, HIL, system is expressed in Figure 6.15. The optimization OPF program run on a host computer and then control signals are transferred to the RT simulator.

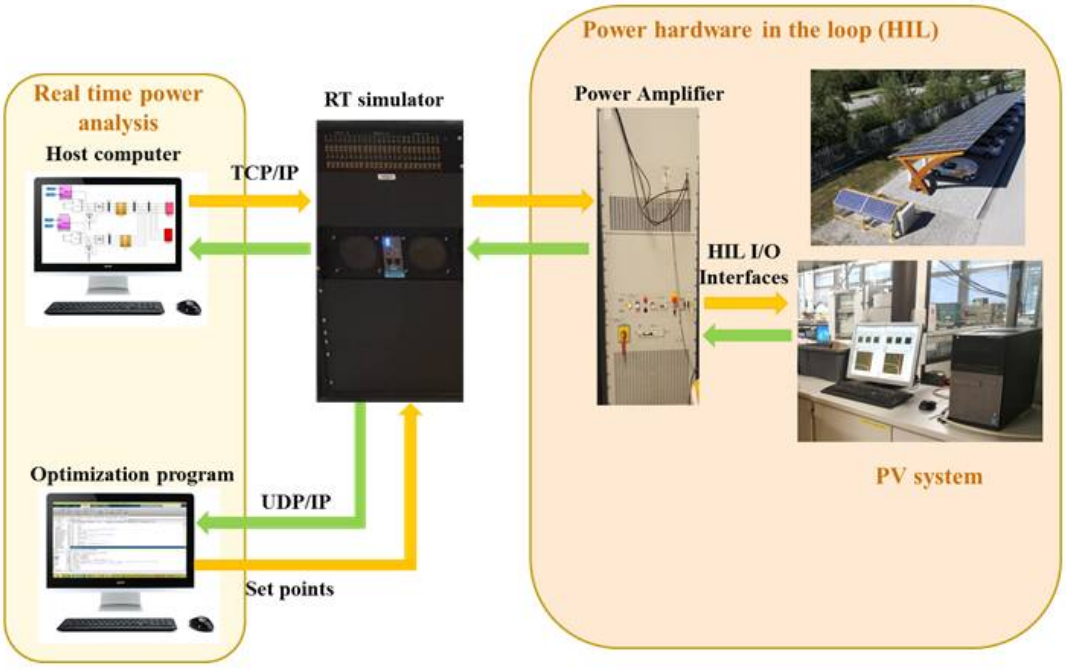

Figure 6.15. The configuration of Hardware in the loop simulation

Technical specifications of OP5142 RT-Lab are expressed as follow:

(i) Digital I/O:

Number of channels: 256 input/output configurable in 1- to 32-bit groups

Compatibility: 3.3 V

Power-on state: High impedance

(ii) Bus:

Dimensions (not including connectors): PCI-Express x1

Data transfer: 2.5 Gbit/s

(iii) FPGA:

Device: Xilinx Spartan 3

I/O Package: fg676

Embedded RAM available: 216 Kbytes

Clock: 100 MHz

Platform options: XC3S5000

Logic slices: 33,280

Equivalent logic cells: 74,880

Available I/O lines: 489

Technical specifications of the PC used for RT-Lab simulations: Microsoft Windows XP (32-bit version), Xilinx ISE design suite v10.1 with IP update 3, Xilinx System Generator for DSP v10.1, MATLAB R2007b.

6.5.1. Results simulation of transient responses

The simulation results of a transient response for a load change of every hours at bus 3 are expressed in Figure 6.16 showing the output power of generators, while frequency and the three phase voltage at the generators are described specifically in the Figures from 6.17 to figure 6.19.

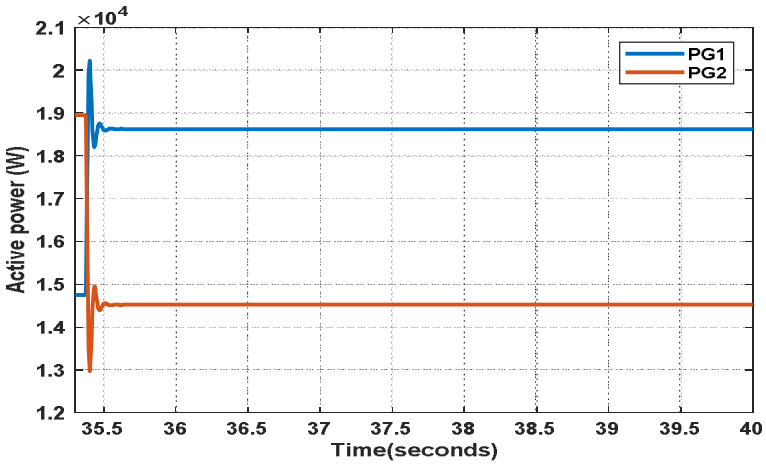

Figure 6.16. Output active power at DG1 and DG2 at nodes 1 and 2

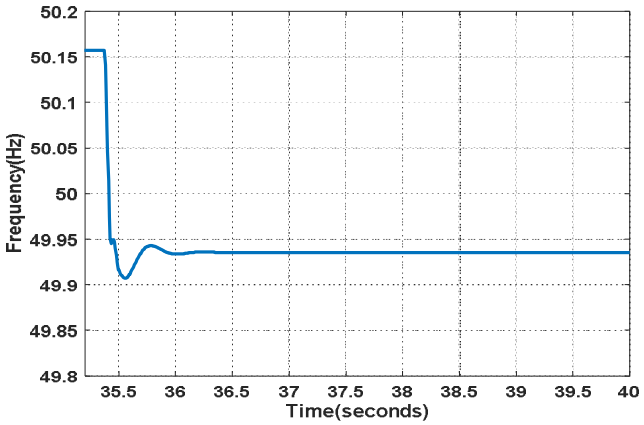

Figure 6.17. Transient frequency of the simulated test system

The voltage of three phases at G1 and G2 are showing in the following figures

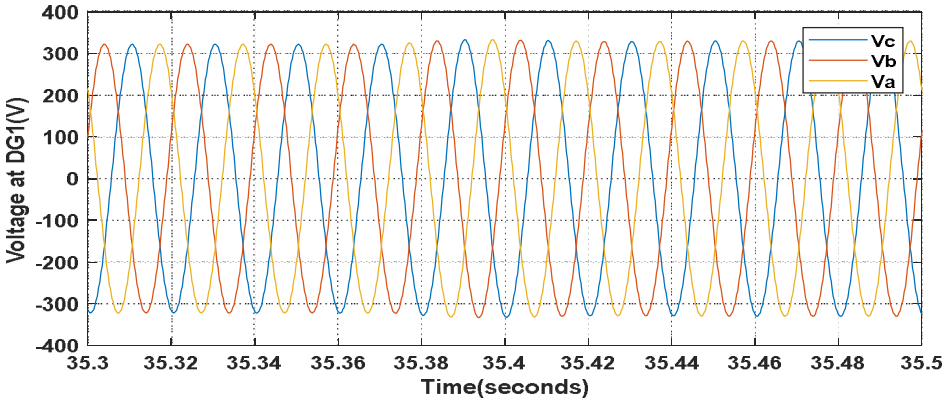

Figure 6.18. Voltage at the three phases in DG1

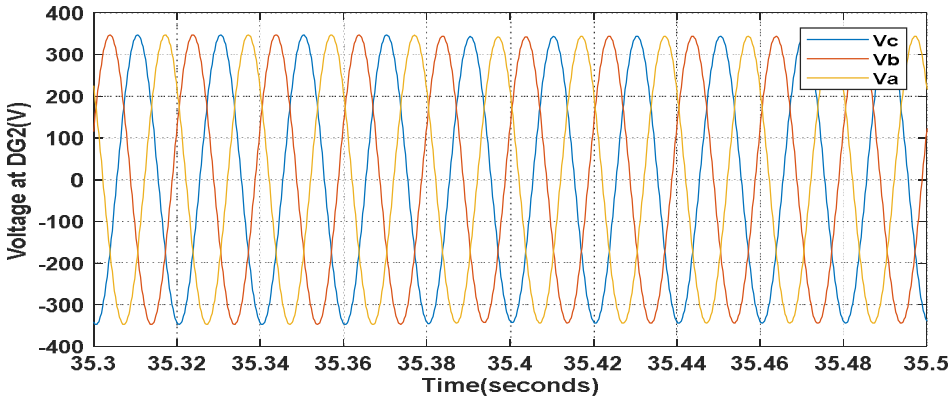

Figure 6.19. Voltage at three phases in DG2

It can be observed that all values of frequency and voltage satisfy their limitations and are stable after changing K_G to a new optimized value for the new loading condition.

6.5.2. Results for 24 hours simulation

Figure 6.20 shows a comparison in the 24 hours of the generated power at the inverted interfaced unit where the optimized droop curve is set. The active power in the system turns to be reduced and frequency is kept within the limitations, as confirmed by Figures 6.21 and Figure 6.23

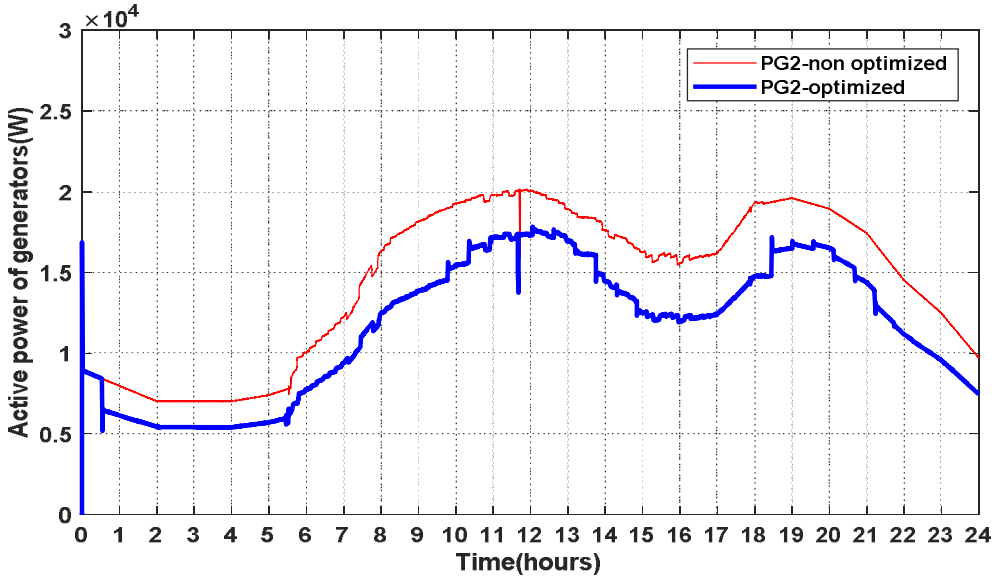

Figure 6.20. Active output power of DGs in 24 hours

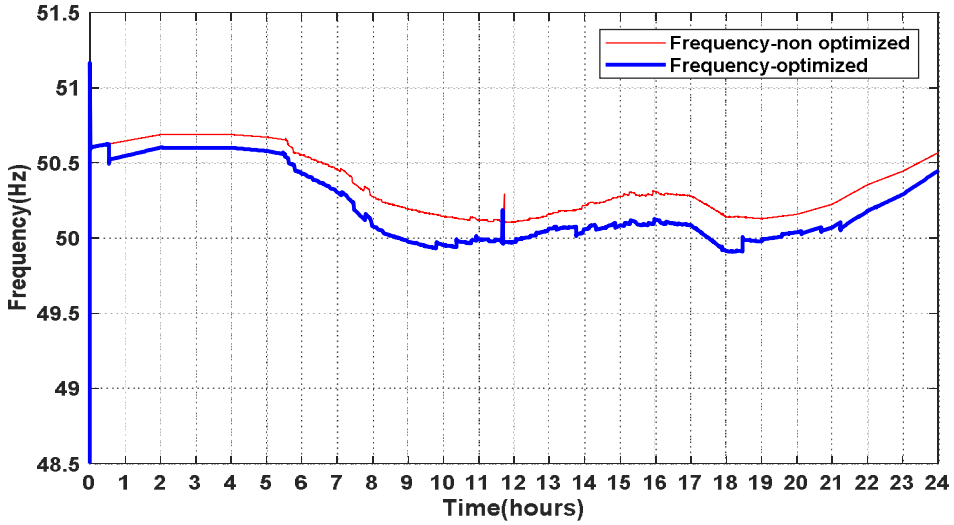

Figure 6.21. Frequency of system in 24 hours

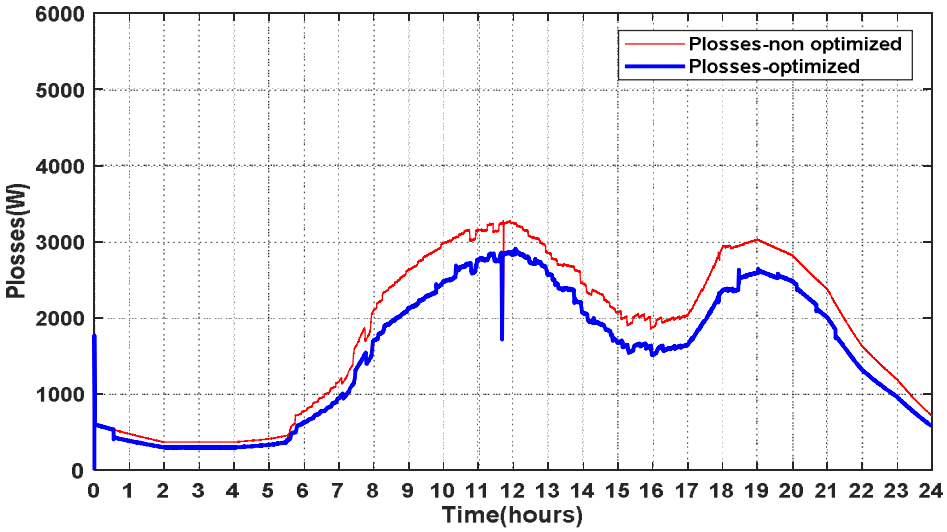

Figure 6.22. The power loss of system in 24 hours

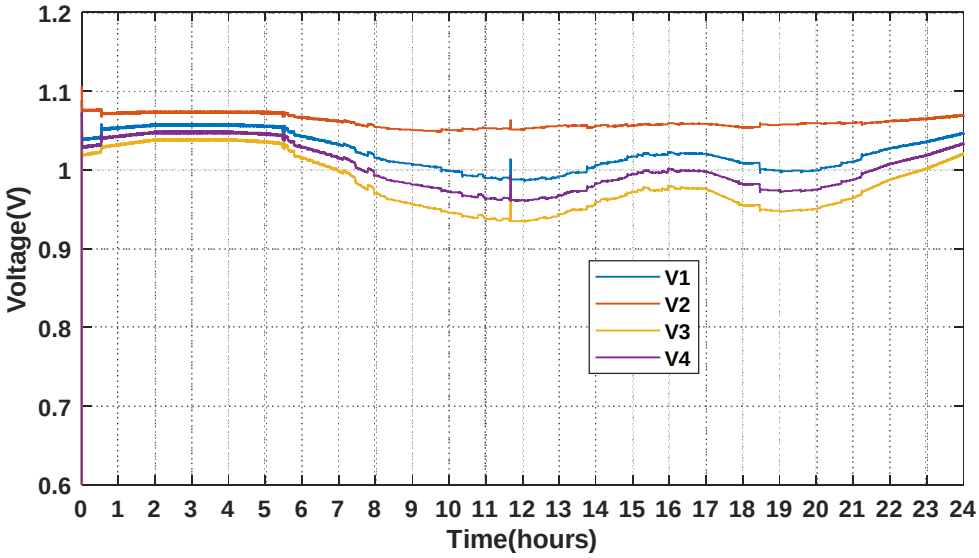

Figure 6.23. Voltage profile of DGs in 24 hours

The following Figure 6.24 shows the improvement in terms of energy losses with an overall improvement as compared to conventional droop of 16,15%.

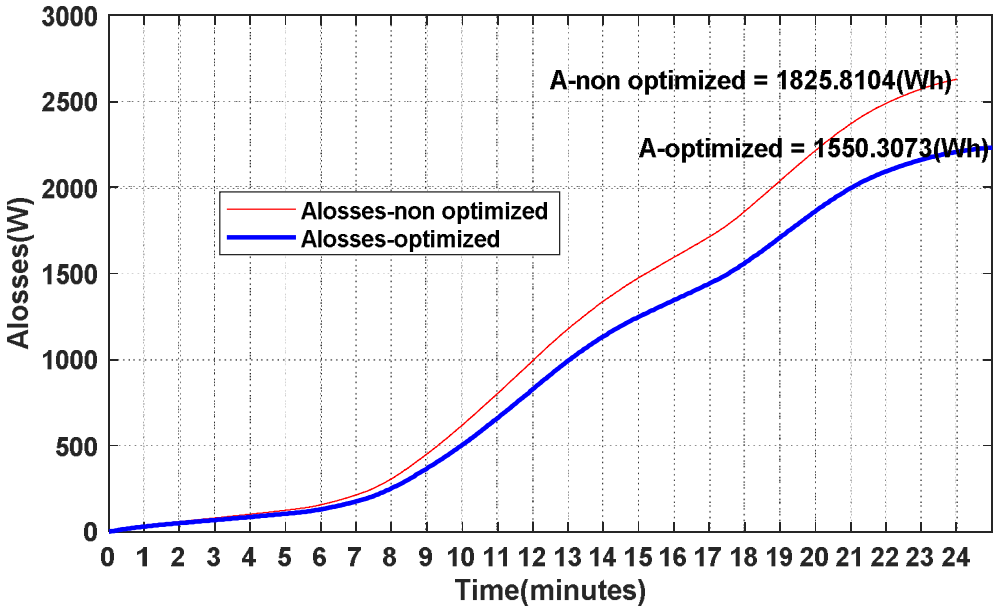

Figure 6.24. The energy loss of system in 24 hours

System frequency fluctuates within their limits, as shown in Figure 6.20, from 49.9 Hz to 50.7 Hz. The frequency response in Figure. 6.21 shows that the response

of frequency is smooth. The DG2 is adjusted to inject enough power in the system in a way that minimizes power losses for the system. The energy losses illustrated in Figure. 6.24 shows that the new regulation method gives smaller losses operation as compared to conventional regulation method of about 16,15%. It is expected that larger systems and LV systems may provide even larger absolute values of power loss reduction. From the proportion of power sharing and the obtained values of frequency, it can be observed that the new regulation demonstrates its powerful efficiency compared to conventional droop method, the system operates in a more effective way at every changing load step.

6.6. Conclusion

In this chapter, a new droop regulation method is proposed for inverter-interfaced units in islanded microgrids. The results have been compared with conventional droop control to prove the effectiveness of the new droop control curve. The results are also simulated using RT lab simulator and to test operating characteristics of the system with hardware in the loop simulation. Further works will produce similar droop regulation curves in larger systems, also optimizing other operating features as fuel cost or operating cost. The proposed on-line procedure ensures a robust optimized operation, since no 24-hours scheduling or rolling horizon approaches are needed for tertiary regulation. In future works, as already outlined in the conclusions of Chapter III, the consideration of storage units will provide even more flexibility and possibility to improve the operational features even more. Other works, will also consider optimized voltage adjustment in droop control.

CHAPTER VII

CONCLUSIONS AND FUTURE WORKS

7.1 Research Summary and Contribution

This research focuses mainly on studying an improved droop regulation methodology for islanded microgrids. The following presents the highlights of its contributions:

- In the new methodology of droop control regulation, solving an OPF problem, new feasible and optimized set points for distributed generators are found to minimize the microgrid operation losses and satisfy the grid and generators constraints. In this way, the frequency and voltage are kept within the desired limits and the energy volumes are relieved for secondary and tertiary regulation purposes. The GSO algorithm is selected to solve the OPF problem, for its ability of looking for global optimization and its fast convergence rate.

- A case study was implemented for demonstrating the effectiveness of the proposed method in different loading conditions and a Matlab/Simulink model was built for testing the operating characteristics of the system. The achieved results were compared to those obtained with the conventional droop regulation. It was shown that, when a load variation occurs, the proposed droop regulation adjusts the droop coefficients, minimizes the power losses, and maximizes the efficiency of power sharing between distributed generators.

- The results are also simulated using RT lab simulator and to test operating characteristics of the system with hardware in the loop simulation.

- The GSO method was applied to keep the energy operation cost for the system to a minimum by regulating droop coefficients in a 24 hours time frame. A test was implemented on a sample 6-bus system to verify the results. The achieved results demonstrated that this method is effective, feasible and can adapt to all technical constraints, whereas it can get a minimum operating cost.

The publications arisen from the work presented in this thesis are provided in Appendix.

7.2 Directions for Future Work

In continuation of this work, the following subjects are suggested for future studies:

- In further works, the optimization procedure, that currently considers only the minimization of the microgrid's power losses, will be modified in order to generate new droop regulation curves for larger systems, and to minimize also the microgrid's operating cost, optimizing other operating features as fuel cost or operating cost

- Moreover, the new regulation method will be applied to battery storage systems to provide wider regulation possibility for further studies since they are currently showing their potential to enhance system stability in grid-connected and in islanded microgrids. The consideration of storage units will provide even more flexibility and possibility to improve the operational features even more.

- With the high penetration of distributed energy storage and controllable loads in smart grids, Demand Side Management (DSM) will be used an effective solution for future grids. Futher studies will address the problem of also considering the demand side management programs. A rolling horizon approach can be also deployed to cope with possible sudden weather variations.

- Further studies will investigate the possibility to have different generators with different speed of response. In this case, some generators will be considered with constant output power others will be variable and will take part to the OPF because speed of response is higher and can follow loads change or sudden power generation variations. Also, a rolling horizon approach for the whole architecture needs to be considered in order to compensate possible weather changes or loads requests. Finally, the price of electricity from the PV and storage system have not been considered, although for the battery a cost can be considered due to depth of discharge issue and the number of operations producing a reduction of their lifetime.

REFERENCES

[1] I. E. Agency, " Technology Roadmap Solar photovoltaic energy," 2010.

[2] A. Ali, W. Li, R. Hussain, X. He, W. B. Williams, and H. A. Memon, "Overview of Current Microgrid Policies, Incentives and Barriers in the European Union, United States and China," *Sustainability,* vol. 9, 2017.

[3] L. Yunwei, D. M. Vilathgamuwa, and L. Poh Chiang, "Design, analysis, and real-time testing of a controller for multibus microgrid system," *IEEE Transactions on Power Electronics,* vol. 19, pp. 1195-1204, 2004.

[4] F. Katiraei and M. R. Iravani, "Power Management Strategies for a Microgrid With Multiple Distributed Generation Units," *IEEE Transactions on Power Systems,* vol. 21, pp. 1821-1831, 2006.

[5] A. Soundarrajan, S. Sumathi, and G. Sivamurugan, "Voltage and frequency control in power generating system using hybrid evolutionary algorithms," *Journal of Vibration and Control,* vol. 18, pp. 214-227, 2012/02/01 2011.

[6] S. Frank and S. Rebennack, "An introduction to optimal power flow: Theory, formulation, and examples," *IIE Transactions,* vol. 48, pp. 1172-1197, 2016/12/01 2016.

[7] M. Soshinskaya, W. H. J. Crijns-Graus, J. M. Guerrero, and J. C. Vasquez, "Microgrids: Experiences, barriers and success factors," *Renewable and Sustainable Energy Reviews,* vol. 40, pp. 659-672, 2014/12/01/ 2014.

[8] " U.S.-Canada Power System Outage Task Force. Final report on the August 14, 2003 blackout in the United States and Canada: causes and recommendations," U.S. Department of Energy2004.

[9] A. Hirsch, Y. Parag, and J. Guerrero, "Microgrids: A review of technologies, key drivers, and outstanding issues," *Renewable and Sustainable Energy Reviews,* vol. 90, pp. 402-411, 2018/07/01/ 2018.

[10] J. M. Guerrero, J. C. Vasquez, J. Matas, L. G. d. Vicuna, and M. Castilla, "Hierarchical Control of Droop-Controlled AC and DC Microgrids—A General Approach Toward Standardization," *IEEE Transactions on Industrial Electronics,* vol. 58, pp. 158-172, 2011.

[11] C.-S. Karavas, G. Kyriakarakos, K. G. Arvanitis, and G. Papadakis, "A multi-agent decentralized energy management system based on distributed intelligence for the design and control of autonomous polygeneration microgrids," *Energy Conversion and Management,* vol. 103, pp. 166-179, 2015/10/01/ 2015.

[12] R. Atia and N. Yamada, "Sizing and Analysis of Renewable Energy and Battery Systems in Residential Microgrids," *IEEE Transactions on Smart Grid,* vol. 7, pp. 1204-1213, 2016.

[13] N. Hatziargyriou, H. Asano, R. Iravani, and C. Marnay, "Microgrids," *IEEE Power and Energy Magazine,* vol. 5, pp. 78-94, 2007.

[14] T. L. Vandoorn, J. D. M. De Kooning, B. Meersman, and L. Vandevelde, "Review of primary control strategies for islanded microgrids with power-electronic interfaces," *Renewable and Sustainable Energy Reviews,* vol. 19, pp. 613-628, 2013/03/01/ 2013.

[15] R. Majumder, "Some Aspects of Stability in Microgrids," *IEEE Transactions on Power Systems,* vol. 28, pp. 3243-3252, 2013.

[16] P. Basak, S. Chowdhury, S. Halder nee Dey, and S. P. Chowdhury, "A literature review on integration of distributed energy resources in the perspective of control, protection and stability of microgrid," *Renewable and Sustainable Energy Reviews,* vol. 16, pp. 5545-5556, 2012/10/01/ 2012.

[17] W. Su and J. Wang, "Energy Management Systems in Microgrid Operations," *The Electricity Journal,* vol. 25, pp. 45-60, 2012/10/01/ 2012.

[18] G. Graditi, M. L. D. Silvestre, R. Gallea, and E. R. Sanseverino, "Heuristic-Based Shiftable Loads Optimal Management in Smart Micro-Grids," *IEEE Transactions on Industrial Informatics,* vol. 11, pp. 271-280, 2015.

[19] Zaheeruddin and M. Manas, "Renewable energy management through microgrid central controller design: An approach to integrate solar, wind and biomass with battery," *Energy Reports,* vol. 1, pp. 156-163, 11// 2015.

[20] W.-M. Lin, C.-S. Tu, and M.-T. Tsai, "Energy Management Strategy for Microgrids by Using Enhanced Bee Colony Optimization," *Energies,* vol. 9, p. 5, 2016.

[21] M. Marzband, E. Yousefnejad, A. Sumper, and J. L. Domínguez-García, "Real time experimental implementation of optimum energy management system in standalone Microgrid by using multi-layer ant colony optimization," *International Journal of Electrical Power & Energy Systems,* vol. 75, pp. 265-274, 2// 2016.

[22] E. Riva Sanseverino, M. L. Di Silvestre, Q. Ninh Nguyen, L. Mineo, J. M. Guerrero, A. C. Luna, *et al.*, "Energy Management Systems and tertiary regulation in hierarchical control architectures for islanded microgrids," in *Environment and Electrical Engineering (EEEIC), 2015 IEEE 15th International Conference on*, 2015, pp. 144-149.

[23] H. Borhanazad, S. Mekhilef, V. Gounder Ganapathy, M. Modiri-Delshad, and A. Mirtaheri, "Optimization of micro-grid system using MOPSO," *Renewable Energy,* vol. 71, pp. 295-306, 11// 2014.

[24] S. Ghaem Sigarchian, M. S. Orosz, H. F. Hemond, and A. Malmquist, "Optimum design of a hybrid PV–CSP–LPG microgrid with Particle Swarm Optimization technique," *Applied Thermal Engineering,* vol. 109, Part B, pp. 1031-1036, 10/25/ 2016.

[25] A. A. Moghaddam, A. Seifi, and T. Niknam, "Multi-operation management of a typical micro-grids using Particle Swarm Optimization: A comparative

study," *Renewable and Sustainable Energy Reviews*, vol. 16, pp. 1268-1281, 2// 2012.

[26] A. J. Litchy and M. H. Nehrir, "Real-time energy management of an islanded microgrid using multi-objective Particle Swarm Optimization," in *2014 IEEE PES General Meeting | Conference & Exposition*, 2014, pp. 1-5.

[27] R. Yang and L. Wang, "Energy management of multi-zone buildings based on multi-agent control and particle swarm optimization," in *Systems, Man, and Cybernetics (SMC), 2011 IEEE International Conference on*, 2011, pp. 159-164.

[28] S. A. Pourmousavi, M. H. Nehrir, C. M. Colson, and C. Wang, "Real-Time Energy Management of a Stand-Alone Hybrid Wind-Microturbine Energy System Using Particle Swarm Optimization," *IEEE Transactions on Sustainable Energy*, vol. 1, pp. 193-201, 2010.

[29] A. H. Habib, V. R. Disfani, J. Kleissl, and R. A. d. Callafon, "Quasi-dynamic load and battery sizing and scheduling for stand-alone solar system using mixed-integer linear programming," in *2016 IEEE Conference on Control Applications (CCA)*, 2016, pp. 1476-1481.

[30] A. C. Luna, N. L. D. Aldana, M. Graells, J. C. Vasquez, and J. M. Guerrero, "Mixed-Integer-Linear-Programming based Energy Management System for Hybrid PV-wind-battery Microgrids: Modeling, Design and Experimental Verification," *IEEE Transactions on Power Electronics*, vol. PP, pp. 1-1, 2016.

[31] T. Ding, K. Sun, C. Huang, Z. Bie, and F. Li, "Mixed-Integer Linear Programming-Based Splitting Strategies for Power System Islanding Operation Considering Network Connectivity," *IEEE Systems Journal*, vol. PP, pp. 1-10, 2015.

[32] "Salahi, S., and Bahramara, S. (2016) Modeling Operation Problem of Micro-grids Considering Economical, Technical and Environmental issues as Mixed-

Integer Non-Linear Programming. Int. Journal of Renewable Energy Development, 5(2), 139-149.."

[33] J. Silvente, G. M. Kopanos, E. N. Pistikopoulos, and A. Espuña, "A rolling horizon optimization framework for the simultaneous energy supply and demand planning in microgrids," *Applied Energy*, vol. 155, pp. 485-501, 10/1/ 2015.

[34] C. Wouters, E. S. Fraga, and A. M. James, "An energy integrated, multi-microgrid, MILP (mixed-integer linear programming) approach for residential distributed energy system planning – A South Australian case-study," *Energy*, vol. 85, pp. 30-44, 6/1/ 2015.

[35] X. Pan, X. Niu, X. Yang, N. Chamollet, and D. Zheng, "Robust scheduling for microgrid energy management optimization," in *2016 China International Conference on Electricity Distribution (CICED)*, 2016, pp. 1-5.

[36] Y. Sun, N. S. Hang, and Z. Y. Sun, "Power Flow Calculation Method for Islanded Power Network," in *Power and Energy Engineering Conference, 2009. APPEEC 2009. Asia-Pacific*, 2009, pp. 1-5.

[37] J. A. Momoh, M. E. El-Hawary, and R. Adapa, "A review of selected optimal power flow literature to 1993. II. Newton, linear programming and interior point methods," *IEEE Transactions on Power Systems*, vol. 14, pp. 105-111, 1999.

[38] M. M. A. Abdelaziz, H. E. Farag, E. F. El-Saadany, and Y. A. R. I. Mohamed, "A Novel and Generalized Three-Phase Power Flow Algorithm for Islanded Microgrids Using a Newton Trust Region Method," *IEEE Transactions on Power Systems*, vol. 28, pp. 190-201, 2013.

[39] E. Riva Sanseverino, Q. Ninh Nguyen, G. Zizzo, M. L. Di Silvestre, and J. M. Guerrero, "A parametric study on unbalanced three phase islanded microgrids with inverter interfaced units," in *AEIT Annual Conference, 2013*, 2013, pp. 1-6.

[40] S. Bruno, S. Lamonaca, G. Rotondo, U. Stecchi, and M. L. Scala, "Unbalanced Three-Phase Optimal Power Flow for Smart Grids," *IEEE Transactions on Industrial Electronics,* vol. 58, pp. 4504-4513, 2011.

[41] A. Elrayyah, Y. Sozer, and M. Elbuluk, "A novel load flow analysis for particle-swarm optimized microgrid power sharing," in *Applied Power Electronics Conference and Exposition (APEC), 2013 Twenty-Eighth Annual IEEE,* 2013, pp. 297-302.

[42] A. Khorsandi, S. H. Hosseinian, and A. Ghazanfari, "Modified artificial bee colony algorithm based on fuzzy multi-objective technique for optimal power flow problem," *Electric Power Systems Research,* vol. 95, pp. 206-213, 2// 2013.

[43] M. H. Hemmatpour, M. Mohammadian, and A. A. Gharaveisi, "Optimum islanded microgrid reconfiguration based on maximization of system loadability and minimization of power losses," *International Journal of Electrical Power & Energy Systems,* vol. 78, pp. 343-355, 6// 2016.

[44] Q. Ninh Nguyen, E. Riva Sanseverino, A. Madonia, M. L. Di Silvestre, and J. M. Guerrero, "GSO-based Optimal Power Flow in islanded microgrids with inverter interfaced units," *AEIT Annual Conference, Trieste, Italia. IEEE CONFERENCE PUBLICATIONS,* 2014.

[45] Q. Ninh Nguyen, E. Riva Sanseverino, M. L. Di Silvestre, A. Madonia, L. Chendan, and J. M. Guerrero, "Optimal power flow based on glow worm-swarm optimization for three-phase islanded microgrids," in *AEIT Annual Conference - From Research to Industry: The Need for a More Effective Technology Transfer (AEIT), 2014*, 2014, pp. 1-6.

[46] M. C. Chandorkar, D. M. Divan, and R. Adapa, "Control of parallel connected inverters in standalone AC supply systems," *IEEE Transactions on Industry Applications,* vol. 29, pp. 136-143, 1993.

[47] E. T. Andrade, P. E. M. J. Ribeiro, J. O. P. Pinto, C. L. Chen, J. S. Lai, and N. Kees, "A novel power calculation method for droop-control microgrid systems," in *2012 Twenty-Seventh Annual IEEE Applied Power Electronics Conference and Exposition (APEC)*, 2012, pp. 2254-2258.

[48] A. Klem, M. H. Nehrir, and K. Dehghanpour, "Frequency stabilization of an islanded microgrid using droop control and demand response," in *2016 North American Power Symposium (NAPS)*, 2016, pp. 1-6.

[49] M. Ramezani and S. Li, "Voltage and frequency control of islanded microgrid based on combined direct current vector control and droop control," in *2016 IEEE Power and Energy Society General Meeting (PESGM)*, 2016, pp. 1-5.

[50] Z. Ahmad and S. N. Singh, "DROOP Control Strategies of Conventional Power System Versus Microgrid Based Power Systems - A Review," in *2015 International Conference on Computational Intelligence and Communication Networks (CICN)*, 2015, pp. 1499-1504.

[51] A. Villa, F. Belloni, R. Chiumeo, and C. Gandolfi, "Conventional and reverse droop control in islanded microgrid: Simulation and experimental test," in *2016 International Symposium on Power Electronics, Electrical Drives, Automation and Motion (SPEEDAM)*, 2016, pp. 288-294.

[52] Y. Guan, J. M. Guerrero, X. Zhao, and J. C. Vasquez, "Comparison of a synchronous reference frame virtual impedance-based autonomous current sharing control with conventional droop control for parallel-connected inverters," in *2016 IEEE 8th International Power Electronics and Motion Control Conference (IPEMC-ECCE Asia)*, 2016, pp. 3419-3426.

[53] C. Sao and P. Lehn, "Control and power management of converter fed microgrids," in *IEEE PES General Meeting*, 2010, pp. 1-1.

[54] N. Jayasekara, P. Wolfs, and M. A. S. Masoum, "An optimal management strategy for distributed storages in distribution networks with high

penetrations of PV," *Electric Power Systems Research*, vol. 116, pp. 147-157, 11// 2014.

[55] A. A. R. Lasserter, C. Marnay, H.Stephens, J. Dagle, R. Gutromson, A. S. Meliopoulous, R. Yinger, and J. Eto, "The CERTS microgrid concept," *in Proc. CERTS*, 2002.

[56] M. I. Azim, M. A. Hossain, M. J. Hossain, and H. R. Pota, "Droop Control for islanded microgrids with compensating approach," in *2015 Australasian Universities Power Engineering Conference (AUPEC)*, 2015, pp. 1-6.

[57] C. Rowe, T. J. Summers, and R. E. Betz, "A novel parallel voltage and current control scheme implementing P-F and Q-V droop in a microgrid," in *Proceedings of the 2011 14th European Conference on Power Electronics and Applications*, 2011, pp. 1-10.

[58] K. D. Brabandere, B. Bolsens, J. V. d. Keybus, A. Woyte, J. Driesen, and R. Belmans, "A Voltage and Frequency Droop Control Method for Parallel Inverters," *IEEE Transactions on Power Electronics*, vol. 22, pp. 1107-1115, 2007.

[59] F. Cingoz, A. Elrayyah, and Y. Sozer, "Plug-and-Play Nonlinear Droop Construction Scheme to Optimize Islanded Microgrid Operations," *IEEE Transactions on Power Electronics*, vol. PP, pp. 1-1, 2016.

[60] M. Sinha, S. Dhople, B. Johnson, N. Ainsworth, and F. Dörfler, "Nonlinear supersets to droop control," in *2015 IEEE 16th Workshop on Control and Modeling for Power Electronics (COMPEL)*, 2015, pp. 1-6.

[61] V. Mariani, F. Vasca, and J. M. Guerrero, "Dynamic-phasor-based nonlinear modelling of AC islanded microgrids under droop control," in *2014 IEEE 11th International Multi-Conference on Systems, Signals & Devices (SSD14)*, 2014, pp. 1-6.

[62] S. M. Ashabani and Y. A. R. I. Mohamed, "General Interface for Power Management of Micro-Grids Using Nonlinear Cooperative Droop Control," *IEEE Transactions on Power Systems*, vol. 28, pp. 2929-2941, 2013.

[63] Y. Sun, W. Huang, G. Wang, W. Wenjun, D. Wang, and Z. Li, "Study of control strategy of DG based on nonlinear droop characteristic," in *2012 China International Conference on Electricity Distribution*, 2012, pp. 1-4.

[64] H. C. Chiang, K. K. Jen, and G. H. You, "Improved droop control method with precise current sharing and voltage regulation," *IET Power Electronics*, vol. 9, pp. 789-800, 2016.

[65] E. Tegling, D. F. Gayme, and H. Sandberg, "Performance metrics for droop-controlled microgrids with variable voltage dynamics," in *2015 54th IEEE Conference on Decision and Control (CDC)*, 2015, pp. 7502-7509.

[66] C. A. Hernandez-Aramburo, T. C. Green, and N. Mugniot, "Fuel consumption minimization of a microgrid," *IEEE Transactions on Industry Applications*, vol. 41, pp. 673-681, 2005.

[67] L. A. Carniato, R. B. Godoy, J. O. P. Pinto, C. A. Canesin, and P. E. M. J. Ribeiro, "Dynamic adaptation of droop control curves for microgrid connected inverters with variable input power," in *2013 Brazilian Power Electronics Conference*, 2013, pp. 1022-1028.

[68] "Off-grid opportunities and challenges in Vietnam," Winrock International Institute for Agricultural Development and SNV Netherlands Development Organisation Hanoi, Vietnam2014.

[69] V. E. Corporation, "The "dream" of rural electrification," ed. Hanoi, Vietnam, 2016.

[70] "Report on the Off-grid Lighting Status for Southeast Asia and the Pacific," United Nations Environment Programme (UNEP) and Global Environment Facility (GEF)2014.

[71] N. H. B. Nguyen Anh Tuan, "Current Situations and Solutions for Renewable Energy Development in Vietnam," *Asia Pacific Journal of Sustainable Agriculture, Food and Energy,* 2015.

[72] "Renewable Energy in Vietnam ", Hanoi, VietnamAugust 2017.

[73] MOIT, "The National Master Plan for Power Development Plan period 2011-2020 with

the vision to 2030," 2011.

[74] "Bibliography on load models for power flow and dynamic performance simulation," *IEEE Transactions on Power Systems,* vol. 10, pp. 523-538, 1995.

[75] M. V. P. Maulik J. Patel, Janak Sorathiya "Real Power Loss Allocation Based on Circulating Current between Generators," *International Journal of Emerging Technology and Advanced Engineering,* vol. 3, 2013.

[76] D. Zhang, F. F. Wang, R. Burgos, and D. Boroyevich, "Common-Mode Circulating Current Control of Paralleled Interleaved Three-Phase Two-Level Voltage-Source Converters With Discontinuous Space-Vector Modulation," *IEEE Transactions on Power Electronics,* vol. 26, pp. 3925-3935, 2011.

[77] Z. X. Li M., Zhao W., " A Novel Stability Improvement Strategy for a Multi-Inverter System in a Weak Grid Utilizing Dual-Mode Control," *Energies* 2018.

[78] M. Hosseinzadeh and F. R. Salmasi, "Power management of an isolated hybrid AC/DC micro-grid with fuzzy control of battery banks," *IET Renewable Power Generation,* vol. 9, pp. 484-493, 2015.

[79] M. P. Asha Gowda Karegowda, "A Survey of Applications of Glowworm Swarm Optimization Algorithm," presented at the IJCA Proceedings on International Conference on Computing and information Technology 2013 IC2IT, 2013.

[80] D. G. Krishnanand N. Kaipa, *Glowworm Swarm Optimization: Theory, Algorithms, and Applications* vol. 698: Springer, Cham, 2017.

[81] A. Sheikh, T. Youssef, and O. Mohammed, "AC Microgrid Control Using Adaptive Synchronous Reference Frame PLL," in *2017 Ninth Annual IEEE Green Technologies Conference (GreenTech)*, 2017, pp. 46-51.

[82] "IEEE Recommended Practice for Functional and Performance Characteristics of Control Systems for Steam Turbine-Generator Units," *IEEE Std 122-1985*, p. 0_1, 1985.

[83] J. Zhao, X. Lyu, Y. Fu, X. Hu, and F. Li, "Coordinated Microgrid Frequency Regulation Based on DFIG Variable Coefficient Using Virtual Inertia and Primary Frequency Control," *IEEE Transactions on Energy Conversion*, vol. 31, pp. 833-845, 2016.

[84] N. N. Quang, E. R. Sanseverino, M. L. D. Silvestre, A. Madonia, C. Li, and J. M. Guerrero, "Optimal power flow based on glow worm-swarm optimization for three-phase islanded microgrids," in *AEIT Annual Conference - From Research to Industry: The Need for a More Effective Technology Transfer (AEIT), 2014*, 2014, pp. 1-6.

[85] A. Elrayyah, F. Cingoz, and Y. Sozer, "Construction of Nonlinear Droop Relations to Optimize Islanded Microgrid Operation," *IEEE Transactions on Industry Applications*, vol. 51, pp. 3404-3413, 2015.

[86] E. R. Sanseverino, T. T. T. Quynh, M. L. D. Silvestre, G. Zizzo, N. Q. Ninh, A. C. Luna, *et al.*, "Optimal power flow for technically feasible energy management systems in islanded microgrids," in *2016 IEEE 16th International Conference on Environment and Electrical Engineering (EEEIC)*, 2016, pp. 1-6.

[87] M. Bacic, "On hardware-in-the-loop simulation," in *Proceedings of the 44th IEEE Conference on Decision and Control*, 2005, pp. 3194-3198.

APPENDIX I

Chapter III

Table III.1. Results by conventional droop control methods with K_{G1}=7,5 and K_{G2}=5 in pu

	Initial load		**results in pu**			
	P_{L1}	P_{L2}	P_{G1}	P_{G2}	P_{L1}	P_{L2}
1	0,10	0,10	0,1233	0,0822	0,1004	0,1004
2	0,12	0,10	0,1357	0,0905	0,1202	0,1002
3	0,14	0,10	0,1482	0,0988	0,1400	0,1000
4	0,16	0,10	0,1607	0,1071	0,1598	0,0999
5	0,18	0,10	0,1732	0,1155	0,1794	0,0997
6	0,20	0,10	0,1858	0,1239	0,1990	0,0995
7	0,22	0,10	0,1985	0,1323	0,2186	0,0994
8	0,24	0,10	0,2112	0,1408	0,2380	0,0992

Table III.2. Results by conventional droop control methods with K_{G1}=7,5 and K_{G2}=5 in pu

P_{loss}	f	I_{13}	I_{24}	I_{34}
0,0049	1,0036	0,1205	0,0830	0,0201
0,0058	1,0019	0,1331	0,0914	0,0127
0,0069	1,0002	0,1457	0,0998	0,0071
0,0082	0,9986	0,1585	0,1083	0,0087
0,0096	0,9969	0,1714	0,1168	0,0155
0,0112	0,9952	0,1842	0,1253	0,0232
0,0129	0,9935	0,1973	0,1340	0,0315
0,0147	0,9918	0,2106	0,1427	0,0399

Table III.3. Results by with different ranges of KG1 =[5 7,5]; KG2 =5 in pu

	Initial load		**Results in pu**			
	P_{L1}	**P_{L2}**	**P_{G1}**	**P_{G2}**	**P_{L1}**	**P_{L2}**
1	0,10	0,10	0,1022	0,1022	0,1000	0,1000
2	0,12	0,10	0,1144	0,1107	0,1197	0,0998
3	0,14	0,10	0,1278	0,1180	0,1395	0,0996
4	0,16	0,10	0,1412	0,1255	0,1592	0,0995
5	0,18	0,10	0,1557	0,1320	0,1788	0,0994
6	0,20	0,10	0,1682	0,1404	0,1984	0,0992
7	0,22	0,10	0,1826	0,1471	0,2179	0,0991
8	0,24	0,10	0,1959	0,1550	0,2374	0,0989

Table III.4. Results by with different ranges of KG1 =[5 7,5]; KG2 =5 in pu

P_{loss}	**f**	**I_{13}**	**I_{24}**	**I_{34}**
0,0045	0,9996	0,1012	0,1010	0,0009
0,0056	0,9979	0,1136	0,1095	0,0083
0,0067	0,9964	0,1272	0,1170	0,0155
0,0080	0,9949	0,1408	0,1247	0,0230
0,0094	0,9936	0,1555	0,1316	0,0296
0,0110	0,9919	0,1682	0,1401	0,0379
0,0127	0,9906	0,1830	0,1472	0,0448
0,0146	0,9890	0,1968	0,1554	0,0527

Table III.5. Results by with different ranges of KG1 =[6 7,5]; KG2 =5 in pu

	Initial load		**Results in pu**			
	P_{L1}	**P_{L2}**	**P_{G1}**	**P_{G2}**	**P_{L1}**	**P_{L2}**
1	0,10	0,10	0,1118	0,0931	0,1001	0,1001
2	0,12	0,10	0,1230	0,1025	0,1199	0,1000
3	0,14	0,10	0,1343	0,1119	0,1397	0,0998
4	0,16	0,10	0,1456	0,1213	0,1593	0,0996
5	0,18	0,10	0,1569	0,1308	0,1789	0,0994
6	0,20	0,10	0,1686	0,1400	0,1984	0,0992
7	0,22	0,10	0,1824	0,1473	0,2179	0,0991
8	0,24	0,10	0,1956	0,1552	0,2373	0,0989

Table III.6. Results by with different ranges of KG1 =[6 7,5]; KG2 =5 in pu

P_{loss}	**f**	**I_{13}**	**I_{24}**	**I_{34}**
0,0046	1,0014	0,1099	0,0928	0,0090
0,0056	0,9995	0,1214	0,1021	0,0021
0,0067	0,9976	0,1330	0,1115	0,0099
0,0080	0,9957	0,1448	0,1210	0,0191
0,0094	0,9938	0,1566	0,1305	0,0284
0,0110	0,9920	0,1686	0,1397	0,0375
0,0127	0,9905	0,1828	0,1474	0,0449
0,0146	0,9890	0,1966	0,1557	0,0530

Chapter IV

Table IV.1. The results in pu with linear droop regulation

Case	KG2	Kd2	PG1	PG2	Ploss*100	f
1	20.0	6.0	0.7432	0.4955	0.5125	0.9952
2	20.0	6.0	0.7724	0.515	0.5396	0.9943
3	20.0	6.0	0.8016	0.5344	0.5704	0.9933
4	20.0	6.0	0.8599	0.5732	0.643	0.9913
5	20.0	6.0	0.9179	0.612	0.7296	0.9894
6	20.0	6.0	0.9759	0.6506	0.8313	0.9875
7	20.0	6.0	1.0626	0.7084	1.0136	0.9846
8	20.0	6.0	1.149	0.766	1.2334	0.9817

Table VI.2. The results in pu with linear droop regulation

Case	QG1	QG2	V1	V2	V3	V4	V5	V6	V7	V8	V9
1	0.2248	0.1111	1.015	1.0215	0.9989	1.0127	0.9945	0.9988	0.9864	1.0013	0.9974
2	0.233	0.1138	1.0141	1.021	0.9979	1.0121	0.9935	0.9979	0.9852	1.0003	0.9959
3	0.2414	0.1167	1.0132	1.0206	0.9968	1.0114	0.9924	0.997	0.984	0.9991	0.9944
4	0.259	0.1229	1.0112	1.0195	0.9945	1.01	0.9901	0.995	0.9814	0.9967	0.9913
5	0.2747	0.1286	1.0095	1.0186	0.9925	1.0087	0.988	0.9932	0.9792	0.9946	0.9885
6	0.2922	0.1353	1.0075	1.0174	0.9901	1.0072	0.9857	0.9912	0.9766	0.9921	0.9855
7	0.3239	0.1483	1.004	1.0153	0.9857	1.0042	0.9812	0.9872	0.9717	0.9875	0.9798
8	0.3631	0.165	0.9997	1.0125	0.98	1.0002	0.9755	0.9822	0.9655	0.9817	0.9727

Table IV.3. The results in pu with improved droop regulation

Case	KG2	Kd2	PG1	PG2	Ploss*100	f
1	12.3	4.1	0.8741	0.3580	0.4248	0.9909
2	12.1	4.2	0.9108	0.3690	0.4262	0.9896
3	12.0	4.9	0.9480	0.3796	0.4295	0.9884
4	12.0	4.4	1.0162	0.4068	0.4399	0.9861
5	12.1	4.1	1.0827	0.4355	0.4582	0.9839
6	12.0	4.5	1.1507	0.4622	0.4842	0.9816
7	14.0	5.0	1.1991	0.5595	0.6313	0.9800
8	17.8	5.5	1.1995	0.7101	1.0348	0.9800

Table IV.4. The results in pu with improved droop regulation

Case	QG1	QG2	V1	V2	V3	V4	V5	V6	V7	V8	V9
1	0.2377	0.1025	1.0136	1.0148	0.9946	1.0063	0.9902	0.9937	0.9826	0.9974	0.9956
2	0.2447	0.1060	1.0128	1.0150	0.9940	1.0062	0.9896	0.9934	0.9818	0.9968	0.9945
3	0.2483	0.1131	1.0124	1.0169	0.9945	1.0075	0.9901	0.9942	0.9819	0.9972	0.9941
4	0.2698	0.1143	1.0100	1.0141	0.9912	1.0047	0.9868	0.9911	0.9785	0.9938	0.9903
5	0.2881	0.1156	1.0080	1.0119	0.9886	1.0025	0.9841	0.9886	0.9757	0.9911	0.9871
6	0.3021	0.1237	1.0064	1.0126	0.9876	1.0025	0.9831	0.9880	0.9742	0.9900	0.9850
7	0.3278	0.1371	1.0036	1.0128	0.9850	1.0019	0.9805	0.9862	0.9710	0.9872	0.9803
8	0.3641	0.1579	0.9995	1.0114	0.9799	0.9994	0.9754	0.9819	0.9654	0.9817	0.9730

Chapter V

Table V.1. Energy profile of load demand at bus 4,5,6 and PV system at bus 2

	EG2 MWh	**EL1 MWh**	**EL2 MWh**	**EL3 MWh**
1	0	8,7478	12,9683	7,5099
2	0	8,1156	10,5767	7,9624
3	0	6,8553	9,3810	7,8470
4	0	6,2975	9,1246	7,6325
5	0	6,9163	9,4644	7,9168
6	0	6,3678	9,2264	7,7177
7	0	7,7922	14,2173	7,6452
8	6,9530	8,9760	14,3301	7,7058
9	21,5583	13,3456	18,2453	6,7066
10	32,3888	18,4328	21,7910	8,7643
11	38,6728	22,4162	30,6748	51,9590
12	39,2953	18,7684	20,9293	16,0118
13	34,1483	16,1656	17,8833	16,6536
14	24,1671	9,4183	11,0961	19,7784
15	10,9496	7,6488	9,4201	20,8812
16	0,0001	8,0638	9,4583	20,9659
17	0	16,7960	20,3975	16,9826
18	0	9,6524	13,2085	20,2700
19	0	15,0794	19,6032	14,7579
20	0	16,7661	21,4136	8,4442
21	0	16,7690	22,4371	7,2940
22	0	16,8333	19,8940	6,3060
23	0	14,4480	17,6897	6,2670
24	0	9,3760	18,4756	6,1818

Table V.2. Results optimizing the production cost of the system in pu

	PG1	PG2	PG3	Ploss	f	PL1/pu	PL2/pu	PL3/pu
1	16,7075	4,8586	10,0749	0,0029	1,0489	0,0943	0,1385	0,0804
2	17,0519	1,9005	10,0109	0,003	1,0498	0,0879	0,1133	0,0854
3	15,4469	0,7583	10,0026	0,0027	1,05	0,0744	0,1006	0,0844
4	15,1018	0	10,0007	0,0027	1,05	0,0684	0,0979	0,0821
5	16,4696	0	10,0002	0,003	1,05	0,0751	0,1014	0,0851
6	14,9139	0,3067	10,1193	0,0026	1,0482	0,069	0,0989	0,0829
7	20,2977	0,1343	11,2765	0,0047	1,0309	0,0829	0,1489	0,0805
8	18,6809	4,3677	10,3783	0,0036	1,0443	0,0965	0,1521	0,0821
9	16,504	14,5834	10,041	0,0035	1,0494	0,1423	0,1939	0,0717
10	16,8488	25,3762	10,0668	0,006	1,049	0,1939	0,2302	0,0928
11	29,0304	48,2875	21,9028	0,0282	0,9531	0,2117	0,2863	0,466
12	19,0196	29,3659	10,5664	0,0081	1,0415	0,1962	0,2191	0,1662
13	13,3855	30,7811	10,0388	0,0078	1,0494	0,1704	0,1894	0,1745
14	10,0386	23,1185	10,0386	0,0053	1,0494	0,1006	0,1185	0,2077
15	11,0298	19,5406	10,0754	0,0048	1,0489	0,0821	0,1006	0,219
16	20,4966	8,7339	11,387	0,006	1,0292	0,0856	0,0989	0,2157
17	29,9743	4,046	18,8121	0,0095	0,9502	0,1627	0,194	0,1621
18	27,764	0,0032	15,4244	0,0094	0,9686	0,0967	0,1291	0,1968
19	29,8299	0,0003	18,719	0,0099	0,9514	0,1468	0,187	0,1417
20	29,5307	0	16,4059	0,0092	0,9539	0,1633	0,205	0,0818
21	29,4662	0	16,3701	0,0094	0,9544	0,1633	0,2149	0,0708
22	27,6982	0	15,3879	0,0081	0,9692	0,1665	0,194	0,0624
23	25,2725	0	14,0403	0,0067	0,9894	0,1463	0,1767	0,0634
24	22,8853	0	12,7141	0,0061	1,0093	0,0975	0,1887	0,0637

Table V.3. Results optimizing the production cost of the system in pu

	QL1/pu	QL2/pu	QL3/pu	V1	V2	V3	V4	V5	V6
1	0,0174	0,0255	0,0148	1,0228	1,013	1,0166	1,0139	1,0089	1,0106
2	0,0162	0,0208	0,0157	1,0244	1,0124	1,0169	1,0155	1,0099	1,011
3	0,0136	0,0184	0,0155	1,0243	1,0127	1,0177	1,0163	1,0108	1,0119
4	0,0126	0,018	0,0151	1,0245	1,0125	1,0181	1,0167	1,011	1,0123
5	0,0137	0,0186	0,0157	1,0252	1,0121	1,0175	1,0167	1,0106	1,0117
6	0,0127	0,0182	0,0153	1,0242	1,0126	1,0181	1,0165	1,011	1,0123
7	0,0158	0,0285	0,0153	1,0266	1,01	1,0171	1,0162	1,0079	1,0105
8	0,0179	0,0283	0,0152	1,0241	1,012	1,0161	1,0142	1,008	1,0098
9	0,0262	0,0356	0,0132	1,0172	1,0153	1,015	1,0077	1,0062	1,0088
10	0,0357	0,0423	0,0171	1,012	1,0181	1,0115	1,0015	1,0036	1,0048
11	0,0472	0,0639	0,1039	1,0126	1,0171	0,9868	0,9954	0,9897	0,97
12	0,0366	0,0409	0,031	1,0132	1,019	1,006	1,0017	1,0025	0,9983
13	0,0313	0,0348	0,0321	1,0107	1,0215	1,0067	1,002	1,0047	0,9994
14	0,0185	0,0218	0,0382	1,0148	1,0211	1,0074	1,0085	1,0084	1,0002
15	0,0151	0,0185	0,0403	1,0177	1,02	1,0072	1,0112	1,0091	1
16	0,0164	0,0189	0,0413	1,0264	1,0138	1,0077	1,0159	1,0077	0,9998
17	0,0365	0,0435	0,0364	1,0254	1,0056	1,0136	1,0096	1,0004	1,0023
18	0,0209	0,0279	0,0426	1,0308	1,0071	1,0108	1,0169	1,0045	1,001
19	0,0328	0,0419	0,0318	1,0271	1,0045	1,0157	1,0116	1,0014	1,0047
20	0,0363	0,0457	0,0182	1,026	1,0048	1,0176	1,0104	1,0018	1,0081
21	0,0364	0,0478	0,0157	1,0258	1,0046	1,0181	1,0102	1,0016	1,0088
22	0,036	0,0419	0,0135	1,0249	1,0058	1,0188	1,0102	1,0031	1,0101
23	0,0303	0,0366	0,0131	1,0251	1,0073	1,0187	1,0117	1,0048	1,0107
24	0,0194	0,0376	0,0128	1,0266	1,0081	1,018	1,0148	1,0057	1,0107

APPENDIX II

The following is the list of the publications arising from the work in this dissertation:

Articles in Refereed Journals

1. A distributed minimum losses optimal power flow for islanded microgrids, Eleonora Riva Sanseverino, Luca Buono, Maria Luisa Di Silvestre, Gaetano Zizzo, Mariano Giuseppe Ippolito, Salvatore Favuzza, Tran Thi Tu Quynh, Nguyen Quang Ninh, Electric Power Systems Research, Volume 152, November 2017, Pages 271-283.

2. Driven Primary Regulation for Minimum Power Losses Operation in Islanded Microgrids, Quynh T.T Tran, Maria Luisa Di Silvestre, Eleonora Riva Sanseverino, Gaetano Zizzo, Thanh Nam Pham, Energies Journal.

3. A methodology for assessing the impact of salinity gradient power generation in urban contexts, A Cipollina, ML Di Silvestre, F Giacalone, GM Micale, E Riva Sanseverino, R Sangiorgio, QTT Tran, V Vaccaro, G Zizzo, Sustainable Cities and Society Journal, Volume 38, Pages 158-173.

Article in Refereed Conference Proceedings

1. Optimal power flow for technically feasible energy management systems in islanded microgrids, E. Riva Sanseverino, T.T.T. Quynh, M. L. Di Silvestre, G. Zizzo, N.Q. Ninh, A. C. Luna and J.M. Guerrero, EEEC 2016: 16th IEEE International Conference on Environment and Electrical Engineering. 8-10 June 2016, Florence, Italy.

2. A multi-agent system reinforcement learning based optimal power flow for islanded microgrids, E. Riva Sanseverino, M. L. Di Silvestre, L. Mineo, S. Favuzza, N.Q. Nguyen, T.T.T. Quynh, 16th IEEE International Conference on Environment and Electrical Engineering (EEEC 2016). 8-10 June, 2016, Florence, Italy

3. A distributed minimum losses optimal power flow for islanded microgrids, Eleonora Riva Sanseverino, Luca Buono, Maria Luisa Di Silvestre, Gaetano Zizzo,

Mariano Giuseppe Ippolito, Salvatore Favuzza, Tran Thi Tu Quynh, Nguyen Quang Ninh, Electric Power Systems Research, Volume 152, November 2017, Pages 271-283.

4. Optimizing droop coefficients for minimum cost operation of islanded micro-grids, E. Riva Sanseverino; Q. T. T. Tran; G. Zizzo; M. L. Di Silvestre; B. V Doan; N. Q Nguyen; J. M. Guerrero, 2017 IEEE International Conference on Environment and Electrical Engineering and 2017 IEEE Industrial and Commercial Power Systems Europe (EEEIC / I&CPS Europe).

5. Nonlinear droop control for minimum power losses operation in islanded microgrids, Q. T. T. Tran; H. Shehadeh; E. Riva Sanseverino; S. Favuzza; M. L. Di Silvestre, 2017 IEEE International Conference on Environment and Electrical Engineering and 2017 IEEE Industrial and Commercial Power Systems Europe (EEEIC / I&CPS Europe).

6. Improved Primary Regulation For Minimum Energy Losses In Islanded Microgrids, Eleonora Riva Sanseverino, Gaetano Zizzo, Maria Luisa Di Silvestre, Salvatore Favuzza, Quynh Tran, Pham Thanh Nam, Kieu Thi Thanh Hoa, The 7th IEEE International Conference on Innovative Smart Grid Technologies (ISGT Europe 2017).

7. Optimal Placements of SVC Devices in Low Voltage Grids with High Penetration of PV Systems, E Riva Sanseverino, QTT Tran, Leon R Roose, Staci T Sadoyama, Thai Tran, BV Doan, NH Nguyen, 2018 9th IEEE International Symposium on Power Electronics for Distributed Generation Systems (PEDG), Charlotte, North Carolina, America, June 2018.

8. Minimum power losses by using droop coefficients regulation method with voltage and frequency constraints in islanded microgrids, E Riva Sanseverino, QTT Tran, ML Di Silvestre, G Zizzo, BV Doan, 2018 IEEE International Energy Conference (ENERGYCON), Cyprus, June 2018.

9. Voltage profile improvement for Soc Son’s low-voltage grid with high penetration of PV systems by optimizing the location of SVC devices, E. Riva

Sanseverino, Q. T.T Tran, M. L. Di Silvestre, B.V. Doan, N.Q Nguyen, 2018 IEEE International Conference on Environment and Electrical Engineering and 2018 IEEE Industrial and Commercial Power Systems Europe (EEEIC / I&CPS Europe)

10. Urban energy hubs economic optimization and environmental comparison in Italy and Vietnam, G. Attardo, S. Longo, F. Montana, E. Riva Sanseverino, Q. T. T. Tran, G. Zizzo, 4th International Forum on Research and Technologies for Society and Industry (RTSI 2018), Palermo, Italy, September 2018.